Topological Classification of Floquet-Bloch Systems

Master's Thesis in Physics

Niels Bohr Institute, University of Copenhagen

Frederik S. Nathan
Supervisor: Mark S. Rudner

January 27, 2015

Abstract

Topological insulators are characterized by the existence of universal, robust and highly non-trivial phenomena at their edges. Recently, it has been realized that periodic driving may provide us with a tool versatile enough to induce these robust edge phenomena into otherwise ordinary systems. These periodically driven (Floquet) systems actually have a richer topological structure than non-driven systems, and for this reason we need to develop a new topological classification. In this thesis we present a unified and intuitive way of understanding the topological properties of periodically driven systems. We demonstrate that non-removable degeneracies of the bulk time-evolution operator determine the edge-mode spectrum of such systems. We use this understanding to obtain bulk-edge correspondences of Floquet systems for various cases of dimensionality and symmetry class.

The approach presented here provides a general way of obtaining bulk-edge correspondences for periodically driven systems. The approach can furthermore be used to systematically construct Floquet systems that exhibit non-trivial edge phenomena.

Aknowledgements

I would first and foremost thank my supervisor, Mark S. Rudner for guidance and useful discussions, and for being very helpful in the entire process that led to this thesis. Also thanks to Konrad Wölms for reading through the thesis and coming with useful feedback and comments. Finally, thanks to the CMT group, and the lunch club in particular, for providing a friendly and welcoming environment that made the past year of writing enjoyable.

Contents

Chapter 1

Introduction

In recent years, a class of materials known as topological insulators has been under intensive study. These systems are characterized by the existence of universal, robust and highly non-trivial phenomena at their edges. Besides from being interesting on their own, these phenomena have current and possible applications ranging from metrology, over spintronics to quantum computation. A theory that provides a unified description for topological insulators has been developed recently. The core idea is that these universal edge phenomena are all expressions of some non-trivial property of the bulk systems, the topological phase of the system. The stability of the topological phase is what gives the edge phenomena their robustness. By identifying the topological phase of the system, that is, topologically classifying the bulk Hamiltonian, one can predict the class of phenomena that occurs at the edge.

However, although theoretically well-understood, topological insulators are rarely found in nature. Since the edge phenomena are determined by the bulk properties of a system, their appearance is limited by the choice of materials. There exist tools for manipulating materials, such as applying a strong magnetic field to a sample. However, these are, with some few notable exceptions [1], not sufficient to make desired edge phenomena observable.

More recently, it has been realized that periodic driving might provide us with a tool for "engineering" Hamiltonians that is versatile enough to do this. Periodically driven systems (Floquet systems) are in some respects very analogous to non-driven systems, and edge phenomena in these can be relevant to consider for the same reasons as their non-driven counterparts [2]. Several proposals have been made for experiments that can drive otherwise ordinary systems into exhibiting these non-trivial edge-phenomena, using materials and driving protocols achievable with current technology [3–8]. In this way, periodic driving opens up a new possibility for observing otherwise unobtainable edge phenomena.

The fact that these Floquet systems are governed by time-dependent Hamiltonians means that they have some fundamental differences with static systems however [9–11]. For example, even though the theory of topological insulators generalizes straightforwardly to periodically driven systems, periodically driven systems actually have a richer topological structure than non-driven systems. This is manifested in the existence of *anomalous* edge phenomena in Floquet systems that are not possible to obtain in non-driven systems [10, 12, 13]. This richer structure opens up some new possibilities (see for example Sec. 5.3.1), but it also means that our classification

of non-driven topological insulators is not easily generalized. We thus need to develop a new topological classification for periodically driven systems.

For non-driven systems, topological classification amounts to identifying one or more invariant quantities of the bulk Hamiltonian. These invariants define its topological phase and determine whether the system has non-trivial edge phenomena or not. This relationship between invariants of the bulk system and the edge phenomena is the fundamental idea in the theory of topological insulators. Knowing the invariants that determine the edge physics is helpful for identifying which materials exhibit non-trivial edge phenomena, as was done in Refs. [14, 15].

For periodically driven systems, one can also identify such invariants. As for the non-driven systems, such invariants are helpful for identifying materials and driving protocols that result in non-trivial edge phenomena. Very recently, several invariants have been obtained that relate various classes of edge-configurations with the bulk-properties of driven systems [10, 12, 13, 16]. These invariants were obtained with very different approaches however, and do not give a clear general understanding of the topological structure of periodically driven systems. Furthermore, they do not all provide an immediate intuition that can be used for devising driving schemes that result in non-trivial behaviour.

In this thesis we present a unified and intuitively appealing way of understanding the topological properties of periodically driven systems. We demonstrate for a periodically driven system that the eigenvalues of the bulk time-evolution operator define a well-defined band structure, analogous - but fundamentally different - from the energy band structure of non-driven systems. Note that this is **not** the quasi-energy band structure. This band-structure can have protected degeneracies similar to Weyl nodes [17] for a 2+1-dimensional system, as we demonstrate in Chapter 4. In other dimensions, similar protected degeneracies also appear when symmetries are present. We refer to them as *topological singularities*. We demonstrate in this thesis that topological singularities play a crucial role for the topological properties of periodically driven systems. We show for multiple cases of symmetry class and dimensionality that the edge-phenomena of Floquet systems have a direct relationship with these protected degeneracies. The topological singularities account for the additional topological richness of periodically driven systems and give rise to the anomalous edge phenomena that are unobtainable in non-driven systems.

The results in this thesis seem to make it generally possible to systematically devise driving schemes that result in non-trivial edge behaviour. The approach presented here furthermore provides a general way of obtaining correspondences for Floquet systems. This we demonstrate in Chapter 5 where we derive the bulk-edge correspondences for a wide range of systems.

This thesis is structured as follows: In Chapter 2, we give an introduction to the topic of topological insulators. In Chapter 3 we then introduce the theory of periodically driven systems in quantum mechanics, and generalize the concept of topological insulators to also encompass such Floquet systems. In Chapter 4 we present the main ideas of this thesis: the band-structure picture of the time-evolution operator and the existence of topological singularities. We demonstrate that the number of chiral edge modes in a 2-dimensional Floquet system have a direct and simple relationship with the topological singularities of the bulk time-evolution operator. This system was studied in Ref. [10]. In chapter 5 we generalize the ideas of chapter 4 to also include systems with symmetries. We use the approach outlined there to derive bulk-edge correspondences for periodically driven systems of various symmetry classes. Chapter 6 contains a group of results that follow immediately from the ideas in chapter 4, but are not fully developed. This chapter is

not strictly relevant for the main theme of thesis. In Chapter 7 awe discuss the results of this thesis as well as possible future directions of study. Chapters 1-3 thus introduce the relevant topics, while Chapters 4 and 5 constitute the bulk of the thesis.

Appendix A gives a complete overview of all currently known topological invariants of periodically driven single-particle systems.

Appendix C contains an alternative approach to topological classification of Floquet systems that was attempted in spring 2014. This approach eventually turned out to be inconvenient. This appendix is not a part of the thesis, and can be skipped if necessary. However, the approach still provides a useful and complementary view on the theory of periodically driven systems. It furthermore contains some useful and non-trivial results. Among these is the generalization of the winding number invariant [10] to any even dimension. For completeness we therefore include this approach as appendix.

Chapter 2

Topological Insulators

In this chapter, we introduce the topic of topological insulators. The concept of topological insulators provides a unified description for a great variety of interesting phenomena in condensed matter physics. Examples of topological insulators include the spin quantum Hall effect (Fig. 2.1a), the integer quantum Hall effect (shown on Fig. 2.1b), and Majorana modes at the ends of a super-conducting nano-wire (Fig. 2.1c). Apart from these well-known realizations, there are many other types of topological insulators as well.

What the above systems have in common is that they are in some respect trivial in the bulk, but exhibit interesting phenomena at the edges. These edge phenomena are furthermore "protected" by some fundamental property of the system - for example the locality of the Hamiltonian or a symmetry. The core idea in the theory of topological insulators is that the interesting edge phenomena do not depend on details of the edge itself. Rather, they can be seen as expressions of some inherent bulk property of the system. This gives the edge phenomena their robustness, and thus opens up for a wide range of interesting possible applications in for example metrology, spintronics, and quantum computation.

In this chapter we will explain in more detail what the above means. In order to do this, we first introduce the concept of edge phenomena in single-particle systems with discrete translational invariance. Following this, we demonstrate that certain aspects of the edge-mode spectra can be protected by topology or symmetry. We then discuss the consequences and applications of this phenomenon, and examine the above mentioned examples in a little more detail. Finally, we outline a general theory for these types of phenomena, namely the theory of topological insulators.

In this chapter and the next, continuous deformations of Hamiltonians will play a central role. For continuous deformations of Hamiltonians, we implicitly assume that translational invariance and locality is maintained.

2.1 Edge-mode phenomena in systems with discrete translational invariance

We begin with a general discussion of edge-mode phenomena in single-particle systems with discrete translational invariance in the bulk. Although topological insulators in general do not need translational invariance, it is for illustration very helpful to work with this. The systems we

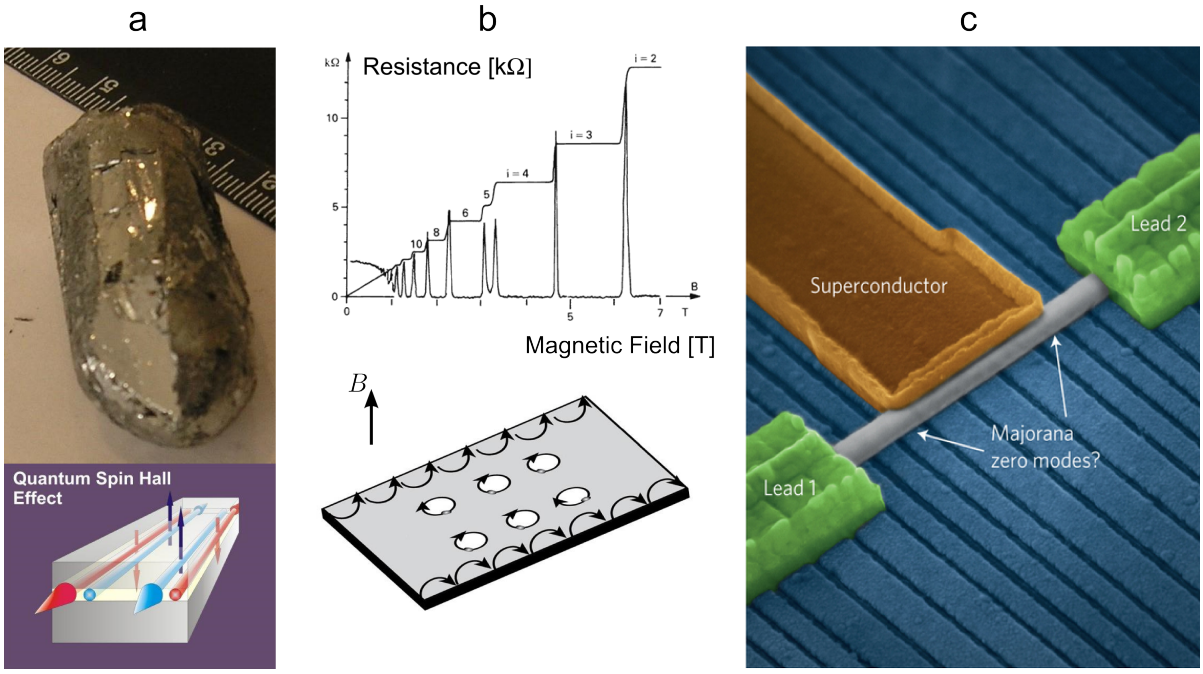

Figure 2.1: Different realizations of topological insulators. a): spin quantum Hall effect. Top shows a picture of BiSe, a time-reversal symmetry protected topological insulator. Bottom: a schematic depiction of the spin quantum Hall-effect. b): An Integer Quantum Hall Effect (IQHE) system . Top shows the quantized current response to an applied voltage gradient in an IQHE system. Bottom: Skipping orbits in an IQHE system, the mechanism behind the quantized current response (this is explained in more detail in Sec. 2.4). c): Majorana fermions in a quantum wire. Experimental setup that might have Majorana fermions at its edge. Image sources in order of mentioning: [18–22].

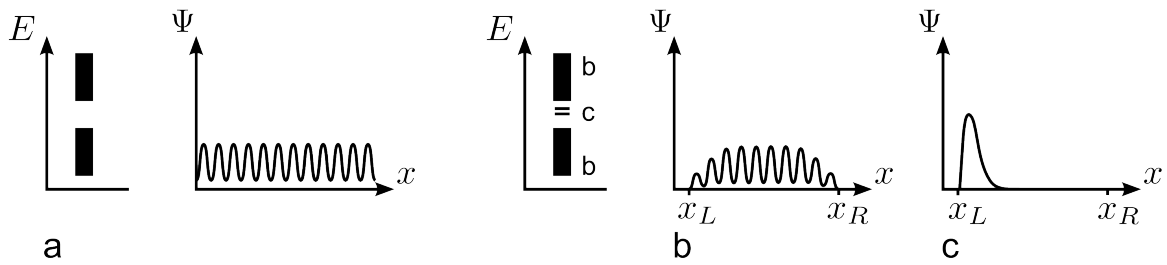

Figure 2.2: a) Depiction of the energy spectrum and eigenstates of an infinite system with discrete translational symmetry. b,c): energy spectrum and eigenstates when edges are introduced at x_L and x_R. b): bulk spectrum and bulk eigenstates. c): edge spectrum and edge modes

consider here are non-driven systems with discrete translational invariance in d spatial dimensions, defined on an infinite lattice. The systems are governed by a time-independent single-particle Hamiltonian H, and in order to be able to properly distinguish bulk phenomena from the edge-mode phenomena that we are eventually interested in, we require that this Hamiltonian is local in space; i.e. it only couples points in the system that are near each other. Consider first an infinite system governed by the Hamiltonian H. The Bloch theorem implies that the spectrum of H forms continuous energy bands, while its eigenstates are plane waves. This situation is depicted in Fig. 2.2 a. Suppose now edges are introduced in the system. The locality condition means that sufficiently far from the edges, the eigenstates and spectrum of the Hamiltonian are unaffected by the introduction of edges (assuming the edges are placed sufficiently far apart). We will refer to this region as the *bulk*. In the bulk it is still possible to identify the energy bands and eigenstates of the infinite system, as in Fig. 2.2b., and this part of the spectrum forms the *bulk energy bands* of the finite system. The eigenstates of the Hamiltonian appear in the bulk as plane waves and are completely delocalized (at least until disorder is introduced).

Near the boundary of the system, however, the spectrum and eigenstates of the Hamiltonian gets distorted by the presence of edges. In this region, the Hamiltonian can acquire localized eigenstates whose energies lie in the bulk gaps [23]. These eigenstates are known as *edge modes*, and their energies form the *edge-mode spectrum* (these are depicted on Fig. 2.2c).

For some systems, the presence or absence of edge states (and their corresponding energies) sensitively depends on the details of the boundary itself. Intriguingly, in other cases, very precise statements can be made about the appearance and energies of edge states, without needing to know almost anything about the details of the boundary. When this is the case, the system is known as a *topological insulator*. An example of such a system is the Chern Insulator, which we will now discuss.

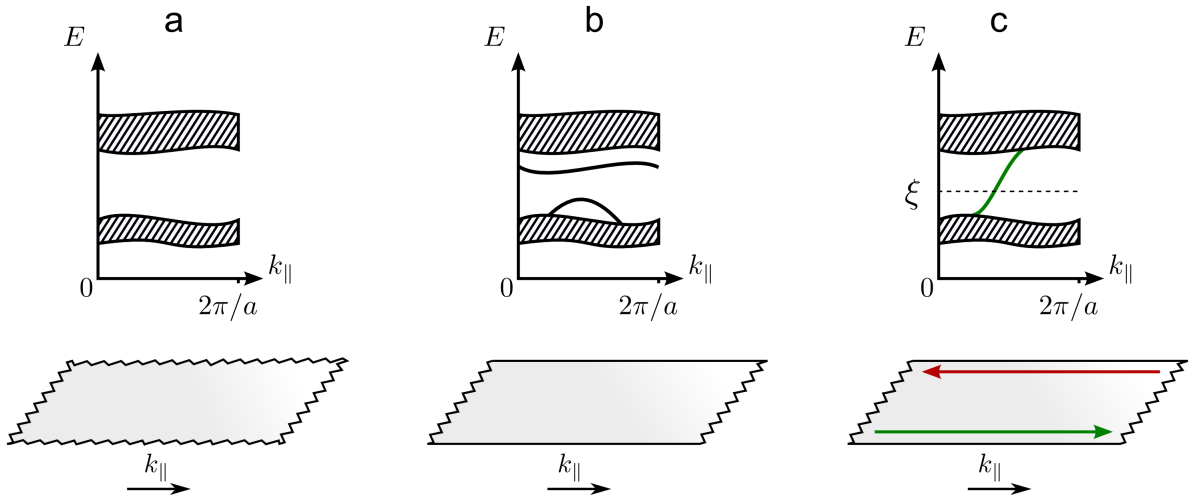

Figure 2.3: a): The spectrum of a Hamiltonian with discrete translational symmetry in an infinite geometry, as a function of the crystal momentum coordinate $k_\parallel$. $k_\parallel$ is defined within a Brillouin zone, and a is the size of the unit cell in the direction of $k_\parallel$. b) An example spectrum of an ordinary insulator in a strip geometry, with the edge-mode spectrum at one edge displayed. c) The spectrum of a topological (Chern) insulator in a strip geometry, with the edge-mode spectrum on one edge displayed. At the opposite edge the two bulk bands are connected by an edge-mode with the opposite slope. The number of chiral edge modes ν_ξ in the gap for this system is 1, and this number cannot change as long as the bulk gap stays open. When the chemical potential lies in the bulk gap, the protected edge mode give rise to a localized current propagating in one direction along the edge.

2.2 Protection of edge-mode phenomena by topology: the Chern Insulator

Consider an insulator in 2-dimensions which is infinite in extent or large and subject to periodic boundary conditions. Ignoring disorder, such a system is governed by a Hamiltonian H with discrete translational symmetry. From the Bloch Hamiltonian we can define a set of continuous energy bands $\{E_n(\mathbf{k})\}$ that depend on crystal momentum $\mathbf{k}$. Since the system is an insulator, the system has a well-defined energy gap that separates a group of energy bands from another. When the energy bands $\{E_n(\mathbf{k})\}$ of this system are projected onto one direction in momentum, one obtains the spectrum of H as a function of a single crystal momentum coordinate $k_\parallel$, as in Fig. 2.3a. Since crystal momentum is defined within a Brillouin zone, the dependence of the spectrum on $k_\parallel$ is $2\pi/a$-periodic, where a is the width of the unit cell in the direction of $k_\parallel$.

Suppose now that edges are introduced along $k_\parallel$, such that the system now becomes an infinitely long strip (Fig. 2.3b bottom). Since the edges were introduced in only one direction, $k_\parallel$ is still a good quantum number, and we can thus still obtain the spectrum of the strip-geometry Hamiltonian as a continuous function of $k_\parallel$ (see Fig. 2.3b top). If the two edges of the strip are far enough apart, we can still identify the bulk energy spectrum of the system. Near the edges of the strip however, the system can acquire edge modes. As for the rest of the spectrum, the energies of the edge modes on each edge will be continuous functions of $k_\parallel$, but it is possible for the edge modes to merge with a bulk band under a continuous change of momentum. This situation is also depicted on Fig. 2.3b. The edge modes in this figure can be altered by changing the shape and form of the edge, and adding perturbations to the Hamiltonian. In particular, it is in general possible to merge the edge modes completely with the bulk bands under an adiabatic change of the Hamiltonian without closing the bulk gap.

Consider now the situation depicted in Fig. 2.3c. Suppose that an edge mode on one edge connects two bulk bands on each side of a bulk gap. This connection cannot be broken under a continuous change of the Hamiltonian, unless the bulk energy gap is closed during the deformation: there is no way to collapse the entire edge mode into either of the two bulk bands without "ripping" the spectrum apart (breaking continuity in $k_\parallel$). Hence the connecting edge mode is a topologically protected feature of the edge-mode spectrum. It is also possible to have a larger number of edge-modes connecting two bulk bands. In general, we can define ν_ξ to be the difference in the number of times the edge modes on one edge crosses the bulk gap at energy ξ from below and above, respectively, as $k_\parallel$ goes from 0 to $2\pi/a$ (see Fig. 2.3c). Note that ν_ξ cannot change under any continuous deformation of the Hamiltonian that keeps the bulk gap open. The number ν_ξ is thus a topologically protected characteristic of the edge-mode spectrum. Since the number of states in a bulk band should not change by winding $k_\parallel$ from 0 to $2\pi/a$, one can show that the net the number of times an edge mode crosses the gap from below should be $-\nu_\xi$ at the opposite edge.

The guaranteed existence of protected edge modes of a Chern insulator means that the system will always be conducting at the edge when connected with a particle reservoir that has chemical potential in the bulk gap. However, there will be a different number of left-moving and right-moving edge modes, and this difference, the net number of chiral edge modes, is given by ν_E. A nonzero number of chiral edge modes means the system will have a current propagating

along the edges of the system, as depicted in Fig. 2.3. If the chemical potential is different at the two edges, there will be a net current along the edges of the system, due to the different filling of edge modes, and the associated "transverse" conductivity is quantized as $\sigma_{xy} = 2\nu_E\sigma_0$, where $\sigma_0 = 7.75 \cdot 10^{-5}\ \Omega^{-1}$ is the conductance quantum .

The phenomenon discussed above is one the most striking features of the integer quantum Hall effect, and in fact systems exhibiting this effect can be seen as a Chern insulators. The quantum Hall effect is discussed in more detail in Sec. 2.4.

2.2.1 Bulk-edge correspondence of the Chern insulator

In the previous subsection we saw that the number ν_ξ of chiral edge modes in a bulk-energy gap ξ was invariant under any continuous deformation of the Hamiltonian that kept the bulk gap open. For a Hamiltonian of a 2d system with discrete translational symmetry, it turns out that there only exist *two* independent quantities with this behaviour [24], and these quantities can be found directly from the bulk properties of the system. The first, $B_\xi[H]$ is simply the number of bulk bands below the energy ξ, when ξ is set inside one of the gaps of the bulk spectrum. The second is the so-called *Chern Number* of the occupied bands.

The Chern number is found as follows: first we express the Bloch Hamiltonian of the system in the form

$$H(\mathbf{k}) = \sum_{n=1}^{N} P_n(\mathbf{k})E_n(\mathbf{k}), \tag{2.1}$$

where the continuous eigenspace projector $P_n(\mathbf{k})$ is given by $P_n(\mathbf{k}) = |\Psi_n(\mathbf{k})\rangle\langle\Psi_n(\mathbf{k})|$ with $|\Psi_n(\mathbf{k})\rangle$ being the n'th eigenstate of $H(\mathbf{k})$, given some arbitrary ordering. The locality of H means that $\{P_n(\mathbf{k})\}$ can be taken to be continuous in $\mathbf{k}$. The Chern number of the band is defined as

$$C[P_n] = \frac{1}{2\pi i}\int \mathrm{d}^2\mathbf{k}\mathrm{Tr}[P_n\partial_{k_x}P_n\partial_{k_y}P_n] - x \leftrightarrow y. \tag{2.2}$$

The Chern number is an integer, and it cannot change under any adiabatic deformation of the projector $P_n(\mathbf{k})$ that preserves its continuity [25]. Furthermore, one can show that for multiple orthogonal projectors $\{P_n\}$, $\sum_n C[P_n] = C\left[\sum_n P_n\right]$. These two properties mean that the sum of Chern numbers of the bands below the energy gap,

$$C_\xi[H] = \sum_{E_n<\xi} C[P_n], \tag{2.3}$$

is a topological invariant of the bulk system. It stays invariant under any continuous deformation of the system that keeps the bulk energy gap E_{gap} open. The indices B_ξ and C_ξ are the *only* independent quantities with this property [24]; any two systems with the same $B_\xi[H]$ and $C_\xi[H]$ can be continuously deformed into each other while keeping the bulk energy gap open. The net number of edge modes ν_ξ defined above is also invariant under such deformations however, and this means that ν_ξ must be given by some function of $B_\xi[H]$ and $C_\xi[H]$. Indeed, it can be proven in several ways [26] that

$$\nu_\xi = C_\xi[H]. \tag{2.4}$$

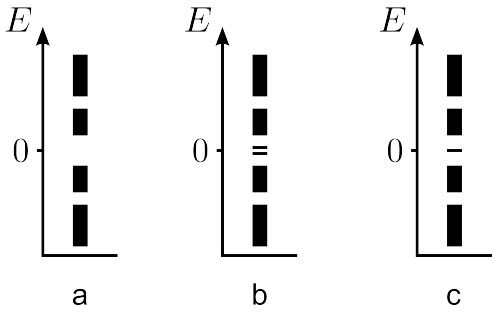

Figure 2.4: a) Energy spectrum of a 1-dimensional system with even particle-hole symmetry in infinite boundary conditions. b) Spectrum of a system in a finite setting, with the edge-mode spectrum at one edge displayed. This system has a trivial edge-mode configuration. c) The spectrum of a system with a non-trivial edge-mode spectrum. The system has a single zero-energy mode that is forced to stay at energy zero.

This non-trivial relation shows that the bulk properties of the system determines the configuration of the edge-mode spectrum: the number of chiral edge modes in a gap is given by the sum of Chern numbers of the bulk bands below the gap.

A relation that identifies the edge-mode configuration with a bulk topological invariant is known as a *bulk-edge correspondence*, and the existence of such a relation is the *key* feature of topological insulators. This notion is therefore referred to extensively in the following, and subsequent chapters will to a large extent focus on generalizing this concept. In Sec. 2.5, a more general discussion of bulk-edge correspondences is given.

2.3 Protection of edge-mode phenomena by symmetry and topology

The chiral edge modes in a Chern insulator are protected purely by topology. That is, the robustness of these modes comes directly from the necessity of maintaining continuity of the spectrum, as described above. However, if one or more additional symmetries are present, the symmetries themselves may also contribute to the protection of the edge modes, thus allowing for new protected configurations of edge modes.

To illustrate the concept that edge modes can be protected by symmetry, we now consider zero-energy edge modes on the edges of 1-dimensional systems with particle-hole symmetry.

Consider a 1-dimensional system, whose Hamiltonian H is particle-hole symmetric, i.e. the Hamiltonian satisfies $H = -H^*$ in some basis. The symmetry means that if $|\Psi_n\rangle$ is an eigenstate of H with energy E_n, $|\Psi_n^*\rangle$ also is, with energy $-E_n$, where $|\Psi_n^*\rangle$ is the complex conjugate of $|\Psi_n\rangle$ with respect to the same basis. The spectrum of H is thus symmetric around $E = 0$ and is depicted in Fig. 2.4a for an infinite system. Suppose now this system has a bulk gap around $E = 0$ and has edges. The Hamiltonian will in general have edge modes, and these also have to satisfy particle-hole-symmetry. Thus, if at one edge the Hamiltonian has an edge mode with

energy E, there will at the same edge be a localized mode with energy $-E$. Edge-modes with nonzero energy thus come in pairs as on Fig. 2.4b.). Importantly, however, zero-energy edge modes can be their own conjugates, since $E = -E$ for $E = 0$. The symmetry then forces such edge modes to stay at energy zero. In this way, particle-hole symmetry ensures that the number of edge modes with zero energy cannot change its parity ν unless the bulk energy gap at zero is closed: the parity ν is a protected characteristic of the edge-mode spectrum.

Similarly to the Chern insulator case, there only exist a limited number of independent quantities invariant under continuous deformations that preserve particle-hole symmetry and keep the bulk gap at energy zero open. These quantities can also be obtained directly from the bulk system, and ν can thus be found from an invariant quantity of the bulk system. Such an expression for ν in terms of the bulk Hamiltonian was found in [27]. There it was shown that ν is given by the expression

$$\nu = \mathrm{sgn}\mathrm{Pf}[H(0)]\mathrm{Pf}[H(\pi)], \tag{2.5}$$

where $\nu = -1$ corresponds to an odd number of zero-energy edge-modes. Here $H(\mathbf{k})$ is the Bloch Hamiltonian of the 1d system at crystal momentum $\mathbf{k}$ in the basis where $H = -H^*$, and where the width of the unit cell is taken to be 1. The Pfaffian Pf is a quantity defined for skew-symmetric matrices that is invariant under orthogonal transformations (more information about these can be found in Ref. [28]).

2.3.1 Symmetry classes

The 1-dimensional particle-hole symmetric system was just one example where a symmetry contributed to the protection of certain characteristics of the edge-mode spectrum. In fact, a wide range of symmetry classes can support systems whose edge mode spectrum have non-trivial properties that are protected by a combination of symmetry and topology. The most interesting symmetry classes from a physical perspective are symmetries insensitive to disorder, as disorder is always present in real-world solid state systems. Of these disorder-insensitive symmetries, the most important ones are time-reversal symmetry, particle-hole symmetry, and chiral symmetry. They can each be expressed as a condition on the Hamiltonian of the form

$$H = rSHS^{-1}, \tag{2.6}$$

where S is some unitary or anti-unitary[1] operator, and r is 1 or -1. The four different cases correspond to the different symmetries: a system is said to be time-reversally symmetric if the Hamiltonian satisfies the above relation for some anti-unitary S and with $r = 1$. Particle-hole symmetry is present if S is anti-unitary and $r = -1$, and chiral symmetry is present if S is unitary and $r = 1$. The last type of condition where S is unitary and $r = 1$ is always satisfied. If S is anti-unitary, one can furthermore show that S must square to either 1 or -1, and these two cases correspond to physically distinct situations. In this way, there actually exist two types of time-reversal symmetry and two types of particle-hole symmetry.

From the symmetry conditions discussed above, it is possible to show that there are in total 10 independent combinations of particle-hole, time-reversal and chiral symmetries that Hamiltonians

[1] Anti-unitary operators are operators on the form UK, where U is a unitary operator and K is the complex conjugation operator with respect to some basis

Symmetry				d							
AZ	Θ	Ξ	Π	1	2	3	4	5	6	7	8
A	0	0	0	0	$\mathbb{Z}$	0	$\mathbb{Z}$	0	$\mathbb{Z}$	0	$\mathbb{Z}$
AIII	0	0	1	$\mathbb{Z}$	0	$\mathbb{Z}$	0	$\mathbb{Z}$	0	$\mathbb{Z}$	0
AI	1	0	0	0	0	0	$\mathbb{Z}$	0	$\mathbb{Z}_2$	$\mathbb{Z}_2$	$\mathbb{Z}$
BDI	1	1	1	$\mathbb{Z}$	0	0	0	$\mathbb{Z}$	0	$\mathbb{Z}_2$	$\mathbb{Z}_2$
D	0	1	0	$\mathbb{Z}_2$	$\mathbb{Z}$	0	0	0	$\mathbb{Z}$	0	$\mathbb{Z}_2$
DIII	-1	1	1	$\mathbb{Z}_2$	$\mathbb{Z}_2$	$\mathbb{Z}$	0	0	0	$\mathbb{Z}$	0
AII	-1	0	0	0	$\mathbb{Z}_2$	$\mathbb{Z}_2$	$\mathbb{Z}$	0	0	0	$\mathbb{Z}$
CII	-1	-1	1	$\mathbb{Z}$	0	$\mathbb{Z}_2$	$\mathbb{Z}_2$	$\mathbb{Z}$	0	0	0
C	0	-1	0	0	$\mathbb{Z}$	0	$\mathbb{Z}_2$	$\mathbb{Z}_2$	$\mathbb{Z}$	0	0
CI	1	-1	1	0	0	$\mathbb{Z}$	0	$\mathbb{Z}_2$	$\mathbb{Z}_2$	$\mathbb{Z}$	0

Figure 2.5: Periodic table of topological insulators. The table shows the topological classification of edge-mode spectra for systems with all types of twofold symmetries. The Greek letters Θ, Ξ and Π indicate whether, respectively, time-reversal, particle-hole or chiral symmetry are present. These symmetries are explained in more detail in Sec. 2.3.1. For the two first, the sign indicates whether the symmetry operator squares to 1 or -1. Given the dimension d and symmetry class, the table shows how many topologically distinct edge-mode configurations are possible, where 0 corresponds to all edge-mode spectra being topologically identical. The leftmost column shows the Altland-Zirnbauer naming convention for the symmetry classes [29]. The table was obtained in [30, 31].

can satisfy (including the trivial cases). These were described in Ref. [29], where a naming convention - the Altland-Zirnbauer (AZ) classification - was also introduced. In Refs. [30, 31] it was found how many distinct edge-mode configurations each of these 10 symmetry classes could support in a given dimension. This "periodic table" of edge-mode configurations is shown on Fig. 2.5, with an explanation.

The symmetries on the periodic table are not the only types of symmetries that can support protected edge modes however. Other symmetries than the 10 AZ classes can also give rise to protected edge mode configurations. These can for example be crystal symmetries, such as inversion symmetry [26], but there could in principle also exist other disorder-insensitive symmetry classes that support new types of protected edge-mode configurations. This could for example be the case if a Hamiltonian satisfies the condition with S unitary and $r = 1$ for multiple independent operators S.

2.4 Topological insulators

In the previous section we found that there existed a wide range of systems that had edge-mode phenomena protected by symmetry and topology. Such systems are collectively known as *topological insulators*. Topological insulators host a wide range of interesting physical phenomena

that are characterized by their robustness and may have useful applications [32].

The most striking example observed so far in experiments is the quantum Hall effect. This phenomenon is found in a 2-dimensional electron gas, such as for example a GaAs/AlGaAs interface, subject to a perpendicular magnetic field [25]. Such a system can bee seen as a realization of the Chern insulator. The magnetic field causes the electrons at the edge to move in skipping orbits along the edge, constituting chiral edge modes (see Fig. 2.1b bottom). The quantized current response discussed in Sec. 2.2.1 is what gives rise to one of the most noticeable features of the integer quantum Hall effect, namely the plateaus formed by the transverse resistivity as a function of the magnetic field (see Fig. 2.1b top). The plateaus arise because the number of transversely conducting edge modes can be changed by tuning the magnetic field. But since this number can only take integer values, the transverse conductance must change stepwise. The topological nature of the edge modes protects this effect against disorder—actually and most remarkably, the quantum Hall effect would not exist without disorder [33]. Due to this robustness, the quantum Hall effect can be observed in relatively large and uncontrolled systems. Furthermore, the quantum Hall conductance is universal: it has the same value, regardless of sample, experiment, or lab. The quantum Hall conductance is so precisely quantized that its value can be measured to a accuracy of a few parts per billion. This accuracy, achieved in a wild and relatively uncontrolled solid state sample, is as good as any measurement in atomic physics . Due to its universality and robustness, the Quantum hall conductance is used as a practical standard of electrical resistance. [34].

Another example of a topological insulator was the 1-dimensional system discussed in Sec. 2.3 whose edge-mode spectrum was protected by particle-hole symmetry. Examples of Hamiltonians with this type of symmetry are Boguliubov-de Gennes (BdG) Hamiltonians that are used as a mean-field description of fermionic systems with superconductivity. BdG-Hamiltonians act in a space containing two particle-hole conjugate copies of the same system, and the symmetry is thus artificially imposed. Nevertheless, such systems can have edge-modes with zero energy that are their own conjugates [27]. The modes corresponding to a many-body excitations that are their own antiparticles - so-called Majorana fermions. These excitations have non-trivial exchange statistics and can potentially be used for quantum computation. The Majorana fermions have been proposed to be observable in a 1-dimensional wire with the correct band-structure properties, in the proximity of superconductivity. An experimental setup is shown in Fig. 2.1c. Although no definite observation has been made so far, these edge states are currently subject of intensive investigations [35].

Another prominent example of a topological insulator protected by symmetry is the two dimensional topological insulator with time reversal symmetry [36, 37]. These systems have a time-reversally conjugate pair of edge modes at their boundary. The edge modes have opposite chirality, so in contrast to the Chern insulator, the edge modes do not carry a charge current along the edge of the system, but instead for example a spin current [36] (see Fig. 2.1a). This type of phenomenon can be realized in graphene and HgTeCd quantum well-structures. Time-reversal symmetry also allows for a distinct protected edge-mode configuration in 3-dimensional systems, and in this way, there also exists a distinct type of 3-dimensional topological insulator protected by time-reversal symmetry. On such systems, the edge modes live on 2D surfaces. of these systems have an odd number of Dirac-points in their dispersion, and these are protected by symmetry. These 3D topological insulators can be found in nature, for instance in the materials BiSb, BiSe

(sample depicted on Fig. 2.1), BiTe and SbTe. Topological insulators protected by time-reversal symmetry have potential applications in quantum information processing and spintronics [32]

The protection of edge-mode spectra by symmetry and topology thus give rise to a wide range of robust and physically interesting phenomena that may have useful applications.

2.5 Topological classification of topological insulators and superconductors

In this section, we introduce a simple but powerful idea that gives us some fundamental insight into the nature of topological insulators. The concepts we introduce here furthermore provide a useful framework for describing topological insulators that will be used extensively in the subsequent. The main idea is that bulk Hamiltonians with a given symmetry fall into some distinct topological classes or phases, related by continuous deformations. The protected edge-mode configurations we have discussed turn out appear at the boundary between Hamiltonians of different classes.

Given a symmetry, two Hamiltonians are defined to be *topologically equivalent* if it is possible to continuously deform one into the other without closing any energy gap, breaking locality or the symmetry. If this is not possible, the Hamiltonians are *topologically distinct*. This equivalence relation defines a natural grouping of Hamiltonians: Two Hamiltonians belong to the same *topological class* or *phase* if and only if they are topologically equivalent. A quantity that is invariant under any continuous deformation of the Hamiltonian that maintain all symmetries and keeps all bulk gaps open is known as a *topological invariant* of the Hamiltonian. Per definition, Hamiltonians in the same topological phase share the same invariants. Furthermore, the invariants of a Hamiltonian usually determines its topological class. The identification of the topological phase of a Hamiltonian is known as *topological classification*.

For every type of topological insulators, the edge-mode configuration in a bulk gap defines a topological invariant. Often, if not always, it is only possible to define a limited number of independent topological invariants of a system, and these invariants can also be found directly from the bulk Hamiltonian. It is therefore possible to identify one of these topological invariants with the edge mode configuration, such as was done with the Chern number in Sec. 2.2.1. The identification is known as the *bulk-edge correspondence*, and the existence of a bulk-edge correspondence is is the key property of a topological insulator. Identifying the bulk-edge correspondence for a class of topological insulators provides non-trivial insight into the mechanism behind the edge-mode phenomena. More importantly, it can be used to identify materials that exhibit the non-trivial edge mode phenomena. As was demonstrated for the Chern insulator in Sec. 2.2.1, the bulk-edge correspondence is not necessarily the only independent topological invariant one can define for a bulk system. There can be more distinct phases of bulk systems than there are distinct edge-mode configurations.

Since the topological categorization of Hamiltonians requires a specification of symmetry class and dimensionality, every class of topological insulators is defined by these two properties. For example, a Chern insulator is classified as a 2-dimensional topological insulator with no symmetries (symmetry class A), while the 1d system with Majorana edge modes is a 1-dimensional topological insulator with particle-hole symmetry (class D), and the spin quantum Hall effect is found in 2d topological insulators with time-reversal symmetry (class AII). For topological insulators with

the symmetry classes studied in the periodic table (Fig. 2.5), all bulk-edge correspondences are known in every dimension [30].

It is important to note that not all combinations of dimensionality and symmetry class can support a topological insulator - for example there exists no 1-dimensional version of the Chern insulator. In fact, in each dimension only 5 of the 10 symmetry classes in the periodic table (Fig. 2.5) support a topological insulator. If a symmetry class and dimensionality supports topological insulators, it means there exist distinct topological phases, but one of these is always trivial. Hence, it is always possible for a system with of a given symmetry and dimensionality to be topologically trivial even though topological insulators are supported. For instance, not all 2-dimensional systems are Chern insulators.

Chapter 3

Periodically driven quantum systems

In the last chapter we discussed a class of materials known as topological insulators. This type of systems was characterized by having robust and interesting phenomena at their edges. Besides from being physically interesting on their own, these edge phenomena have several possible applications, and are thus desirable to obtain in experiments for many reasons. The core property that makes the edge phenomena interesting is that they can be seen as expressions of some inherent bulk property of the system. This gives the topological edge phenomena their robustness.

This also has an unfortunate consequence however: the fact that the edge modes were determined by the bulk properties of the systems means that the observation of topological edge phenomena is limited by the choice of materials, and although interesting, topological insulators are rarely found in nature. There exist a few methods of manipulating the band-structure of non-driven systems into exhibiting the edge phenomena, such as applying a strong magnetic field to a sample. However, with some few exceptions, these tools are in general not enough to make desirable topological edge phenomena easily obtainable in experiments.

However, recently [3,6] it has been realized that periodic driving can provide us with a tool for band-structure manipulation that is versatile enough to drive systems into non-trivial topological phases, and thereby induce non-trivial protected edge phenomena. The existence of stationary states of the time-evolution operator means that periodically driven systems are in some respects very similar to non-driven systems. Many results for non-driven systems can thus be generalized to periodically driven systems. In particular, it is for periodically driven systems possible to talk of band-structure of some effective Hamiltonian that acts in a way analogous to non-driven systems. The concept of topological insulators also has a direct and immediate generalization to periodically driven systems, as we discuss in Sec. 3.3. The relevant bulk properties of driven systems are in some cases very dependent on the driving field., and in this way periodic driving gives us a new way of "engineering" effective Hamiltonians. This can be used to induce topological edge phenomena into otherwise ordinary systems.

In this chapter we first present the theory of periodically driven quantum systems. Such systems are also known as Floquet systems, dubbed after the French 19th century Mathematician whose theorem [38] for periodic linear differential equations provides us with a basis for understanding periodically driven quantum systems. After having presented the theory of periodically driven system, we generalize the concept of topological insulators from non-driven systems to also include

driven systems. These types of systems are the subject of study in the rest of this thesis.

3.1 Theory of periodically driven systems

In this section we introduce the subject of periodically driven systems in quantum mechanics. According to the laws of quantum mechanics, the state of a physical system associated with a vector $|\psi(t)\rangle$. The time-evolution is of the system is then governed by the Schrödinger equation

$$i\partial_t|\psi(t)\rangle = H(t)|\psi(t)\rangle, \tag{3.1}$$

where $H(t)$ is the Hamiltonian operator of the system. In the above equation we set $\hbar = 1$, and we will do so in the rest of the thesis. If the Hamiltonian is independent of time, the problem of solving the Schrödinger equation is made simpler by the diagonalization of the Hamiltonian. Obtaining a complete set of solutions $\{E_n, |\Psi_n\rangle\}$ to the static Schrödinger equation

$$H|\Psi_n\rangle = E_n|\Psi_n\rangle \tag{3.2}$$

allows one to compute the time-evolution of any state analytically, given an initial state: the solutions to the Schrödinger equation take the form

$$|\psi(t)\rangle = \sum_n c_n|\Psi_n\rangle e^{-iE_nt}, \tag{3.3}$$

where the amplitudes $\{c_n\}$ are constant in time, and can be found from the initial conditions: $c_n = \langle\psi(0)|\Psi_n\rangle$. We will refer to systems governed by time-independent Hamiltonians as *non-driven*.

The simplification for non-driven systems arose from the continuous time-translation symmetry of the problem. If the Hamiltonian $H(t)$ is time-dependent, it is in general impossible to obtain the time-evolution of a state analytically. The best one can do is to formally integrate the Schrödinger equation, obtaining

$$|\psi(t)\rangle = U(t)|\psi(0)\rangle, \tag{3.4}$$

where the *time-evolution operator* is given by

$$U(t) = \mathcal{T}e^{-i\int_0^t H(t')dt'} \tag{3.5}$$

$$= \lim_{\delta t\to 0} e^{-iH(t)\delta t}e^{-iH(t-\delta t)\delta t}e^{-iH(t-2\delta t)\delta t}\dots e^{-iH(0)\delta t}. \tag{3.6}$$

Here $\mathcal{T}$ is the time-ordering operator that orders the factors of $H(t')$ in the expansion of the exponential in order of increasing time, such that the later times are to the left of earlier times. The time-evolution operator is a unitary operator that from Eq. (3.4) should satisfy $U(0) = 1$. Furthermore, there is a one-to-one correspondence between time-evolution operators and Hamiltonians, since $H(t) = i\partial_t U(t)\cdot U^\dagger(t)$. Eqs. (3.4)-(3.6) gives a formal solution to the time-dependent Schrödinger equation, but they are basically a restatement of the problem. Their solution is in general computationally involved, and equally important, it does not provide much physical insight into the behaviour of the system. For systems governed by time-dependent Hamiltonians however, this is in general the best one can do.

There are some exceptions though. importantly, if the Hamiltonian depends *periodically* on time, such that $H(t) = H(t+T)$ for some driving period T, we can actually do much better in describing and understanding the behaviour of the system. We will refer to this type of system as a *periodically driven system*. The discrete time-translational symmetry of a periodically driven system makes it possible to analyse the time-evolution of a periodically driven system in a similar fashion to non-driven systems. The reason for this is that the time-evolution operator of a periodically driven system satisfies

$$U(t+mT) = U(t)U(T)^m \tag{3.7}$$

for integer m, as can be shown from Eq. (3.6). In particular, $U(mT) = U(T)^m$.

Each time a driving period has passed, the eigenstates of $U(T)$ have thus evolved into themselves, gaining a complex phase. Whereas for non-driven systems we wanted to diagonalise the Hamiltonian, we are for periodically driven systems instead interested in diagonalizing the so-called *Floquet operator*, defined as the time-evolution operator $U(T)$ of the system over one driving period. The central eigenvalue problem for periodically driven systems thus looks like

$$U(T)|\Psi_n\rangle = e^{-i\varepsilon_n T}|\Psi_n\rangle. \tag{3.8}$$

Knowing the eigenvalues and eigenstates of the Floquet operator, one can easily obtain the time-evolution of any initial state stroboscopically. At any integer multiple of the driving period, the evolution of a state can be obtained as

$$|\psi(mT)\rangle = \sum_n c_n|\Psi_n\rangle e^{-i\varepsilon_n mT}, \tag{3.9}$$

where, as for non-driven systems, $\{c_n\}$ are determined by the initial state: $c_n = \langle\psi(0)|\Psi_n\rangle$. For periodically driven systems, it is thus possible to analytically obtain the time evolution of a state at integer multiples of the driving period by diagonalizing the Floquet operator.

Comparing the above to Eqs. (3.2), (3.3), we see that the parameter ε plays a role analogous to energy for the time-evolution of a state of a non-driven system. For this reason, it is known as *quasi-energy*. Like energy, it determines the time-evolution of a system and is a conserved quantity[1]. Unlike energy however, it is periodic: equation (3.8) only defines ε_n up to an integer multiple of the driving frequency $2\pi/T$. So whereas energy lives on the line of real numbers, quasi-energy lives on a circle. The periodicity of quasi-energy constitutes one of the main qualitative differences in the analysis of non-driven and periodically driven systems, and it has important implications.

If we want to know the evolution of observables (say, the position of particles), at time-scales longer than the driving period, the stroboscopic evolution given by Eq. (3.9) will often, but not always, give all relevant information about the physical behaviour of the system (see eg. Refs. [9, 39] for examples where the stroboscopic evolution does not provide an adequate description).

It is also possible to obtain the time-evolution of a state at intermediate times, using the so-called *Floquet states* $\{|\Psi_n(t)\rangle$, that are defined as $|\Psi_n(t)\rangle = U(t)|\Psi_n\rangle$. From Eq. (3.7), we

[1]This can be seen by explicitly writing the change of the quasi-energy expectation value over one driving period

know the Floquet states must evolve with the form

$$|\Psi_n(t)\rangle = e^{-i\varepsilon_n t}|\Phi_n(t)\rangle, \tag{3.10}$$

where the state $|\Phi_n(t)\rangle = |\Phi_n(t+T)\rangle$ is T-periodic. Eq. (3.10) is known as the *Floquet theorem*, and is a result that dates back to 1883 [38] (although not in the context of quantum mechanics). Knowing the quasi-energies and the Floquet states, it is possible from to obtain the time-evolution of any state, for all times:

$$|\psi_n(t)\rangle = \sum_n c_n|\Phi_n(t)\rangle e^{-i\varepsilon_n t}, \tag{3.11}$$

where the amplitudes $\{c_n\}$ are determined from the initial conditions.

Note the similarity between the Floquet states in Eq. (3.10) and the Bloch wave functions of a periodic crystal. The Bloch theorem states that when a system has discrete translational symmetry, the eigenstates of the Hamiltonian takes the form of a periodic function times a complex plane wave. The wavelength of the plane wave defines the crystal momentum of the state, and this is just defined up to a multiple of $2\pi/a$ with a being the lattice constant. Quasi-energy can thus be seen as the time-translation analogue to crystal momentum.

3.2 Floquet-Bloch systems

For the topic of this thesis, we are interested interested in driven systems with translational symmetry. For studying such systems, it is very important to note that many of the ideas about band structure can carry over from non-driven systems, only with the Hamiltonian being replaced by the Floquet operator, and energy with quasi-energy.

If a non-driven systems has discrete translational symmetry, the Hamiltonian H diagonalizes with respect to crystal momentum. We can then represent it by a Bloch Hamiltonian $H(\mathbf{k})$ that determines the time-evolution of states with crystal momentum $\mathbf{k}$. If the Hamiltonian of a Floquet system has discrete translational invariance, the time-evolution operator still block-diagonalizes with respect to crystal momentum. We can in the same way represent the time-evolution operator $U(t)$ by a Bloch time-evolution operator $U(\mathbf{k}, t)$ that gives the time-evolution of states with crystal momentum $\mathbf{k}$. The Bloch time-evolution operator is given by

$$U(\mathbf{k}, t) = \mathcal{T}e^{-i\int_0^t dt' H(\mathbf{k},t')}, \tag{3.12}$$

where $H(\mathbf{k}, t)$ is the Bloch Hamiltonian of the system. The locality and boundedness of the Hamiltonian is equivalent to $U(\mathbf{k}, t)$ being continuous in crystal momentum and time, respectively. We can in particular represent the Floquet operator in Bloch space, and its eigenvalue equation becomes:

$$U(\mathbf{k}, T)|\Psi_n(\mathbf{k})\rangle = e^{-i\varepsilon_n(\mathbf{k})T}|\Psi_n(\mathbf{k})\rangle. \tag{3.13}$$

$\{\varepsilon_n(\mathbf{k})\}$ are known as the *quasi-energy bands*. Together, the Floquet eigenstates and quasi-energies form the Floquet bands of the system. This effective band structure describe the physics of a single-particle system in an analogous way to the protected edge-modes of a non-driven system. Although the many-body problem is currently not as well-understood, [10], Floquet bands play a

role similar to energy bands for the transport properties of a multi-particle system in at least some cases of weak driving [2].

Single-particle systems with discrete translational symmetry in the bulk will be known as *Bloch systems*. If the system is furthermore periodically driven, we refer to it as a *Floquet-Bloch* system.

3.3 Topological phenomena in Floquet-Bloch systems

The close analogy between periodically driven and non-driven systems means that the concept of topological insulators has an immediate analogy in periodically driven systems. When edges are introduced to a Floquet-Bloch system, the Floquet operator maintains its bulk spectrum and eigenstates, but can acquire edge modes whose quasi-energies form an edge-mode spectrum. In the same way as for the non-driven case, it is possible for the Floquet operator to have features of its edge-modes spectrum that are protected by topology or symmetry. The protected edge-modes of non-driven systems discussed in the previous chapter can actually be seen as a special case of this phenomenon as one can also define a quasi-energy spectrum for non-driven systems. In this way, Floquet-Bloch systems with topologically protected edge modes can be seen as generalizations of topological insulators. Floquet-Bloch systems in general have a richer topological structure than their non-driven special cases. For example, there exist multiple cases of Floquet-Bloch systems with configurations of edge modes that are not obtainable in any non-driven system [10, 12, 13]. Such configurations will be known as *anomalous edge modes* and they will be discussed in more detail in the subsequent.

For the understanding of the edge-phenomena of periodically driven systems, it is also very useful develop a topological classification for periodically driven systems. Two driven systems are defined to be topologically equivalent if the *quasi*-energy gaps to stay open during a continuous deformation from one system to another, and with this definition the results in Sec. 2.5 still apply: the time-evolution operators of periodically driven systems fall into distinct topological classes or phases, and the topological phase of a system is determined by a set of topological invariants. One of these invariants determines the edge-mode configuration of the Floquet operator. In this way, periodically driven systems also have a bulk-edge correspondence.

However, that while the bulk invariant of a non-driven system determining the edge mode configuration related to the bulk Hamiltonian, it turns out that the bulk-edge correspondence for driven systems actually depends on the entire time-evolution of the system [10]

There are no obvious generalization of the bulk-edge correspondences of non-driven systems to periodically driven systems. Although recently bulk-edge correspondences for several cases have been obtained [10, 12, 13, 16], there are still many cases of symmetry class and dimensionality for which the bulk-edge correspondence is not known.

We now present an example of a Floquet-Bloch system with non-trivial edge mode configurations, analogous to the 2-dimensional system discussed in Sec. 2.2.1. and present its bulk-edge correspondence that was obtained in ref. [10]. The this system will be examined in more detail in the next chapter, and hence the following section serves as a starting point for the next chapter... .

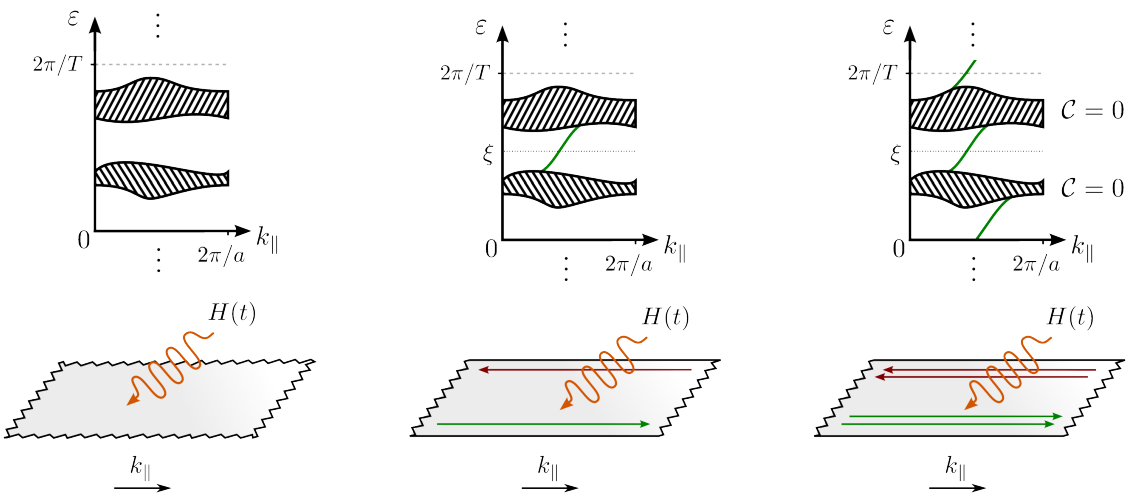

Figure 3.1: a) Quasi-energy band-structure of a periodically driven system in infinite boundary conditions. The dots above and below the spectrum indicate the periodicity of quasi-energy. b) quasi-energy spectrum of a system in a strip geometry whose Floquet operator has a single chiral edge mode in the quasi-energy gap ξ . c) Floquet topological insulator with anomalous edge modes. The Chern numbers of the bulk Floquet bands are zero, but the Floquet operator still has chiral edge modes in its bulk gaps.

3.3.1 Chiral edge modes in a 2-dimensional periodically driven system

Consider a 2-dimensional periodically driven system with translational invariance, defined on an infinite geometry, subject to periodic driving. This system has a single-particle time-evolution operator in Bloch Space $U(\mathbf{k}, t)$ and a bulk-quasi-energy band structure $\{\varepsilon_n(\mathbf{k})\}$, as depicted on Fig. 3.1a. Suppose now edges are introduced in one direction, along $k_\parallel$. In the same way as for the Chern insulator, the Floquet operator of this system can also acquire chiral edge modes in its bulk quasi-energy gap, as depicted on Fig. 3.1b. The edge-mode configuration depicted here can also be found for the Floquet operator of a non-driven Chern Insulator, but the quasi-energy spetrum on Fig. 3.1c is impossible to have in a non-driven system. Here the Chern numbers of the Floquet bands are zero, but there are chiral edge modes in every bulk quasi-energy gap, and a non-driven system whose bulk bands have Chern number zero should have no chiral edge modes. This anomalous edge-mode configuration is possible to have in periodically driven systems however, and appear in several known models [10].

As for the Chern insulator, the number ν_ξ of chiral edge-modes in a bulk quasi-energy gap at quasi-energy ξ is determined from some quantity of the bulk system. In contrast to non-driven systems however, the Chern numbers of the Floquet bands are not enough to determine the number of chiral edge modes, as can also be seen from the appearance of anomalous edge modes. Hence further information is needed to determine the number of edge modes. This information is contained in the entire time-evolution of the system.

The bulk-edge correspondence of this system was found in [10]. In order to find the number ν_ξ of chiral edge modes in a bulk gap at quasi-energy ξ, we consider the bulk time-evolution operator $U(\mathbf{k}, t)$ in Bloch space. We then let $U_\xi(\mathbf{k}, t)$ be any time-evolution operator that satisfies $U_\xi(\mathbf{k}, T) = 1$ and can be continuously deformed into $U(\mathbf{k}, t)$ without closing the gap at quasi-energy ξ. In practice, U_ξ can be obtained as follows. We define the effective Hamiltonian $H^\xi_{\text{eff}}(\mathbf{k})$ as the unique operator that satisfies

$$U(\mathbf{k}, T) = e^{-iH^\xi_{\text{eff}}(\mathbf{k})T}, \tag{3.14}$$

and takes eigenvalues between ξ and $\xi + 2\pi/T$. Then U_ξ can be taken to be

$$U_\xi(\mathbf{k}, t) = U(\mathbf{k}, t)e^{iH^\xi_{\text{eff}}(\mathbf{k})t}. \tag{3.15}$$

With $U_\xi(\mathbf{k}, t)$ defined, ν_ξ can then be obtained as

$$\nu_\xi = W[U_\xi] \equiv -\frac{1}{8\pi^2}\int_0^T \mathrm{d}t \int \mathrm{d}^2\mathbf{k}\,\mathrm{Tr}\left[U_\xi^\dagger \partial_t U_\xi \cdot U_\xi^\dagger \partial_{k_x} U_\xi \cdot U_\xi^\dagger \partial_{k_y} U_\xi - x \leftrightarrow y\right]. \tag{3.16}$$

where $W[U_\xi]$ is referred to as the *winding number* of U_ξ. In the next chapter we will derive an alternative, complementary expression for ν_ξ.

Chapter 4

Topological classification of Floquet systems without symmetries

In the last chapter we discussed the possibility of engineering effective Hamiltonians using periodic driving. The quasi-energy spectrum of a periodically driven system in general depends non-trivially on the applied driving potential [6], and periodic driving gives a new and versatile way of manipulating the effective band-structure of a quantum system. In particular, periodic driving can be used to drive an otherwise ordinary system into a topologically non-trivial phase with topologically protected edge modes at its boundary [2, 10].

However, there are still some major qualitative/fundamental differences between the description of driven and non-driven systems, and the field of periodically driven quantum systems is not entirely well-understood yet. An important question is understanding what bulk properties give rise to protected edge mode phenomena in driven systems. As we saw in section 3.3.1, the bulk-edge correspondences of non-driven systems do not have immediate generalizations to driven systems. There are multiple examples of topological phenomena in driven systems, so-called *anomalous edge phenomena*, that do not have equivalents in non-driven systems [10, 12, 40, 41]. It is therefore necessary to gain a better understanding for topological structure of periodically driven systems. This better understanding will be helpful for gaining a deeper theoretical insight into topological phenomena in single-particle quantum systems. But also, more importantly, it is a powerful tool for identifying materials and devising driving schemes that can result in topologically protected edge modes.

In this chapter, we present the main idea of this thesis, namely that there is a relationship between topologically protected degeneracies of the time-evolution operator and the edge mode spectrum of the Floquet operator in a finite geometry. We first show that by diagonalizing Bloch space time-evolution operator of a driven system, it is possible to represent it by a time-dependent band structure, analogous to the energy band structure of a non-driven system. We then demonstrate that, for a 2-dimensional system, there are cases where the time-evolution operator can have topologically protected degeneracies in its band structure, analogous to Weyl nodes in a 3D topological semi-metal [17]. These degeneracies can in some cases prevent us from continuously deforming the time-evolution operator of a driven system into that of a non-driven system. Hence they must play a role for the topological properties of a periodically driven system.

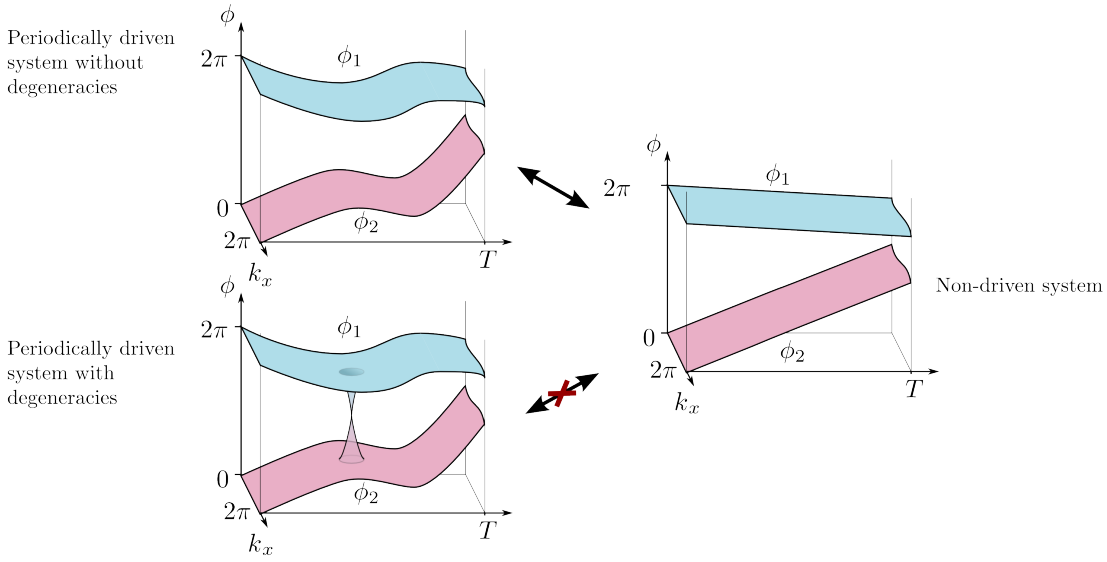

Figure 4.1: A periodically driven system whose time-evolution operator has no degeneracies is topologically equivalent to at non-driven system: it can always be continuously deformed into a non-driven system without closing any quasi-energy gap or breaking the continuity of the time-evolution operator. If the time-evolution operator of the system *has* degeneracies, such a deformation can in general not be done. Periodically driven systems of this type are therefore topologically distinct from non-driven systems. These types of systems can have anomalous edge modes in finite geometry.

We finally show that there indeed is a direct and simple relationship between the topological singularities and the winding number invariant [10] that determines the edge-mode spectrum of a 2D driven system.

In Ref. [12], it was mentioned that there was a connection between the topological properties of periodically driven systems and the continuous evolution of the eigenvalues of the time-evolution operator. This idea will now be generalized and its consequences examined in more detail.

4.1 Band-structure picture of the time-evolution operator

In this section we will present a new principle for finding topological invariants of periodically driven systems, analogous to the band-flattening procedure used for non-driven systems. The core idea is that degeneracies of the time-evolution operator play an important role for the topological properties of periodically driven systems. In the second half of the section we will show that these degeneracies are closely related with the appearance of anomalous edge-mode phenomena.

The systems we consider are periodically driven, meaning they are subject to a Hamiltonian that depends periodically on time, with driving period T. For our purpose, it is no longer convenient to use the Hamiltonian to describe such systems. We will instead work with the

time-evolution operator $U(t)$ of the system that contains the same amount of information as the Hamiltonian. We will furthermore work in Bloch space such that the time evolution operator $U(\mathbf{k}, t)$ depends on crystal momentum as well as time. The locality and the boundedness of the Hamiltonian then translates to $U(\mathbf{k}, t)$ being continuous in both momentum and time. Our starting point is to note that we can write $U(\mathbf{k}, t)$ in the diagonal form

$$U(\mathbf{k}, t) = \sum_{n=1}^{d} P_n(\mathbf{k}, t) e^{-i\phi_n(\mathbf{k},t)}, \tag{4.1}$$

where $P_n(\mathbf{k}, t)$ is the projector into the n'th eigenstate of $U(\mathbf{k}, t)$ and $e^{-i\phi_n(\mathbf{k},t)}$ is the corresponding eigenvalue, given some arbitrary labelling of eigenstates. We take the real functions $\phi_n(\mathbf{k}, t)$ to take values zero at the beginning of the driving and be continuous in $\mathbf{k}$ and t, although not necessarily differentiable. Furthermore, they can always be chosen to never cross, such that if it holds for one point in $\mathbf{k}, t$-space that $\phi_n(\mathbf{k}, t) \geq \phi_m(\mathbf{k}, t)$, it holds everywhere $\mathbf{k}, t$-space. With this choice, the continuous functions $\{\phi_n(\mathbf{k}, t)\}$ are uniquely determined for any system, and they can grow to take any value on the real line. We will refer to the functions $\{\phi_n(\mathbf{k}, t)\}$ as the phase bands (not to be confused with the topological phase of a system). The phase bands of the time-evolution operator define a band structure for a periodically driven system, analogous to the energy bands of a non-driven system. In contrast to the energy bands, the phase bands of a driven system depend on time as well as crystal momentum. At $t = 0$, the phase bands all take value zero, and at $t = T$, they give the quasi-energy bands of the system. An example of a phase-band structure is shown on Fig. 4.1. The periodic nature of the phases $\{\phi_n(\mathbf{k}, t)\}$ means that there should be copies of the two depicted bands above and below the depicted bands. For compactness we only show the one copy of each phase band.

We want to find the edge-mode spectrum of the Floquet operator $U(\mathbf{k}, T)$ associated with this system. To begin, we consider the case of a two dimensional system with no symmetries beyond those of the lattice. While this situation was studied previously in ref. [10], here we use a different approach which will naturally generalize to other symmetry classes. In the subsequent sections, we will then generalize the results of this section to systems with additional symmetries. For static systems, the topological nature of the edge modes allows us to perform a band flattening procedure. A continuous deformation of the eigenvalues of the Hamiltonian will not change the number of edge modes in any gap, as long as no bulk gap is closed and the Hamiltonian stays continuous in momentum. As was noted in ref. [10], the edge-mode spectrum of the Floquet operator is also topologically protected, meaning number of chiral edge modes will be invariant under any continuous transformation of the system that preserves locality and keeps every quasi-energy gap open. For periodically driven systems, we can thus develop a procedure similar to band-flattening, where we continuously deform the time-evolution operator through its eigenvalues without changing its edge-mode spectrum. The only requirements are that we keep the time-evolution operator continuous in momentum and time, and no quasi-energy gap is closed during the deformation. Such a deformation can be implemented by continuously deforming the functions $\phi_n(\mathbf{k}, t)$ in a way that keeps their initial and final values constant. The only other constraint on the deformation lies in regions where the band projectors $\hat{P}_n(\mathbf{k}, t)$ are not continuously defined. This can only happen where two bands are degenerate, and we can thus in general *not* lift degeneracies of the time-evolution operator without breaking locality.

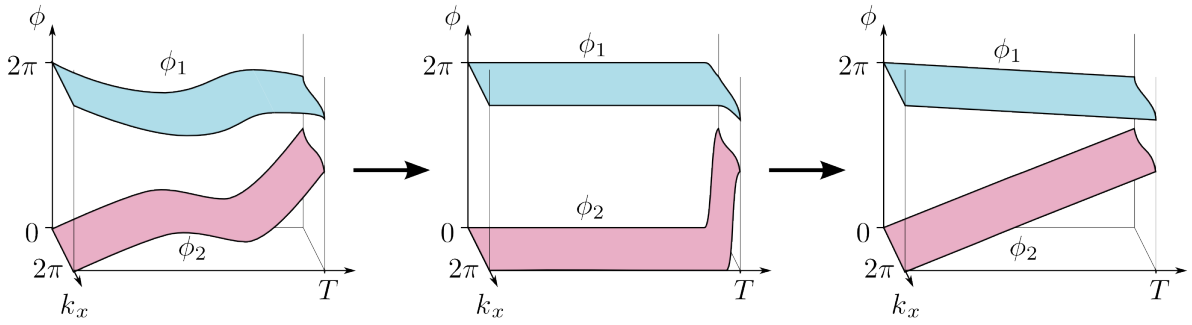

Figure 4.2: Graphical depiction of the deformation described in sec. 4.1, where the time-evolution operator of a periodically driven system is deformed into the time-evolution operator of a non-driven system. This deformation is always possible if the time-evolution operator has no degeneracies.

Naively, one might expect a generic time-evolution operator of a periodically driven system to have no degeneracies. If this were true, we would always be able to deform our system into a non-driven system using our band-flattening procedure: for any n simply deform $\phi_n(\mathbf{k}, t)$ to zero everywhere until a small time-interval δt before T, after which we let it grow linearly to its final value. If this interval is small enough we can assume that $P_n(\mathbf{k}, t) = P_n(\mathbf{k}, T)$ here. After this deformation is done, we then let $\delta t \to T$. The deformed system is now non-driven and described by the Hamiltonian

$$h(\mathbf{k}) = \frac{1}{T} \sum_n \phi_n(\mathbf{k}, T) P_n(\mathbf{k}, T). \tag{4.2}$$

We note that this is an effective Hamiltonian of the system. Since the quasi-energy spectrum has been kept constant, and the time-evolution operator stayed continuous, the edge-mode spectrum has not changed during the deformation. If the edge-mode spectrum depends on some symmetry being present a similar deformation to non-driven systems could be performed without breaking the symmetry, as long as no degeneracies are present. We will demonstrate this in the following sections. When the deformation is done, any topological invariant could then be calculated by simply analysing the resulting non-driven system, and we would thus have a general prescription for finding topological invariants of periodically driven systems. A consequence of a nondegenerate time-evolution operator would also be that we would have no anomalous edge modes: the edge-mode spectrum of a system with a nondegenerate time-evolution operator can always be found in a non-driven system with the same bulk Floquet operator (4.2). By definition, this excludes the possibility of anomalous edge modes. This result indicates that degeneracies of the time-evolution operator *are* a generic feature in periodically driven systems, as anomalous edge modes have been identified in several models [10, 40]. We will now demonstrate how such a degeneracy can appear: consider a 2d non-driven two-level system, with flattened bands 1 and 2 that have opposite and nonzero Chern numbers. The phase bands of the time-evolution operator will look like Fig. 4.3a. The time evolution operator of the system will have a degeneracy at any time t_0 for which $\varepsilon_1 t_0 \equiv \varepsilon_2 t_0 \mod 2\pi$, ε_i being the energy of band i. We now try to lift this degeneracy by adding

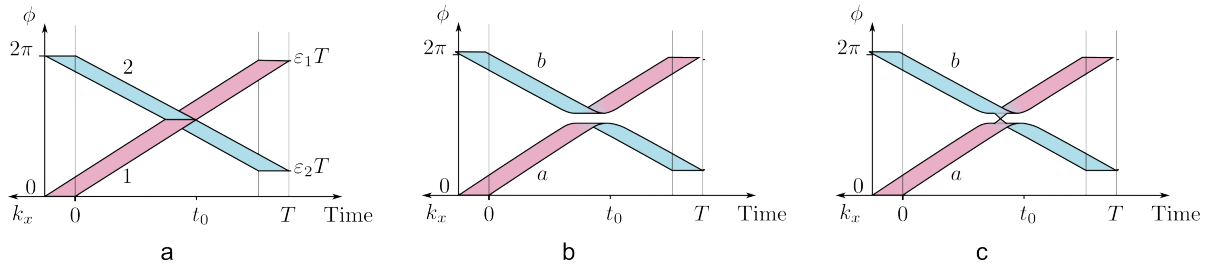

Figure 4.3: a) the phase band-structure of a 2-band non-driven system whose Hamiltonian has flattened band, plotted as a function of k_x for some fixed value of k_y. b) Our naive expectation of the phase band structure after some small time-dependent perturbation has been applied near t_0. c) the actual phase-band structure if band 1 and 2 have different Chern numbers.

a time-dependent perturbation $V(\mathbf{k}, t)$ to the Hamiltonian such that $P_1(\mathbf{k})V(\mathbf{k}, t_0)P_2(\mathbf{k}) \neq 0$. We would then naively expect a gap to open, separating two new hybridized bands a and b, as on Fig. 4.3b. The corresponding eigenstate projectors $P_a(\mathbf{k}, t)$ and $P_b(\mathbf{k}, t)$ must then be continuous in $\mathbf{k}$ and t. Since the perturbation only changed the time-evolution operator near, $t = t_0$ we must have $P_a(\mathbf{k}, t_1) = P_1(\mathbf{k})$, and $P_a(\mathbf{k}, t_2) = P_2(\mathbf{k})$ for times $t_1 \ll t_0 \ll t_2$ (see again Fig. 4.3b). But this must mean that the Chern number of band a changes between t_1 and t_2, and our assumption that $P_a(\mathbf{k}, t)$ was continuous must be wrong. There must then be at least one point in this region of $\mathbf{k}, t$-space where U is degenerate and $P_a(\mathbf{k}, t)$ discontinuous.

We will refer to such a point as a *topological singularity*. A topological singularity is a topologically protected degeneracy of the time-evolution operator at which the degenerate band projectors have a discontinuity. We claim that we can reduce any region where the time-evolution operator is degenerate to a cluster of topological singularities. Topological singularities are closely related to the appearance of anomalous edge-mode phenomena: Their presence prevents us from deforming the system into a non-driven system, thus allowing for the system to exhibit anomalous edge-mode phenomena. Examples of such phenomena are the anomalous edge states found in ref. [10], or the $\omega/2$-quasi-energy modes in a particle-hole symmetric system, found in ref. [12]. As we will demonstrate in this thesis, these anomalous phenomena are all the consequence of topological singularities appearing in the system.

4.2 Relationship between topological singularities and the edge-mode spectrum in two dimensions

In this section we will explicitly show how topological singularities determine the topological properties of 2D systems, in the case without additional symmetries beyond those of the lattice. By using the band-flattening procedure presented in the previous section, we find that the winding number invariant found in Ref. [10] has a simple expression in terms of its Floquet eigenstates and topological singularities, and that there is a direct relation between topological singularities and anomalous edge modes. Before we begin on this, we will first give a more precise definition

of a topological singularity.

4.2.1 Topological singularities in two-dimensional systems

Let $U(\mathbf{k}, t)$ be the bulk time-evolution operator of a two-dimensional system with no other symmetries than discrete translational symmetry. Consider now a point $\mathbf{r}_0 = (\mathbf{k}_0, t_0)$ in $\mathbf{k}, t$-space where the eigenvalues of two bands of U coincide. The two bands are spanned by some basis states $|\psi_1\rangle$ and $|\psi_2\rangle$. The continuity of U means we can assume that the subspace spanned by the two degenerate bands can be assumed constant within some finite-size neighbourhood around $\mathbf{r}_0$ in $\mathbf{k}, t$-space . The remaining non-degenerate bands $\{|\chi_n\rangle\}$ and their associated phases $\{\phi_n\}$ can also be assumed to be constant within this neighbourhood. Close to $\mathbf{r}_0$, the time-evolution operator thus takes the form

$$U(\mathbf{k}, t) = \sum_n |\chi_n\rangle\langle\chi_n| e^{-i\phi_n} + \sum_{a,b=1}^{2} |\psi_a\rangle\langle\psi_b| M_{ab}(\mathbf{k}, t), \tag{4.3}$$

where M is a 2×2 unitary matrix. The fact that M is $U(2)$ means that we can write it as

$$M(\mathbf{r}) = \exp\left[-i\phi_d(\mathbf{r}) - i f_j(\mathbf{r})\sigma_j\right]$$

where summation over repeated indices is used. Here $\phi_d(\mathbf{r})$ is a real function, whose value at $\mathbf{r}_0$ gives the eigenvalue of the two bands that are degenerate here, $\{\sigma_j\}$ are the Pauli matrices, and $\{f_j(\mathbf{r})\}$ are real continuous functions that satisfy $f_i(\mathbf{r}_0) = 0$. We assume that U, and thereby f, is differentiable in some neighbourhood around $\mathbf{r}_0$ such that we can expand f_j around $\mathbf{r}_0$. When we take the neighbourhood small enough we only have to keep the term with lowest order in $(\mathbf{r} - \mathbf{r}_0)$. Since $f_j(\mathbf{r}_0) = 0$, this is the first order term, and M can thus be written

$$M(\mathbf{r}) = \exp\left[-i\phi_d(\mathbf{r}) - i(\mathbf{r} - \mathbf{r}_0)_j S_{jk}\sigma_k\right], \tag{4.4}$$

where $S_{jk} = \partial_j f_k(\mathbf{r}_0)$ is a real 3×3 matrix. The case where the first order term is also zero will be covered shortly.

Let us consider the case where the matrix S has rank 3 such that all three Pauli matrices come into play in the neighbourhood around $\mathbf{r}_0$. In this case, the degeneracy is topologically protected, similarly to the case of a Weyl node [17]: an infinitesimal change of the time-evolution operator can never lift the degeneracy, but rather can only infinitesimally change the location where it appears. The degeneracy can thus not be lifted with a continuous deformation of the system, and is therefore topologically protected. In this way, we define a topological singularity of a two-dimensional system to be a a degeneracy of the time-evolution operator, where the matrix S is invertible. For a topological singularity, the degeneracy will only occur at a single point $\mathbf{r}_0$.

We may also find cases where S is not invertible. This occurs when two bands are degenerate along some line, surface, or 3-dimensional region in $\mathbf{k}, t$-space, such that $\mathbf{r}_0$ is a point on this manifold. The rank of S will then be $3 - D$, where D is the dimension of the manifold. In this case, the degeneracy is not topologically protected: we can completely lift it in the entire neighbourhood where $|\psi_{1,2}\rangle$ are constant, by turning on an infinitesimally small term orthogonal to the image of S in Eq. (4.4). We can only do this in one small neighbourhood at a time

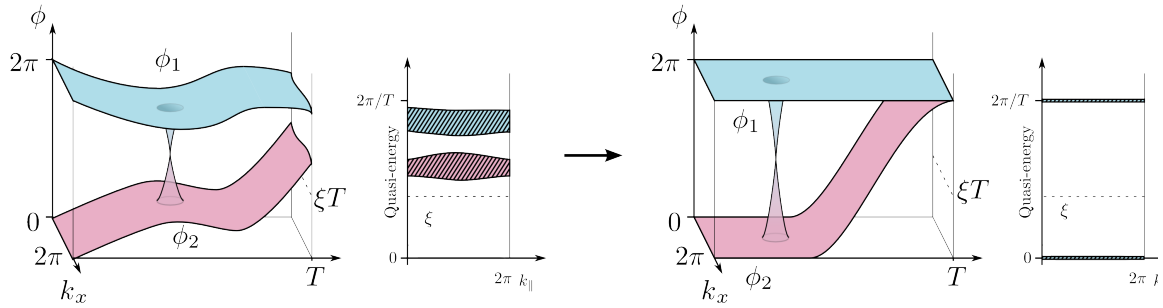

Figure 4.4: Deformation of U to U_ξ

however. If one tries to lift the degeneracy over the entire manifold, two cases are possible: either the degeneracy can be lifted everywhere, or there will be a discrete set of points where topological degeneracies remain. Hence, if the time-evolution operator is degenerate along some finite-dimensional manifold, one can always apply an infinitesimal deformation to the system that either completely lifts the degeneracy, or reduces it to a cluster of topological singularities.

With the definition of a topological singularity in place, we now associate two indices with each singularity that play important roles for the topological properties of the system. These two indices we call the vorticity σ and the branch index ν, which we define as

$$\sigma = \mathrm{sgn}|S|, \quad \nu = |\phi_a(\mathbf{r}_0) - \phi_b(\mathbf{r}_0)|/2\pi, \tag{4.5}$$

where bands a and b are the two bands that become degenerate at the singularity. Note that ν can be non-zero since we defined the bands ϕ_a and ϕ_b by analytic continuation in time from $\phi_{a,b}(\mathbf{k}, 0) = 0$. The two ν and σ are topologically protected, and we define $q \equiv \nu\sigma$ as the charge of the singularity. The total charge of all topological singularities in a system is conserved under any continuous deformation of the system that keeps at least one quasi-energy gap open.

As mentioned in the previous section, there is a relationship between the Chern numbers of the bands of the time-evolution operators and the topological singularities. To be precise, consider a topological singularity where two bands meet. The Chern numbers of the two bands change discontinuously here with time: The Chern number of the band whose phase has a minimum at the singularity changes by σ at the singularity, while the Chern number of the other band changes by $-\sigma$.

4.2.2 Winding number of a two-dimensional system

Having seen how topological singularities appear in a 2-dimensional system, we now investigate their relationship with the edge-mode spectrum of the system in a finite geometry. We want to calculate the number of edge-modes of this system in a quasi-energy gap at quasi-energy ξ, $n_{\mathrm{edge}}(\xi)$. This number can be calculated using the bulk-edge correspondence that was found in ref. [10]. In order to calculate $n_{\mathrm{edge}}(\xi)$, the first step is to deform the time-evolution operator U into a time-periodic time-evolution operator U_ξ such that $U_\xi(T) = 1$. This deformation should be done continuously without ever closing the quasi-energy gap at ξ. The number of edge modes

can then be found by $n_{\text{edge}}(\xi) = W[U_\xi]$, where

$$W[U_\xi] = -\frac{1}{8\pi^2}\int \mathrm{d}^2k dt \mathrm{Tr}\left[U_\xi^\dagger \partial_t U_\xi \cdot U_\xi^\dagger \partial_{k_x} U_\xi \cdot U_\xi^\dagger \partial_{k_y} U_\xi\right] - x \leftrightarrow y. \tag{4.6}$$

We will refer to $W[U_\xi]$ as the winding number of U_ξ. As was noted in ref. [16], a convenient choice for U_ξ is $U(\mathbf{k},t)e^{iH_{\text{eff}}^\xi(\mathbf{k})t}$. Here $H_{\text{eff}}^\xi = i\log U(\mathbf{k},T)/T$, where the logarithm is defined with branch radially from 0 through $e^{-i\xi T}$. In other words, H_{eff}^ξ is the unique effective Hamiltonian of the system with eigenvalues in the interval $[\xi, \xi+\omega)$. With this choice of U_ξ, the eigenstates of $U_\xi(\mathbf{k},t)$ will coincide with the eigenstates of $U(\mathbf{k},t)$ as t approaches T, and the phases $\phi_n^\xi(\mathbf{k},T)$ of $U_\xi(\mathbf{k},T)$ will satisfy

$$\phi_n^\xi(\mathbf{k},T) = 2\pi w_n^\xi, \tag{4.7}$$

where w_n^ξ is the net number of times $e^{-i\phi_n(\mathbf{k},t)}$ crosses $e^{-i\xi T}$ during the driving cycle. We will refer to w_n^ξ as the phase winding number of band n. If ξ lies in a quasi-energy gap, w_n^ξ will be the same for all $\mathbf{k}$, due to the $\mathbf{k}$-continuity of ϕ_n, which is why we haven't indicated at $\mathbf{k}$-dependence.

With the choice of U_ξ given above, we will now find a new expression for the winding number of U_ξ in terms of the phase winding numbers and the charges of the topological singularities. This will be done by using the band-flattening procedure on the deformed time-evolution operator U_ξ. We will first consider two special cases, then discuss the general situation.

Winding number in case of no singularities

Let us first consider the case where $U_\xi(\mathbf{k},t)$ has no topological singularities. We can then continuously deform the time-evolution operator U_ξ into that of a non-driven system without changing $W[U_\xi]$, in the way we described in Sec. 4.1. In this case, $W[U_\xi]$ is simply the winding number of the non-driven system described by the Hamiltonian $\tilde{H}_\xi(\mathbf{k}) = \sum_n P_n(\mathbf{k},T)2\pi w_n^\xi/T$, where P_n is the projector into the n'th eigenstate of $U(\mathbf{k},T)$. The Floquet operator $\tilde{U}_\xi(T)$ of this non-driven system has net number of edge modes $W[\tilde{U}_\xi] = \sum_n (w_{\max}^\xi - w_n^\xi)\mathcal{C}_n$, where $w_{\max}^\xi$ is the maximum phase winding number of the system, and $\mathcal{C}_n$ is the Chern number of the n'th band of $\tilde{H}$. With our choice of U_ξ, hte n'th eigenstate of $\tilde{H}_\xi(\mathbf{k})$ is the same as the n'th eigenstate of $U(\mathbf{k},T)$. Using the fact that $\sum_n \mathcal{C}_n = 0$, we thus find

$$W[U_\xi] = -\sum_n C_n w_n^\xi, \tag{4.8}$$

where C_n is the Chern number of the n'th band of $U(\mathbf{k},T)$. In other words, if no singularities are present, the winding number of U_ξ is simply the sum of Chern numbers of the Floquet bands weighted by their phase winding number. For a non-driven system, w_n will be zero if band n is below the energy gap and 1 if band n is above. In the non-driven case, the above result thus reduces to the well-known bulk-boundary correspondence for the Chern insulator [26] (see Sec. 2.2.1). This follows from the fact that the Chern numbers of all bands sum to zero.

Winding number in case of one singularity

Let us now consider the case where all the phase winding numbers are zero and $U_\xi(\mathbf{k},t)$ has only one singularity, located at $\mathbf{r}_0 = (\mathbf{k}_0, t_0)$. In this case we can deform the phases to zero

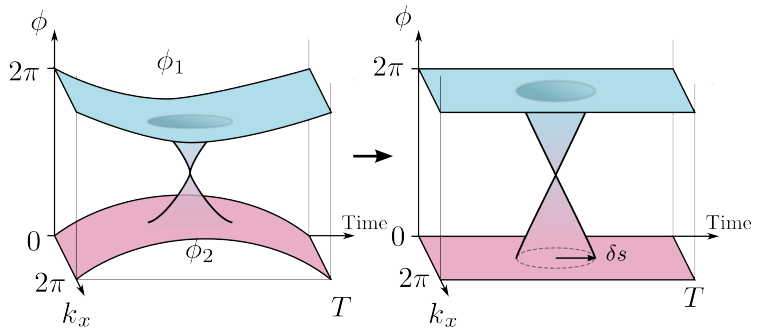

Figure 4.5: Deformation of an isolated singularity

everywhere, except in some arbitrarily small neighbourhood that contains the singularity. Under this deformation we keep the eigenstates of $U_\xi(\mathbf{r})$ constant, and keep the time-evolution operator fixed at the singularity. The deformed time-evolution operator is the identity everywhere, except in the small region of radius δs around the singularity (see fig. 4.5). If we choose δs small enough, the time-evolution operator is then of the form (4.3) within the neighbourhood, since the eigenstates of U_ξ have not changed under the deformation:

$$\tilde{U}_\xi(\mathbf{r}) = \sum_n |\chi_n\rangle\langle\chi_n| + \sum_{a,b=1,2} |\psi_a\rangle\langle\psi_b| M_{ab}(\mathbf{r}), \tag{4.9}$$

where $M_{ab}(\mathbf{r})$ is a 2×2 matrix whose eigenvectors are the eigenvectors of $S_{jk}(\mathbf{r}-\mathbf{r}_0)\sigma_k$. Since $\tilde{U}(\mathbf{r})$ should become the identity at the boundary of the neighbourhood, we know that the logarithm of the eigenvalues of M must grow from 0 at the boundary to $-i\phi_d(\mathbf{r}_0)$ and $-i\phi_d(\mathbf{r}_0) - 2\pi i\nu$ at $\mathbf{r}_0$. for $|\mathbf{r}-\mathbf{r}_0| < \delta s$, M thus takes the form

$$M(\mathbf{r}) = v_a^1(\mathbf{r}) v_b^{1*}(\mathbf{r}) e^{i\phi_d(|\mathbf{r}-\mathbf{r}_0|/\delta s - 1)} + v_a^2(\mathbf{r}) v_b^{2*}(\mathbf{r}) e^{i(\phi_d + 2\pi\nu)(|\mathbf{r}-\mathbf{r}_0|/\delta s - 1)} \tag{4.10}$$

while for $|\mathbf{r}-\mathbf{r}_0| > \delta$, M is given by the identity. The vectors $v^1(\mathbf{r})$ and $v^2(\mathbf{r})$ are the eigenvectors of the matrix $S_{jk}(\mathbf{r}-\mathbf{r}_0)\sigma_k$. S is a real, symmetric invertible matrix and can thus be written $S = R_1 \Lambda R_2$, where R_1 and R_2 are orthogonal and Λ is diagonal matrix with positive entries [42]. A continuous deformation of the entries of Λ to 1 results in a orthogonality-preserving continuous interpolation of the eigenvectors $v^1(\mathbf{r})$ and $v^2(\mathbf{r})$ to the eigenvectors of $R_{jk}(\mathbf{r}-\mathbf{r}_0)_j\sigma_k$, where $R = R_1 R_2$. By continuously deforming the vectors v^1 and v^2 in this way, we deform M into

$$M(\mathbf{r}) = \begin{cases} 1, & |\mathbf{r}-\mathbf{r}_0| > \delta s \\ (-1)^\nu \exp\left[\frac{-i\pi\nu}{\delta s}(\mathbf{r}-\mathbf{r}_0)_i R_{ij}\sigma_j \cdot\right], & |\mathbf{r}-\mathbf{r}_0| < \delta s \end{cases}. \tag{4.11}$$

This deformation could be done continuously without breaking continuity at any time. We recall that R is orthogonal and its determinant is the vorticity $\sigma = |R_1||R_2| = \mathrm{sgn}|S|$ of the singularity (see eq. (4.5)). From Eq. 4.6, we explicitly calculate the winding number of this time-evolution operator and find that

$$W[\tilde{U}_\xi] = -\nu|R| = -\nu\sigma \equiv -q. \tag{4.12}$$

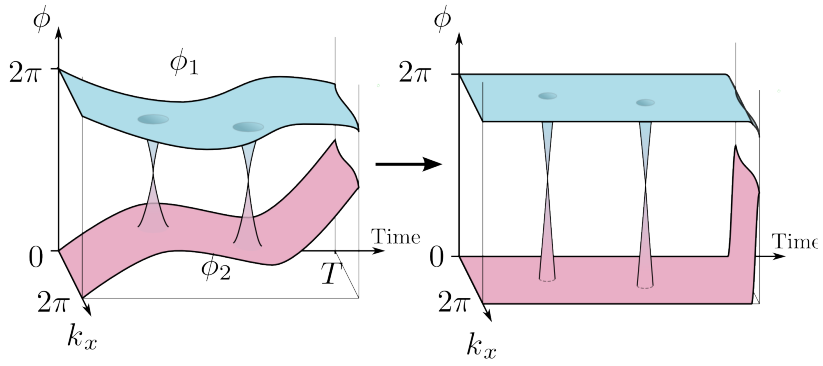

Figure 4.6: Deformation scheme for general case

This calculation is given in appendix B.1. Using $W[U_\xi] = W[\tilde{U}_\xi]$, we thus have

$$W[U_\xi] = -q. \tag{4.13}$$

In other words, if U_ξ contains one isolated singularity, the winding number of U_ξ is given by the corresponding charge of the singularity. This is one of the key results of this work.

The general case

We are now ready to put the pieces together. Consider the general case, where U_ξ has N singularities with charges $\{q_i^\xi\}$, and phase winding numbers $\{w_n^\xi\}$. In order to find the winding number of this system, we deform $U_\xi(\mathbf{k}, t)$ in the following way: we keep the band projectors fixed, but deform $\phi_n^\xi(\mathbf{k}, t)$ to zero everywhere, except for small isolated regions that surround each topological singularity, as well as a small time-interval δt before T, where we let the phases wind linearly to their final values.

We then calculate the winding number of this band-flattened time-evolution operator. The winding number, Eq. (4.6), can expressed as an integral over $\mathbf{k}, t$-space of the curvature function $F_\xi(\mathbf{k}, t) = \frac{1}{8\pi^2}\mathrm{Tr}[U_\xi^\dagger \partial_t U_\xi \cdot U_\xi^\dagger \partial_{k_x} U_\xi \cdot U_\xi^\dagger \partial_{k_y} U_\xi] - x \leftrightarrow y$. For the band-flattened system, F is only nonzero in the regions that surround the singularities and in the small time-interval before T. We can therefore split up the integral of F into a sum of integrals over each of these nontrivial regions. From the first special case we examined, we know that the integral of $F_\xi(\mathbf{k}, t)$ over the region at the time-interval before T equals $\sum_n \mathcal{C}_n w_n^\xi$, where $\mathcal{C}_n$ are the Chern numbers of the Floquet bands, and w_n^ξ are their phase winding numbers. From the second special case, we know that the integral of $F_\xi(\mathbf{k}, t)$ over a region surrounding a topological singularity equals the charge q of the singularity. When we sum the integrals over all regions together we then obtain

$$W[U_\xi] = -\sum_n \mathcal{C}_n w_n^\xi + \sum_{i=1}^{N} q_i^\xi, \tag{4.14}$$

where $\mathcal{C}_n$ is the Chern number of the n'th band of $U(\mathbf{k}, T)$. Now, since U_ξ can be continuously deformed into U without closing the quasi-energy gap, we know from the result in the end of

subsection 4.2.1 that $\sum_i q_i^\xi = \sum_i q_i$, where $\{q_i\}$ are the singularity-charges of the $U(\mathbf{k}, t)$. We finally have the following result for the number of edge-modes in a two-dimensional system:

$$n_{\text{edge}}(\xi) = -\sum_n \mathcal{C}_n w_n^\xi + \sum_i q_i \tag{4.15}$$

This simple expression provides a direct way of evaluating the edge mode count given by the winding number formula found in Ref. [10]. In Ref. [10], it was noted that the number of edge modes of a 2D periodically driven system is determined by its full time-evolution, and not just by the Chern numbers of the Floquet eigenstates. We now see that this information is in fact contained in the topological singularities of the time-evolution operator.

As discussed in Sec. 4.1, topological singularities are what makes a Floquet system topologically inequivalent to a non-driven system - they prevents us from deforming the former into the latter. This inequivalence is reflected by the appearance of anomalous edge modes in periodically driven systems: due to the existence of topological singularities, a system can have chiral edge modes even though the Chern numbers of all the Floquet bands are zero.

4.2.3 Topological singularities in a specific 2-band model

In this subsection we will demonstrate the method we have described on the model that was considered in ref. [10]. The model we will examine is a tight-binding model on a 2D bipartite square lattice, described by the time-dependent Bloch Hamiltonian

$$H(\mathbf{k}, t) = \sum_{n=1}^{4} J_n(t) \left(\sigma^+ e^{i\mathbf{b}_n \cdot \mathbf{k}} + \sigma^- e^{-i\mathbf{b}_n \cdot \mathbf{k}} \right) + V\sigma_z, \tag{4.16}$$

where σ_z and $\sigma^\pm = (\sigma_x \pm i\sigma_y)/2$ are the Pauli-matrices acting on the sublattice, and the vectors $\{\mathbf{b}_n\}$ are given by $\mathbf{b}_1 = -\mathbf{b}_3 = (a, 0)$, and $\mathbf{b}_2 = -\mathbf{b}_4 = (0, a)$, with a being the lattice constant. The Hamiltonian is T-periodic in time, and one driving cycle consists of 5 time intervals of length $T/5$, where in the n'th interval $J_n(t) = \lambda_n$ while all the other hopping amplitudes are set to zero. In the 5th interval, all hopping amplitudes are set to zero.

We now re-evaluate the edge modes of this model in terms of topological singularities. In Ref. [10], the model above was examined in the case where all hopping amplitudes were equal such that $\lambda_n = J$ for some tunable parameter J . In that case anomalous edge modes were observed in certain parameter ranges when the system was put in a strip geometry. Based on the findings of the previous section, this implies that topological singularities are present. Indeed, when this model is in a nontrivial phase, the time-evolution operator exhibits a degeneracy in the second segment of the driving along the entire line $k_x = k_y$.

In order to see whether this degenerate region contains topological singularities, we add a small time-dependent perturbation to the system, such that the degeneracy will only occur at isolated points, if anywhere (see section 4.2.1). We do this by reducing the hopping in the y-direction slightly compared to the x-direction, such that $\lambda_1 = \lambda_3 = J$ and $\lambda_2 = \lambda_4 = (1 - \alpha)J$ for some small parameter α that can be regarded as a perturbation. Starting from fixed values of J and V, we expect the system to stay in the same topological phase when α is increased from 0. We then take $V = 0.8\pi/T$, and numerically calculate time-evolution operator at a representative set of

points in $(\mathbf{k}, t)$-space for the parameter choices $J = -0.5\pi/T$, $J = -1.2\pi/T$, and $J = -2.5\pi/T$ (see Fig. 4.7. From diagonalization of the time-evolution operator we obtain the phase band structures of these models.

Now we examine the band structure of the time-evolution operator for three illustrative cases. For $J = -0.5\pi/T$, we find that the time-evolution operator has no degeneracies anywhere in $\mathbf{k}, t$-space, and this system is thus topologically equivalent to a non-driven system. On Fig. 4.7a is plotted the phase band-structure for this model at a fixed value of k_x. In the two latter cases, however, we find that there is exactly one point where bands beginning at different branches coincide. We recognize this as a topological singularity. For $J = -1.2\pi/T$, the singularity appears at $(k_x a, k_y a, t/T) = (0.0, 0.0, 0.7)$, and for $J = -2.5\pi/T$, the singularity appears at $(k_x a, k_y a, t/T) = (0.5\pi, 0.5\pi, 0.4)$. These locations are found numerically. For $J = -2.5\pi/T$, the time-evolution operator also has another singularity where two phase bands that coincide at $t = 0$ become degenerate. This singularity carries zero charge, and hence we ignore it. In Figs. 4.7 b,c, we show the band structure of U as a function of k_y and t, with k_x held fixed at the value corresponding to the singularity.

Having examined the band-structure of the bulk time-evolution operator, we then numerically compute the Floquet operator of the systems in a strip geometry, and obtain the quasi-energy band structures, shown in Figs. 4.7 d-f. When we compare the band structure of U with the quasi-energy bands in strip geometry, we see a direct connection between the appearance of topological singularities and the chiral edge modes of the Floquet operator. For $J = -0.5\pi/T$, there are no singularities, and the Floquet bands have Chern numbers zero. Hence the Floquet operator should have no edge modes. When we turn the hopping amplitude up to $J = -1.5\pi/T$, the time-evolution operator acquires a topological singularity that connects bands from neighbouring branches. The net topological singularity charge is now nonzero, and there will be one pair of edge modes in the quasi-energy gap at π/T. There will be no edge modes in the gap at quasi-energy 0, since the Floquet bands have acquired nonzero Chern numbers. In this gap they cancel out the contribution from the singularity (see Eq. (4.15)). Finally, when we turn the hopping amplitude up to $-2.5\pi/T$, the bands of U will eventually meet in a singularity at a quasi-energy 0 and the Chern numbers of the Floquet bands become zero again. However, the singularity at quasi-energy π still remains, and there will thus be an edge mode in each quasi-energy gap of the system (see again Eq. (4.15). Through the analysis of this explicit model, we have thus demonstrated the connection between topological singularities and (anomalous) edge modes.

4.3 Complete topological classification of periodically driven systems in 2d

By deforming the time-evolution operator into the form depicted on Fig. 4.6, we see that topological singularities and non-zero phase winding numbers are the only features that prevent us from deforming the time-evolution operator into the identity. By considering how we can change the location of singularities in $\mathbf{k}, t$-space through continuous deformations, it is possible to show that there exist only two independent topological invariants one can define for a periodically driven system in two dimensions in the absence of symmetries. The first is the winding number $W_\xi[U]$, discussed in the above section. The second invariant quantity is the the sum of phase winding

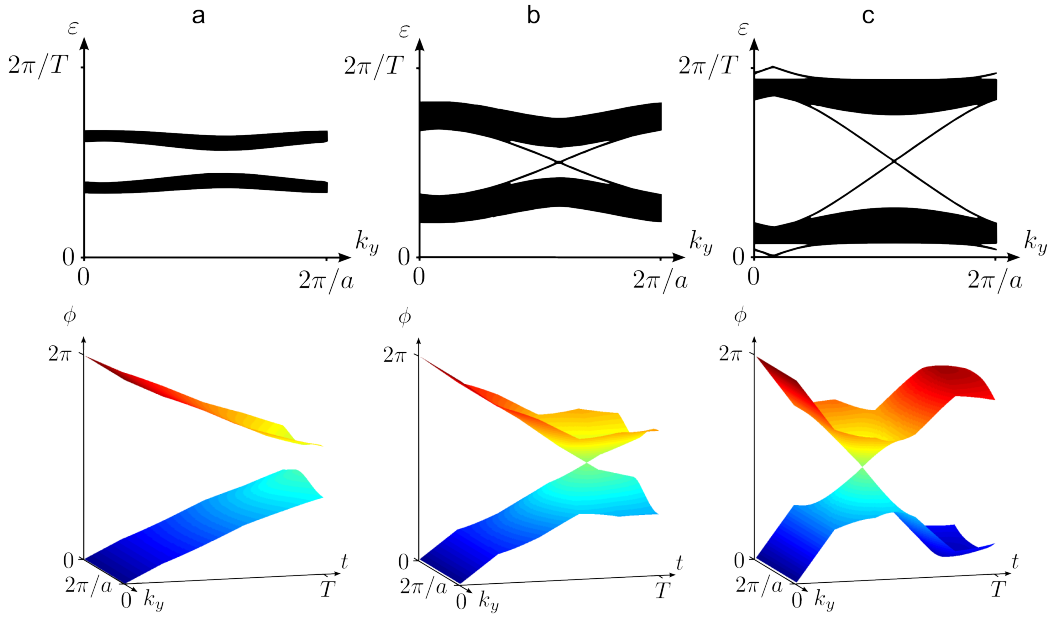

Figure 4.7: Relationship between the band structure of the time-evolution operator and edge modes of the finite-geometry Floquet operator. For various values of the hopping amplitude J, we plot the band structure of the time-evolution operator of the model (4.16) (bottom). For each value of J, we plot the band-structure at a fixed value of k_x. At a) we plot for $J = 0.5\pi/T$ at $k_x = 0$. At b) $J = 1.2\pi/T$ at $k_x = 0$. At c) $J = 2.5\pi/T$ at $k_x = 0.25$. In the latter two cases, the time-evolution operator has a singularity with nonzero charge, and in these cases we plot the band structure at the exact value of k_x where this singularity appears. Also shown is the quasi-energy band structure in a strip geometry for the respective models (top). Notice the correspondence between the phase bands at $t = T$ in the bottom and the quasi-energy bands in the top.

numbers,

$$z_\xi[U] = \sum_n w_n^\xi = \frac{1}{2\pi}\int_0^T \mathrm{d}t \mathrm{Tr}[U_\xi^\dagger(\mathbf{k},t)\partial_t U_\xi(\mathbf{k},t)] \tag{4.17}$$

This invariant is discussed in more detail in Chapter. 6. In the above, the right hand side is independent of the choice of $\mathbf{k}$. The invariants z_ξ and W_ξ provide an *exhaustive* topological classification of periodically driven systems in two dimensions. Two time-evolution operators can be continuously deformed into each other while keeping a quasi-energy gap ξ open if and only if they have the same winding number W_ξ and phase winding number sum z_ξ in this gap.

Chapter 5

Topological classification of Floquet systems with symmetries

In the previous chapter we used a band-flattening procedure to show that for a 2-dimensional system, the winding number of the time-evolution operator had a simple expression in terms of its singularities. So far this approach has given a new perspective on results found previously by different means. However, the previous approaches provided no clear path to generalization. We now illustrate the power of our new approach by using it to generalize the results and obtain an *exhaustive* topological classification, including symmetries.

When the band-flattening approach is applied to systems with symmetries, it becomes apparent that the time-evolution operator can have new types of degeneracies that are protected from a combination of symmetry and topology. While the topological singularities we discussed in Secs. 4.1 ad 4.2 relied on the system being $2+1$-dimensional, particle-hole conjugation invariant systems in any dimension can for example have protected degeneracies. These prevent us from deforming the time-evolution operator into the identity and we see them as new types of topological singularities. From the new types of topological singularities, new topological invariants can be constructed.

In this section we apply the band-flattening procedure to systems with symmetries. Doing this, it is possible to obtain all invariants of a periodically driven system directly as discrete expressions of the type as in Eq. (4.15). We will use this approach to exhaustively classify periodically driven systems with various types of symmetries, and identify the topological invariants that constitute their bulk-edge correspondences. Proofs of exhaustive classification are in some examples left out for clarity and brevity. We will prove that the obtained invariants constitute the bulk-edge correspondence of the system, however. From the invariants we find, we derive expressions that give them directly in terms of the time-evolution operator. The invariants we obtain coincide with those found in Refs. [12, 13, 16].

In many cases, we find more invariants than in the non-driven case, due to the extra quasi-energy gap present in Floquet systems. For example, with no symmetries there is one extra invariant, namely the winding number for the anomalous gap. For a particle-hole symmetric system there exist two quasi-energies that are invariant under particle-hole conjugation and this results in a "squaring" of the $\mathbb{Z}_2$ invariant. We also encounter a case of a topological

invariant that has no analogy in non-driven systems. A 1-d periodically driven 2-band system with particle-hole symmetry has a $\mathbb{Z}$ topological classification, and thus this system provides example of a periodically driven system that has a different topological classification than its non-driven equivalent, at least from a mathematical point of view.

We will in this chapter also demonstrate other examples of nontrivial topological phenomena that do not have equivalents in non-driven systems. For example, we find that a periodically driven two-band system with time-reversal symmetry can host topologically protected edge-modes, while a minimum of four bands is necessary in the non-driven case.

5.1 Symmetries in periodically driven systems

The symmetries we consider in this paper can all be expressed in terms of conditions on the time-evolution operator. These conditions fall into two categories. First, we consider instantaneous symmetries which can be expressed in the form

$$U(t) = SU(t)S^{-1}, \tag{5.1}$$

where S is a unitary of anti-unitary operator. Second, we consider time-non-local symmetries, which are expressed via conditions on the form

$$U(t) = SU(T-t)U^{\dagger}(T)S^{-1}. \tag{5.2}$$

where S is again some unitary or anti-unitary operator. The symmetry is satisfied if the above holds for some proper choice of time origin. The symmetries of the periodic table of topological insulators [30, 31] can all be expressed in the above forms when applied to the Floquet operator. The instantaneous symmetries include spatial symmetries (where S is unitary) and particle-hole (S anti-unitary) classes, while the non-local symmetry classes include chiral symmetry (S unitary) and time-reversal symmetry (S anti-unitary). Symmetry classes where S is anti-unitary furthermore divide into two subclasses, depending on whether S squares to 1 or -1. If $S^2 = 1$ one can always find a basis where S is the complex conjugation operator. One could also consider other types of symmetries than the above, for example, a discrete time-translational symmetry, combined with some unitary or anti-unitary operator S, but this is beyond the scope of this thesis.

What is common for the above types of symmetries is that they allow us to band-flatten the Floquet operator: it is always possible to continuously deform the system such that the Floquet operator becomes some scalar multiplication operator, while keeping at least one quasi-energy gap open (this can be done since the eigenvalues of the Floquet operator are complex exponentials of the Quasi-energies). For each distinct way the Floquet operator can be deformed into a scalar, it is then potentially possible to define a set of topological invariants associated with the gap that stays open. Given a symmetry and quasi-energy gap ξ, we define a topological invariant as a quantity that does not change under any continuous deformation of the system that keeps the quasi-energy gap open and preserves the symmetry and locality. With this definition, any topological characteristic of the edge-mode spectrum in a bulk gap of the system defines such a topological invariant.

We now demonstrate the implications these various types of symmetries on the crystal momentum and time-dependent evolution operator. In the process we obtain topological invariants for these cases using the approach described in the beginning of this section.

5.2 Classification for particle-hole symmetry with $S^2 = 1$

We first consider the topological classification of a 1-dimensional periodically driven system with particle-hole symmetry (Class D in the AZ classification [29]). This case was also considered in Ref. [12], and here topological invariants consistent with the bulk-edge correspondence were obtained. Particle-hole symmetry for a time-dependent system implies that the Bloch Hamiltonian of the system $h(\mathbf{k}, t)$ satisfies $h(\mathbf{k}, t) = -Sh(-\mathbf{k}, t)S^{-1}$, for some antiunitary operator S. In this section we examine the case where $S^2 = 1$. This type of symmetry is present in Boguliubov-de Gennes Hamiltonians. If $S^2 = 1$, we can always find a basis where S is the complex conjugation operator. In this basis, the symmetry condition is equivalent to the time-evolution operator satisfying $U(\mathbf{k}, t) = U^*(-\mathbf{k}, t)$ at each time t. As a consequence, the bands of $U(\mathbf{k}, t)$ come in pairs related by symmetry, and the time-evolution operator of a particle-hole symmetric system with $2N$ bands can always be written in the form

$$U(\mathbf{k}, t) = \sum_{n=1}^{N} \left[P_n(\mathbf{k}, t) e^{-i\phi_n(\mathbf{k},t)} + P_{\bar{n}}(\mathbf{k}, t) e^{-i\phi_{\bar{n}}(\mathbf{k},t)} \right] \tag{5.3}$$

where we can assume the real functions $\phi_n(\mathbf{k}, t)$ to be continuous and non-crossing, and, in the basis specified above,

$$\begin{aligned} P_{\bar{n}}(\mathbf{k}, t) &= P_n^*(-\mathbf{k}, t), \\ \phi_{\bar{n}}(\mathbf{k}, t) &= -\phi_n(-\mathbf{k}, t) \end{aligned} \tag{5.4}$$

Furthermore, any time-evolution of this form is particle-hole symmetric. In the case where the symmetry operator S squares to -1, the time-evolution operator U takes the same form as in Eqs. (5.3), (5.4), but the conjugate bands n and $\bar{n}$ would not relate each other just by complex conjugation.

Particle-hole symmetry still permits a band-flattening of the time-evolution operator by a deformation of the real functions $\{\phi\}$, and we are allowed to freely deform $\{\phi_n\}$ in any region of $(\mathbf{k}, t)$ space where the eigenstates $\{P_n(\mathbf{k}, t)\}$ are continuously defined. Similar to the case of systems without symmetries, studied in Sec. 4.2, the eigenstates $\{P_n(\mathbf{k}, t)\}$ can have topologically protected discontinuities in $\mathbf{k}, t$-space around which the time-evolution operator cannot be flattened to the identity. In fact, symmetry-protected topological singularities can occur in any dimension for particle-hole symmetric systems when $S^2 = 1$. The singularities appear when two particle-hole conjugate bands of $U(\mathbf{k}, t)$ become degenerate at one of the time-reversal invariant points in $\mathbf{k}$-space. In order to see how the singularity arises, suppose that two conjugate bands of the time-evolution become degenerate at $(\mathbf{k}_0, t_0)$, where $\mathbf{k}_0$ is a point in $(\mathbf{k}, t)$-space that is taken unto itself by an inversion in crystal momentum and time. For t close to t_0, we can then write $U(\mathbf{k}_0, t)$ in the form

$$U(\mathbf{k}_0, t) = \sum_n \left(|\chi_n\rangle\langle\chi_n| e^{-i\phi_n(t)} + |\chi_n^*\rangle\langle\chi_n^*| e^{i\phi_n(t)} \right) + \sum_{a,b=1,2} |\psi_a\rangle\langle\psi_b| M_{ab}(t), \tag{5.5}$$

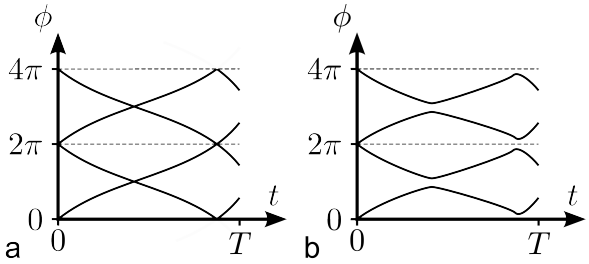

Figure 5.1: a): Evolution of the phases of a generic 2-band system with particle-hole symmetry at a inversion-invariant point in the BZ. At this point in **k**-space the time-evolution operator has one singularity at phase π and one at phase 0. b): the evolution of the phases, at a point in the BZ slightly away from the inversion-invariant point.

where $\{|\chi_n\rangle, |\chi_n^*\rangle\}$ are the eigenstates of $U(\mathbf{k}_0, t_0)$ that do not become degenerate, and $\{|\psi_{1,2}\rangle\}$ are two states that together span the subspace of the degenerate eigenstates. Here $M(t)$ is a continuous 2×2 unitary matrix satisfying $M_{ab}(t_0) = \pm\delta_{ab}$. Now, in the basis where S is the complex conjugation operator, the symmetry (5.4) dictates that $U(\mathbf{k}_0, t)$ must be real for all t. Furthermore, since the two degenerate eigenstates are complex conjugates of each other, we can assume $|\psi_1\rangle, |\psi_2\rangle$ to be real. The first sum in the above expression is also real, so then $M(t)$ must also be real. The latter condition implies that $M(t)$ can be expressed as

$$M(t) = \pm e^{-i\lambda\sigma_y(t-t_0)}, \tag{5.6}$$

where λ is some real number.

From the above, we see that the degeneracy is topologically protected: any local continuous deformation of $U(\mathbf{k}_0, t)$ can only change the value of λ and the the time t_0 where the degeneracy occurs. The topological singularities allow the phases of conjugate bands at the time-reversal invariant points to cross during the time-evolution. At these points in **k**-space, particle-hole symmetry protects this crossing, while elsewhere in **k**-space, the crossing can be avoided by turning on an infinitesimal time-dependent perturbation. See Fig. 5.1. In Ref. [12], a relationship between this winding of phases and the topological classification was mentioned, and we will shortly examine this further.

It is possible to deform the bulk Floquet operator of a particle-hole symmetric system to -1 or 1 while keeping the quasi-energy gap at 0 or π/T open, respectively. Hence it is potentially possible to define two sets of topological invariants associated with these gaps. We will now obtain two indices ν_0 and ν_π for a 1-dimensional system that indicate the number of edge modes with quasi-energy 0 and π/T in the system when the system is defined in a geometry with an edge. The invariants we obtain for the 1-dimensional case coincide with those found in [12].

Classification of 1-dimensional systems

A one-dimensional system with particle-hole symmetry can only have topological singularities at $k = 0$ and $k = \pi$, and the singularities here singularities can have phase 0 or phase π. Hence there

are two types of singularities. In 1 dimension, we furthermore have that all singularities occurring at the same phase are topologically identical if the system has four bands or more: through a local continuous deformation of the eigenstates $|\psi_n\rangle, |\chi_n\rangle$, the time-evolution near all singularities can be made to take the same form in Eq. (5.5). This allows us to create and annihilate pairs of singularities with the same phase at the same point in k-space, without changing the topological phase of the system. Hence the only topologically invariants we can associate with the singularities are the parities of the numbers $N_0(k)$ and $N_\pi(k)$ of 0- and π-singularities that occur at at points $k = 0$ and $k = \pi/a$ in k-space. An exception is when the system has only 2 bands. This case will be discussed in the end of the section.

In order to obtain the invariant ν_0, we can continuously deform the phases such that $\phi_n(t, k) = \pi$ everywhere in k, t-space except around $t = 0$ and around the singularities that appear at phase 0. This deformation keeps ν_0 invariant, and the only information left about the original system is about the singularities at phase 0, and $U(k, t)$ in the limit $t \to 0^+$. This means that any topological invariant associated with the gap at quasi-energy 0 must be some function of $(-1)^{N_0(0)}, (-1)^{N_0(\pi)}$, and $\nu[h_0]$, where $\nu[h_0]$ is the $\mathbb{Z}_2$ index for non-driven systems with particle-hole symmetry [27]. h_0 is the initial particle-hole symmetric Hamiltonian $h_0(k) = h(k, 0)$. From this, we identify

$$\nu_0 = \nu[h_0](-1)^{N_0} \tag{5.7}$$

where $N_0 = N_0(0) + N_0(\pi)$ is the total number of singularities at phase 0.

In order to find ν_π, we note that we can deform the phases ϕ_n to zero everywhere except around the singularities that occur at phase π, without changing any invariant in the gap at quasi-energy π/T. Hence any invariant in this gap is fully determined by the number of singularities at quasi-energy π, and can thus be expressed as some function of $(-1)^{N_\pi(0)}$ and $(-1)^{N_\pi(\pi/a)}$. We identify ν_π as

$$\nu_\pi = (-1)^{N_\pi} \tag{5.8}$$

where N_π is the number of singularities that occur at phase π. From the above two results, it is possible to derive expressions for ν_π and ν_0 directly in terms of the time-evolution operator. In appendix B.2, we show that ν_π and ν_0 can be found by

$$\nu_0 = \operatorname{sgn} \prod_{k=0,\pi} \operatorname{Pf}\left[\frac{1}{2i}(\sqrt{U(k,T)}^\dagger - \sqrt{U(k,T)})\right], \tag{5.9}$$

$$\nu_0\nu_\pi = \operatorname{sgn} \prod_{k=0,\pi} \operatorname{Pf}\left[\frac{1}{2i}(U(k,T)^\dagger - U(k,T))\right] \tag{5.10}$$

where the square root is defined by analytic continuation from $\sqrt{U(k,0)} = 1$. The above expressions are equivalent to the ones that were obtained in Ref. [12] by other means. The equivalence is also explained in appendix B.2.

Through a dimensional reduction argument similar to one used in Ref. [43], it is furthermore possible to show that these two indices give the parities of the numbers of edge modes at quasi-energy 0 and π/T, respectively. It is possible to define a particle-hole symmetric 2-dimensional system $h_{2D}(\mathbf{k}, t)$ that satisfies $h_{2D}(k_x, 0, t) = h(k_x, t)$, while $h_{2D}(k_x, \pi/a, t)$ is some trivial Hamiltonian. Each singularity at phase $0, \pi$, of the 1-dimensional system $h(k, t)$ contributes ± 1 to the winding number of $U_0(\mathbf{k}, t)$, $U_\pi(\mathbf{k}, t)$, respectively. Topological singularities that do

not occur at $k_y \in \{0, \pi/a\}$ have to appear in pairs, and thus contribute by ± 2 to the winding number of U. Furthermore, the Chern number of one conjugate half of the eigenstates of $h(\mathbf{k}, 0)$ can be odd if and only if $\nu[h_0] = -1$, as was shown in Ref. [43]. Using the winding number formula (4.15), we then obtain

$$W[U_0(\mathbf{k}, t)] \equiv \nu_0 \mod 2, \quad W[U_\pi(\mathbf{k}, t)] \equiv \nu_\pi \mod 2. \tag{5.11}$$

Now, suppose edges are introduced along the y-direction. The system will then be described by the Bloch space Hamiltonian $H_{ij}(k_y, t)$, where $H_{ij}(k_y, t)$ is the real space Hamiltonian of the 1-dimensional open-boundary system whose bulk is given by the Bloch Hamiltonian $h(k_x, k_y, t)$. Since the edge mode spectrum of $h(\mathbf{k}, t)$ has to be particle-hole symmetric, $H_{ij}(0, t)$ and $H_{ij}(\pi/a, t)$ will together have an odd number of edge modes with quasi-energy 0 if and only if $W[U_0(\mathbf{k}, t)]$ is odd. Since we chose $h(k_x, \pi/a, t)$ trivial, $H_{ij}(\pi/a, t)$ will have no edge modes. Hence all edge modes will all have to belong to $H_{ij}(0, t)$. A similar result holds for quasi-energy π.This concludes the proof.

Cases where singularities are topologically distinct

We found above that the topological classification was $\mathbb{Z}_2$ for a 1D particle-hole symmetric system with four bands or more. This relied on the fact that topological singularities with the same phase were all topologically identical. However, in some cases the $\mathbb{Z}_2$ invariant do not provide a full topological classification. For example, when the system has 2 bands there will be two distinct types of topological singularities: In Eq. (5.5), we can assume $|\psi_1\rangle$ and $|\psi_2\rangle$ to span the entire Hilbert space, and it is then always possible to choose $|\psi_1\rangle = (1, 0)$ and $|\psi_2\rangle = (0, 1)$. With this choice, one can then define $\mathrm{sgn}(\lambda)$ in Eq. (5.6) to be the charge for each singularity. This charge is conserved, and from a mathematical point of view, the net charge defines a topologically invariant $\mathbb{Z}$ index that is not allowed to change unless the symmetry is broken, or the quasi-energy gap at 0 or π is closed. The physical relevance of this invariant is not presently clear however.

5.3 Classification for time-reversal symmetry with $S^2 = -1$

In this section we apply our framework to the topological classification of periodically driven systems with time-reversal symmetry in the case where the symmetry operator squares to -1 (Symmetry class AII in the AZ classification [29]). This type of system was also considered in Ref. [16] in the 2-dimensional case, and a topological invariant consistent with the bulk-edge correspondence was obtained. We begin the section by demonstrating that if such a system has two bands, periodic driving allows it to have a non-trivial edge-mode configuration. The edge-mode spectrum of such a system is inherently trivial in the non-driven case. We then discuss the topological classification of driven systems with time-reversal symmetry in general terms, before we focus on the cases of 2 and 3 dimensions. For the 2-dimensional case we obtain a complete topological classification and prove the bulk-edge correspondence, and for the 3-dimensional case, we also obtain a bulk-edge correspondence. An exhaustive classification can also be done in the 3D case using band-flattening arguments, but this will not be done here.

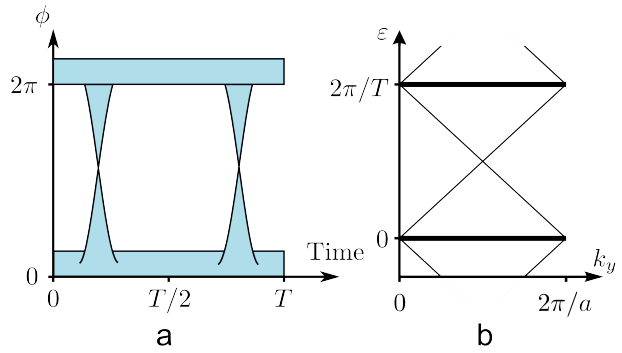

Figure 5.2: a): schematic depiction of the band structure of time-evolution operator of the time-reversally symmetric 2-band system discussed discussed in Sec. 5.3.1. b): quasi-energy band-structure of the model when put in a strip geometry along the y-direction.

5.3.1 Example of a 2-band system with time-reversal symmetry and a non-trivial $\mathbb{Z}_2$ index

In this section we demonstrate that a periodically driven two dimensional two-band system with time-reversal symmetry can have nontrivial $\mathbb{Z}_2$ index in its zone-edge gap (see next chapter for the definition of zone-edge gap). We show through numerical calculation that this model has a nontrivial edge-mode spectrum when defined in a strip geometry. For a non-driven 2-band system, Kramer's theorem guarantees a gapless bulk. Therefore the minimal setting for a non-trivial time-reversal invariant topological insulator involves four bands. However, the periodicity of quasi-energy introduces an additional gap that does not necessarily have to be closed, and this allows for a periodically driven 2-band system with time-reversal symmetry to have topologically protected edge modes. These can only occur when the time-evolution operator has topological singularities.

The model we consider is a 2-orbital square-lattice model given by the T-periodic Bloch space Hamiltonian

$$H(\mathbf{k},t) = \begin{cases} H_0(\mathbf{k},2t), & t < T/2 \\ \sigma_y H_0^*(\mathbf{k},2(T-t))\sigma_y, & t > T/2 \end{cases} \tag{5.12}$$

where $H_0(\mathbf{k},t)$ is non-symmetric Hamiltonian presented in Sec. 4.2.3. With the above definition, $H(\mathbf{k},t)$ is inherently time-reversally symmetric. In Ref. [10], it was noted that the Floquet operator associated with $H_0(\mathbf{k},t)$ was unity when the parameters $\delta_{AB} = 0$, $\lambda_n = 5\pi/2T$ were chosen, and it was shown that the time-evolution operator $U_0(\mathbf{k},t)$ of this system had winding number 1. For our model, we choose $\delta_{AB} = 0$, $\lambda_n = 5\pi/T$. The Floquet operator of the system is 1, and the system has a single gap in its quasi-energy spectrum. A schematic depiction of the band-structure of this model is shown in Fig. 5.2. In order to compare the bulk index with the edge-mode spectrum we numerically calculate the time-evolution operator and obtain the Floquet operator of this system when put in a strip-geometry. The quasi-energy band structure is plotted in Fig. 5.2. We see that the model has two chiral edge modes at each edge, and these edge modes are time-reversal conjugates of each other.

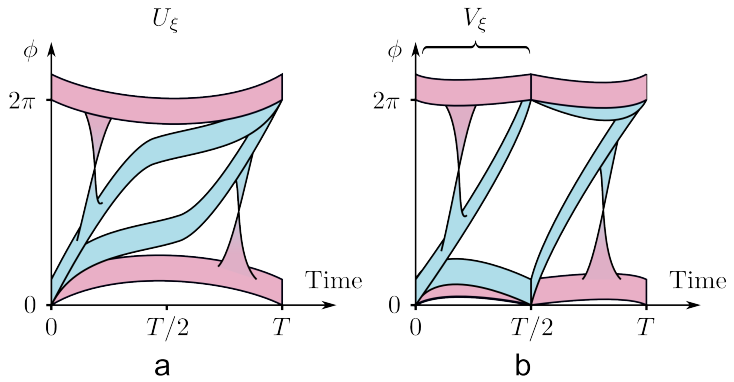

Figure 5.3: a) the band structure of the time-evolution operator of a 2d system with time-reversal symmetry whose bulk Floquet operator is the identity. b) V_ξ is obtained from U_ξ by flattening the bands of U_ξ at $T/2$ in a TR-symmetric way.

Band structure of periodically driven systems with time-reversal symmetry

We now use our approach to classify periodically driven systems with time-reversal symmetry. We first discuss the general features of these systems, and then examine the classification of a 2-dimensional system in more detail. We obtain the bulk-edge correspondence and show that it yields the correct edge-mode configuration for the model discussed above.

In contrast to the particle-hole symmetry discussed in Sec. 5.2, time-reversal symmetry imposes a time-non-local condition on the time-evolution operator. Time-reversal symmetry is defined to be present if, with some proper origin of time, an anti-unitary operator S exists, such that $h(\mathbf{k},t) = Sh(-\mathbf{k},T-t)S^{-1}$ in this basis. In this section we examine the case where $S^2 = -1$. Such anti-unitary operators can be written as $S = \sigma K$, where K is the complex conjugation operator given some basis, and σ is a self-adjoint unitary operator satisfying $\sigma = -\sigma^*$ in this basis. The symmetry condition is then equivalent to the time-evolution operator in this basis satisfying

$$U(\mathbf{k},t) = \sigma U(-\mathbf{k},T-t)^* U^{\mathrm{T}}(-\mathbf{k},T)\sigma. \tag{5.13}$$

For any quasi-energy gap ξ of the system, we can continuously deform $U(\mathbf{k},t)$ into a periodic time-evolution operator $U_\xi(\mathbf{k},t)$ without breaking the symmetry, such that the quasi-energy gap ξ stays open under the deformation. As was noted in Ref. [16], this can be done by using an effective Hamiltonian, in the same way as in the non-symmetric case. Since $U_\xi(\mathbf{k},T) = 1$, the deformed time-evolution operator satisfies $U_\xi(\mathbf{k},t) = SU_\xi^*(-\mathbf{k},T-t)S$. The fact that $S^2 = -1$ means that the eigenstates of $U_\xi(\mathbf{k},t)$ come in pairs that relate to each by symmetry, and we can write $U_\xi(\mathbf{k},t)$ in the form

$$U_\xi(\mathbf{k},t) = \sum_n \left[P_n(\mathbf{k},t) e^{-i\phi_n(\mathbf{k},t)} + P_{\bar{n}}(\mathbf{k},t) e^{-i\phi_{\bar{n}}(\mathbf{k},t)} \right], \tag{5.14}$$

where the functions $\{\phi_n(\mathbf{k},t), \phi_{\bar{n}}(\mathbf{k},t)\}$ are continuous and non-crossing. In contrast to the particle-hole symmetric case, the symmetry relates conjugate bands at different times to each

other:

$$P_{\bar{n}}(\mathbf{k}, t) = \sigma P_n^*(-\mathbf{k}, T - t)\sigma \tag{5.15}$$

$$\phi_{\bar{n}}(\mathbf{k}, t) = 2\pi w_n^\xi - \phi_n(-\mathbf{k}, T - t), \tag{5.16}$$

where the integer $w_n^\xi = \phi_n(\mathbf{k}, T)/2\pi$ is the phase winding number of bands n and $\bar{n}$. An example of a band-structure of U_ξ is given in Fig. 5.3. We note that the symmetry can be expressed as a boundary condition on $U_\xi(\mathbf{k}, t)$ at $t = T/2$: for $t < T/2$, $U_\xi(\mathbf{k}, t)$ can take any form as long as the boundary condition

$$U_\xi(\mathbf{k}, T/2) = \sigma U_\xi^*(-\mathbf{k}, T/2)\sigma \tag{5.17}$$

is satisfied. The symmetry is then automatically satisfied by imposing $U_\xi(\mathbf{k}, t) = SU_\xi^*(-\mathbf{k}, T-t)S$ for $t > T/2$. This means that any topological index defined for gap ξ should stay invariant under any continuous deformation of $U_\xi(\mathbf{k}, t)$ in the first half of the driving that doesn't violate the above boundary condition. If $S^2 = 1$, $U_\xi(\mathbf{k}, t)$ does *not* take the above form . In this case, the bands of U_ξ will be their own conjugates.

We now obtain the topological invariants for a $2d$-system. In particular we are interested in finding the parity ν_ξ of the number of edge-mode pairs in the bulk gap ξ when the system is put in a strip geometry.

Classification in 2D

For a two-dimensional system, we can always continuously deform $U_\xi(\mathbf{k}, T/2)$ into the identity without breaking the condition above. Firstly, it is possible to show that $U_\xi(\mathbf{k}, T/2)$ can not have any topologically protected degeneracies. It is then always possible to deform the function $\{\phi_n(t)\}$ such that $\phi_n(T/2) = 0$, without violating the boundary condition (5.17), see Fig. 5.3. Having deformed $U_\xi(\mathbf{k}, T/2)$ into 1, $U_\xi(\mathbf{k}, t)$ in the first half of the driving is given by a $T/2$-periodic unitary time-evolution operator $V_\xi(\mathbf{k}, t)$ with no special symmetry requirements. The topological properties of U_ξ are thus completely determined by topological classification of V_ξ, and topological invariant of U_ξ should be some function of $z[V_\xi]$ and $W[V_\xi]$ (see Sec. 4.3 for definition of $z_{[}\xi]$). We identify

$$\nu_\xi[U] = W[V_\xi] \mod 2. \tag{5.18}$$

In appendix B.3, we prove that ν_ξ gives the parity of the number of edge-mode pairs, when the system is put in a strip geometry. The invariant obtained here is the same that was found in Ref. [16]. V_ξ was defined in the above paragraph, and can in practice be obtained in many ways: one way is to define a continuous effective Hamiltonian $\tilde{H}_{\text{eff}}(\mathbf{k})$ that satisfies

$$e^{-i\tilde{H}_{\text{eff}}T/2} = U_\xi(\mathbf{k}, T/2), \quad \tilde{H}_{\text{eff}}(\mathbf{k}) = -S\tilde{H}_{\text{eff}}^*(-\mathbf{k})S. \tag{5.19}$$

This is always possible. In the first half of the driving we can then continuously deform $U_\xi(\mathbf{k}, t)$ into $V_\xi(\mathbf{k}, t) = U_\xi(\mathbf{k}, t)e^{i\tilde{H}_{\text{eff}}(\mathbf{k})t}$ without breaking the condition (5.17). The indices ν_ξ and z_ξ are the only topological invariants one can associate with the quasi-energy gap ξ of a 2D system with time-reversal symmetry.

To demonstrate that the invariant $\nu_\xi[U]$ constitutes the bulk-edge correspondence, we evaluate it for the model discussed in the beginning of this section. We recall that the time-evolution

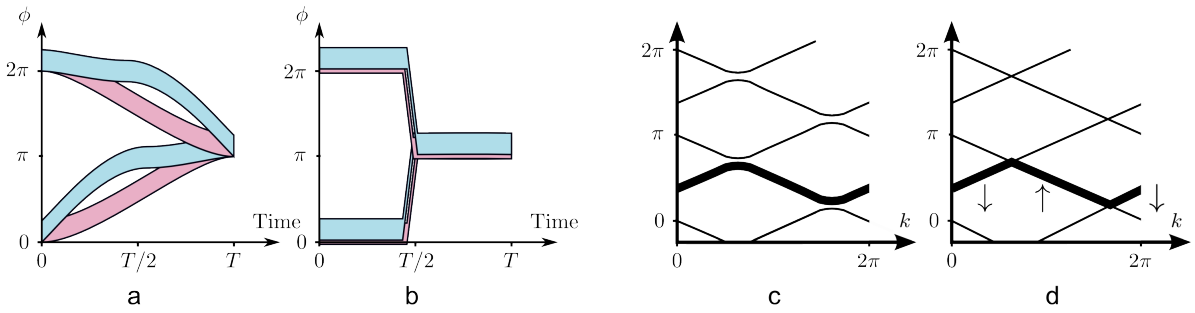

Figure 5.4: Band-structure of U_0 and U_π. a) Band-structure of U_0. b) Band-flattened U_0. c) Band-structure of U_π slightly away from $T/2$. d) Band-structure of U_π at $T/2$ as a function of k, where the S-eigenvalues of one band are indicated. This system has one singularity in each band gap, and $\nu_\pi = 1$. Away from $T/2$, the bands are continuous in k and symmetric in t. At the singularities, the S-eigenvalue of the bands change discontinuously with k.

operator of the model satisfies $U(T/2) = U(T) = 1$, so we do not have to band-flatten the system in order to calculate the $\mathbb{Z}_2$ index. We can take $U_{\pi/T}(\mathbf{k}, t) = U(\mathbf{k}, t)$, and $V_{\pi/T}(\mathbf{k}, t) = U(\mathbf{k}, t)$. $\mathbb{Z}_2$ index of this system is then simply

$$\nu_{\mathrm{TR}} = W[V_{\pi/T}] \bmod 2 = W[U_0] \bmod 2 = 1, \tag{5.20}$$

where U_0 was the time-evolution operator of the non-time-reversally symmetric model discussed in Ref. [10]. the value of ν_ξ thus agrees with the edge-mode spectrum we obtained (see Fig. 5.2b).

$\mathbb{Z}_2$ index for a 3D periodically driven system with time-reversal symmetry

The $\mathbb{Z}_2$ index for 2-dimensional systems (5.18) can also be used to define a $\mathbb{Z}_2$ index ν_ξ^3 that classifies a 3-dimensional system with time-reversal symmetry. The definition is analogous to the non-driven case: for a 3-dimensional system, governed by the time-evolution operator $U(k_x, k_y, k_z, t)$ we define $U^{0,\pi}(k_x, k_y, t)$ as $U(k_x, k_y, 0, t)$ and $U(k_x, k_y, \pi/a, t)$, respectively. Here a is the lattice constant in the z-diretion. These time-evolution operators describe two distinct 2D systems with time-reversal symmetry that share their bulk quasi-energy gaps with the original 3D system. For a bulk gap ξ of the 3D system we then define the $\mathbb{Z}_2$ index $\nu_\xi^3[U]$ as

$$\nu_\xi^3[U] = \nu_\xi[U^0] - \nu_\xi[U^\pi] \mod 2. \tag{5.21}$$

From similar arguments to the non-driven case [26], $\nu_\xi^3[U] = 1$ implies a topologically non-trivial edge-mode configuration in the bulk gap ξ.

5.4 Classification for chiral symmetry

In this section we use our framework to classify periodically driven systems with chiral symmetry. A Hamiltonian $h(\mathbf{k}, t)$ is defined to be chirally symmetric if, given some proper origin of time, a

self-adjoint unitary operator S exists such that $h(\mathbf{k},t) = -Sh(\mathbf{k},T-t)S$. The condition on the time-evolution operator is non-local in time:

$$U(\mathbf{k},t) = SU(\mathbf{k},T-t)U^\dagger(\mathbf{k},T)S. \tag{5.22}$$

There are two ways we can deform this system into a system with a scalar Floquet operator. Without breaking the symmetry, we can deform $U(\mathbf{k},t)$ into $U_0(\mathbf{k},t)$ and $U_\pi(\mathbf{k},t)$, where $U_0(\mathbf{k},T) = -1$ and $U_\pi(T) = 1$, and where, respectively, the quasi-energy gap at 0, π/T stays open during the deformation. From U_π and U_0 it is potentially possible to define topological invariants that classify $U(\mathbf{k},t)$. For a $1D$-system, we can with U_0 and U_π define two such indices ν_0 and ν_π. These indices indicate the number of localized edge modes in the bulk quasi-energy gaps $0, \pi/T$, which appear at each edge of the system when open boundary conditions are imposed. We will now show how to obtain these indices from the bulk time evolution operator of 1-dimensional system system.

Classification of a 1-dimensional system

In this section results that are valid in any dimension are indicated when using $\mathbf{k}$ as momentum, while $1d$-specific results are indicated when using k.

In order to find ν_0, we note that the operator $U_0(\mathbf{k},t)$ satisfies $U_0(\mathbf{k},t) = -SU_0(\mathbf{k},T-t)S$. This means that the bands of U_0 at different times are related pairwise by the symmetry, and we can write U_0 in the form

$$U_0(\mathbf{k},t) = \sum_n \left[P_n(\mathbf{k},t)e^{-i\phi_n(\mathbf{k},t)} + P_{\bar{n}}(\mathbf{k},t)e^{-i(\phi_{\bar{n}}(\mathbf{k},t)}\right], \tag{5.23}$$

where $\{\phi_n, \phi_{\bar{n}}\}$ are continuous and non-crossing, and

$$\begin{aligned} P_{\bar{n}}(\mathbf{k},t) &= SP_n(\mathbf{k},T-t)S \\ \phi_{\bar{n}}(\mathbf{k},t) &= \pi - \phi_n(\mathbf{k},T-t). \end{aligned} \tag{5.24}$$

Since $U_0(\mathbf{k},T) = 1$ and the phases of the bands never cross, we can choose the bands $\{P_n\}$ such that $\phi_n(\mathbf{k},T) = \pi$.

In one dimension, the symmetry (5.23) doesn't protect any topological singularities, and we can therefore assume $U_0(k,t)$ to be nondegenerate for all k,t except at $t = 0$ and $t = T$. The absence of topological singularities allows us to deform the time-evolution operator into one of a non-driven system, in the same way as we did in section 4.1, but with the rapid winding happening in the middle of the driving. See Fig. 5.4ab for a depiction of the deformation. The resulting non-driven system is described by the chiral-symmetric Hamiltonian

$$h_0(k) = \frac{\pi}{T}\sum_n \left[P_n(k,T/2) - SP_n(k,T/2)S\right]. \tag{5.25}$$

The deformation from $h(k,t)$ into $h_0(k)$ could be done without breaking the symmetry or closing the gap at quasi-energy 0, and hence any topological invariant associated with this gap should be a topological invariant of h_0. We identify ν_0 as

$$\nu_0 = \nu[h_0] \tag{5.26}$$

where $\nu[h_0]$ is the chiral $\mathbb{Z}$ index of the static Hamiltonian h_0 [30]. In the end of the section, we will show how to obtain ν_0 directly from $U(\mathbf{k}, t)$. It is immediately clear that ν_0 gives the number of topologically protected edge modes with quasi-energy 0 when open boundary conditions are imposed. We haven't closed the quasi-energy gap at 0 during the deformation or broken the symmetry, and hence the number of edge modes in the gap at quasi-energy 0 is the same for the non-driven system described by h_0 and for the periodically driven system described by $U(\mathbf{k}, t)$.

In order to find the index ν_π, we have to find a topological classification for time-evolution operators $U_\pi(\mathbf{k}, t)$ that satisfy

$$U_\pi(\mathbf{k}, t) = SU_\pi(-\mathbf{k}, T - t)S. \tag{5.27}$$

This condition means that $U_\pi(k, t)$ takes the form

$$U_\pi(k, t) \sum_n P_n(k, t) e^{-i\phi_n(k,t)}, \tag{5.28}$$

where the phases $\{\phi_n(\mathbf{k}, t)\}$ are continuous and non-crossing, and the bands are their own chiral conjugates, i.e. $P_n(\mathbf{k}, t) = SP_n(-\mathbf{k}, T - t)S$ and $\phi_n(\mathbf{k}, t) = \phi_n(\mathbf{k}, T - t)$.

In one dimension, $U_\pi(k, t)$ can have topological singularities, in contrast to $U_0(k, t)$: on the line $t = T/2$, $U_\pi(\mathbf{k}, t)$ commutes with S, and we are forbidden by symmetry to couple bands with opposite S-eigenvalues, so the phases of bands with opposite S-eigenvalues can cross along this line. See Fig. 5.4cd. These crossings we identify as topological singularities. The time-evolution near a singularity at k_0 takes the form

$$U_\pi(k, T/2) = \sum_n |\chi_n\rangle\langle\chi_n| + \sum_{a,b=1,2} M_{ab}(k)|\psi_a\rangle\langle\psi_b|, \tag{5.29}$$

where $|\psi_1\rangle$ and $|\psi_2\rangle$ are two eigenstates of $U(k, T/2)$ with opposite spins that become degenerate at the singularity, while $\{|\chi_n\rangle\langle\chi_n|\}$ are the nondegenerate eigenstates. The matrix M is given by

$$M(k) = e^{-i\phi_d(\mathbf{k}) - i\lambda\sigma_z(k - k_0)}, \tag{5.30}$$

for some real λ. A perturbation that satisfies the symmetry can never lift the degeneracy, only change the values of λ and k_0, and hence the degeneracy is topologically protected. Furthermore, not all singularities are equivalent. If we choose $|\psi_1\rangle$ to have S-eigenvalue 1, we define $\mathrm{sgn}(\lambda)$ to be the charge of the singularity. The total charge Q of singularities between any two neighbouring bands is the same and conserved. Since we can deform the phases to zero everywhere else, any topological invariant of U_π can be expressed as a function of Q. We identify ν_π as

$$\nu_\pi = Q. \tag{5.31}$$

ν_π is the winding number of the eigenvalues of $U_\pi(k, T/2)$ corresponding to eigenstates with positive S-eigenvalue, as k goes from 0 to 2π. One can use a dimensional reduction argument similar to the one used for the 1-dimensional particle-hole symmetric system in Sec. 5.2 to show that ν_π gives the number of edge modes in the quasi-energy gap at π/T.

From the indices obtained in Eqs. (5.26) and (5.31), it is possible to derive expressions for ν_0 and ν_π directly in terms of the time-evolution operator $U(k,t)$, and we obtain the same expressions for ν_0 and ν_π that were found in Ref. [13]: in a basis where S takes the form

$$S = \begin{bmatrix} 1 & 0 \\ 0 & -1 \end{bmatrix}, \tag{5.32}$$

consider the form of $U(k, T/2)$:

$$U(k, T/2) = \begin{bmatrix} A(k) & B(k) \\ C(k) & D(k) \end{bmatrix}. \tag{5.33}$$

ν_0 and ν_π can be found by

$$\nu_0 = \frac{1}{2\pi i} \int_0^{2\pi} dk \mathrm{Tr}[B^{-1}(k)\partial_k B(k)] \tag{5.34}$$

$$\nu_\pi = \frac{1}{2\pi i} \int_0^{2\pi} dk \mathrm{Tr}[A^{-1}(k)\partial_k A(k)]. \tag{5.35}$$

This is shown in appendix B.4.

Chapter 6

The natural quasi-energy zone

In the previous chapter we demonstrated the usefulness of representing the bulk time-evolution operator by its eigenstates $\{P_n(\mathbf{k}, t)\}$ and phase bands $\{\phi_n(\mathbf{k}, t)\}$. In this short chapter we present a group of non-trivial results that follows immediately from the previous chapter but is a diversion from the main theme of this thesis.

In Chapter 3 we mentioned that the quasi-energies of a periodically driven system were only defined modulo the driving frequency $2\pi/T$. Naively, this would lead one to expect that any choice of origin for quasi-energy band labelling is as good as another. However, we here demonstrate that this is not the case, and it is in fact possible to define a "natural" quasi-energy zone. Moreover, this notion seem to have direct physical consequences relevant for all Floquet systems. We finally show that this result is connected with the existence of an additional topological invariant one can define for periodically driven systems.

The results of this section have not been studied in full detail yet, but since they follow immediately from chapter 4, and is useful for understanding the topological properties of periodically driven systems, we will present them here.

6.1 The natural quasi-energy zone

As discussed in Chapter 3, the Floquet operator only defines the quasi-energies of a periodically driven system modulo $2\pi/T$. This means that quasi-energy band of the system can be labelled by two indices n, m, such that

$$\varepsilon_n^m(\mathbf{k}) = \varepsilon_n^0(\mathbf{k}) + 2\pi m/T \tag{6.1}$$

for some zeroth quasi-energy bands $\{\varepsilon_n^0(\mathbf{k})\}$ whose corresponding Floquet eigenstates form an orthonormal basis for the Bloch space. By requiring that two quasi-energies with the same m must not differ by more than $2\pi/T$, this labelling divides the quasi-energy spectrum up into quasi-energy zones of width $2\pi/T$, where $\varepsilon_n^m(\mathbf{k})$ lies in the m'th quasi-energy zone. Naively, the choice of the 0'th quasi-energy zone is just a matter of convention.

However, there is a natural choice. From the previous chapter we remember that the phase bands $\{\phi_n(\mathbf{k}, t)\}$ of a time-evolution operator were the unique solutions to

$$U(\mathbf{k}, t) = \sum_n P_n(\mathbf{k}, t) e^{-i\phi_n(\mathbf{k},t)} \tag{6.2}$$

that were continuous, satisfied $\phi_n(\mathbf{k}, 0) = 0$ and never crossed each other. From this definition, it is possible to show that at a given $\mathbf{k}, t$ two phase bands cannot differ by more than $2\pi/T$. Furthermore, their values at $t = T$ should correspond to the quasi-energies of the system. Hence these therefore define a natural choice for the zeroth quasi-energy zone. In this way, we can define a natural quasi-energy zone of a periodically driven system by picking

$$\varepsilon_n^0(\mathbf{k}) = \phi_n(\mathbf{k}, T)/T. \tag{6.3}$$

With this choice, the index m in Eq. (6.1) then defines a physically meaningful index for each quasi-energy band (see Fig. 6.1a), as we will shortly demonstrate. We will refer to this index as the natural quasi-energy zone (NQZ) index of a band. The NQZ provides a unique well-defined labelling of quasi-energy bands that does not require picking a quasi-energy origin of a system.

The notion of a natural quasi-energy zones has physical consequences that are relevant for all periodically driven systems: the continuity of the time-evolution operator and the phase bands means that *a quasi-energy band can never change its NQZ index under any continuous deformation of the system.* This has implications for the quasi-energy band structure at the edges of a periodically driven system.

Consider a periodically driven 1d system. Suppose that we have an array of these 1d systems next to each other, labelled by a coordinate y (see Fig. 6.1b). Let the 1d system at position y be governed by the Bloch Hamiltonian $H(k_x, y)$, and let us take the Hamiltonians of the 1d systems to depend continuously on y. This continuity then also holds for the quasi-energy bands $\varepsilon_n(k_x, y)$ of this system. Suppose that the 1d systems at $y = y_1$ and $y = y_2$ have the same Floquet operator, with quasi-energy bands $\{\varepsilon_n^m(k_x)\}$, but that these systems have different natural quasi-energy zones, such that $\varepsilon_n^0(k_x, y_1) = \varepsilon_n^0(k_x, y_2) + 2\pi m/T$ This fact tells us that the quasi-energy bands between y_1 and y_2 must connect $\varepsilon_n^0(k_x)$ with $\varepsilon_n^0(k_x) + 2\pi m/T$ and the entire system has no quasi-energy gaps.

This system is a crude model of a 2-d system with hopping in only one direction considered. Presently it has not been studied how this result behaves when hopping in the y-direction is introduced.

Zone-edge gap

The notion of natural quasi-energy zones means that a quasi-energy gap that separates two natural quasi-energy zones is different from the other quasi-energy gaps in some respects. We refer to this gap as the zone-edge gap. The zone-edge gap is the quasi-energy gap that becomes infinitely large when the driving period of the system goes to zero. A system whose time-evolution operator has no degeneracies cannot have any protected edge modes in its zone-edge gap. A non-driven system seen as a driven system cannot have edge modes in it zone-edge gap when the driving frequency becomes wider than the width of the energy spectrum. The fact that a driven system can have non-trivial topological invariants associated with its zone-edge gap means that periodically driven systems in general have a richer classification than their non-driven counterparts. In this way, anomalous edge-phenomena seem to be associated with the existence of edge-modes in the zone-edge gap.

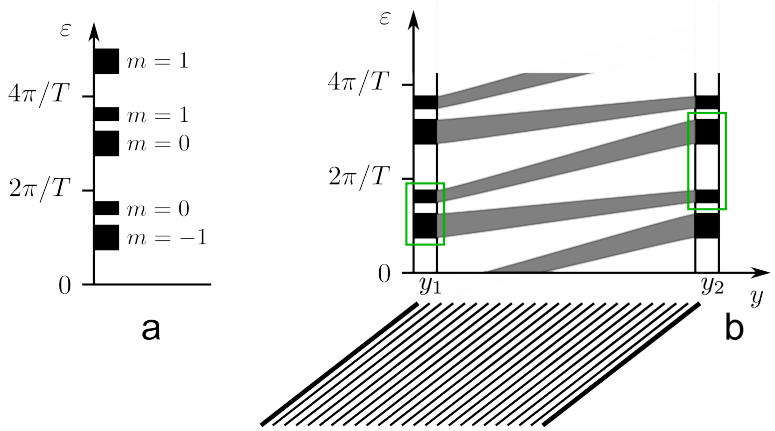

Figure 6.1: a) An example of a quasi-energy spectrum with a natural quasi-energy zone labelling of bands. b) The quasi-energy spectrum for a continuous array of 1-dimensional periodically driven systems. The systems at y_1 and y_2 have the same Floquet operator but different NQZ's. The NQZ's of these two systems are indicated by green boxes. The different NQZ's of the two systems means that the entire two-dimensional array of wires is completely gapless.

6.2 The zeroth winding number

Here we show that the notion of natural quasi-energy zones is connected with the existence of an additional topological invariant associated with periodically driven systems. We recall from the previous chapter, that given a quasi-energy gap ξ, the phase winding numbers $\{w_n^\xi\}$ could only take integer values and were therefore topologically invariant. Apart from the winding number $W_\xi[U]$, we can for each quasi-energy gap ξ thus define an additional topological invariant $z_\xi[U]$ of the time-evolution operator, namely

$$z_\xi[U] = \sum_n w_n^\xi = \frac{1}{2\pi}\int_0^T \mathrm{d}t \mathrm{Tr}[U_\xi^\dagger(\mathbf{k},t)\partial_t U_\xi(\mathbf{k},t)] \tag{6.4}$$

Where the right hand side is the same for any $\mathbf{k}$ in the BZ. The quantity $z_\xi[U]$ is referred to as the zeroth winding number. It is the Floquet analogue of the invariant $B_\xi[H]$ for non-driven systems that gave the number of occupied bulk bands (see sec. 2.2.1). The invariant $B_\xi[H]$ can be seen as a "zeroth" Chern number, hence the name for z_ξ. While B_ξ is usually an uninteresting quantity for non-driven systems, the zeroth winding number is in general less trivial.

The zeroth winding number has a one-to-one relation with the natural quasi-energy zone indices. For a quasi-energy gap ξ, let $\{m_n\}$ be the natural quasi-energy zone indices of the quasi-energy bands that take value in $[\xi - 2\pi/T, \xi]$. With each quasi-energy band we can identify a phase winding number w_n^ξ. From its definition in Sec. 4.2.2, we then have that $\phi_n(\mathbf{k}, T)$ lies in the interval $[\xi T + 2\pi w_n^\xi, \xi T + 2\pi(w_n^\xi - 1)]$. Hence the phase winding number should relate to the

natural quasi-energy zone indices as $w_n^\xi = -m_n$, and

$$z_\xi[U] = \sum_i w_n^\xi = -\sum_i m_i. \tag{6.5}$$

Eqs. (6.6) and (6.5) make it possible to identify the zeroth quasi-energy zone from the invariant z_ξ. In the same way, the zeroth winding number can be used to identify the zone-edge gap: a quasi-energy gap ξ is a zone-edge gap if and only if $z_\xi[U]$ is an integer multiple of the total number of bands.

The zeroth winding number can be found directly from the Hamiltonian and Floquet operator of the systen. The right hand side of Eq. (6.4) can be simplified by recalling that we can take $U_\xi(t) = U(t)e^{iH_{\text{eff}}^\xi t}$ (see sec. 4.2.2 For definition of H_{eff}^ξ). We then have

$$z_\xi[U] = \frac{1}{2\pi}\int_0^T \text{Tr}[h(\mathbf{k},t)]dt - \frac{1}{2\pi}\text{Tr}[H_{\text{eff}}^\xi]T. \tag{6.6}$$

With $h(t)$ being the time-dependent Bloch Hamiltonian of the system. As an aside, the above identity further implies there is a non-trivial relation that holds for any effective Hamiltonian of a periodically driven system, defined with a branch cut in a quasi-energy gap:

$$\text{Tr}[H_{\text{eff}}^\xi] \equiv \text{Tr}\left[\frac{1}{T}\int_0^T h(\mathbf{k},t)dt\right] \mod \frac{2\pi}{T}, \tag{6.7}$$

since $z_\xi[U]$ is always an integer if ξ lies in a quasi-energy gap.

Chapter 7

Discussion and outlook

In this thesis we found that non-removable degeneracies of the bulk time-evolution operator, so-called topological singularities, play a crucial role for the topological classification of periodically driven systems.

This result arises since we are able through a continuous deformation of the eigenvalues of the bulk time-evolution operator to reduce the time-evolution operator to the identity anywhere in $\mathbf{k}, t$-space, except for arbitrarily small regions surrounding the singularities and possibly at the boundary region at the beginning or end of the driving (or at $T/2$ if a time-nonlocal symmetry is present). The deformation can be done without changing the topological class of the system, and this fact implies that *all* topological invariants of a periodically driven system can be seen as quantities relating to the topological singularities in the bulk of the driving, and the topological class of time-evolution operator at the boundary region.

We explicitly demonstrated for several symmetry classes that the bulk-edge correspondence of a periodically driven system has a direct and simple relationship with the topological singularities of the time-evolution operator. To show this, we made use of the the band-flattening scheme mentioned in the above. The band-flattening scheme provides a method for topological classification of periodically driven systems that seems to be universally applicable, or at least applicable for symmetries on the forms discussed in Sec. 5.1. Hence, it can be used as a general way of obtaining bulk-edge correspondences for periodically driven systems. With the method one can obtain all bulk topological invariants of a periodically driven system.

Periodic driving gives an extra freedom to create systems with nontrivial topological edge-mode phenomena. Topologically non-trivial Floquet-Bloch systems are possible in any dimension and symmetry class where topological insulators are possible. However, while every topological insulator has a Floquet analogue, the topological classification of periodically driven systems is actually richer than for non-driven systems. In every symmetry class supporting topologically nontrivial bands, we find new distinct topological configurations which are impossible to obtain in non-driven systems. Examples of such anomalous configurations are the anomalous edge modes in a 2D system with no symmetries encountered in [10], the appearance of edge-modes in a 2-band system with time-reversal symmetry that we described in Sec. 5.3.1, or the edge-modes with quasi-energy π/T in system particle-hole or chiral symmetry. We also encountered an example of a periodically driven system whose bulk topological classification was given by a $\mathbb{Z}$ index, while its

non-driven counterpart classified only by a $\mathbb{Z}_2$ index, meaning the system has an infinite number of topological phases that are inaccessible for a non-driven system. Periodically driven systems thus have a richer topological classification than non-driven systems.

One of the major reasons for the importance of bulk-edge correspondences of non-driven systems is that they are helpful identifying materials that exhibit non-trivial edge phenomena. In the same way, it was hoped that obtaining bulk-edge correspondences for periodically driven systems would help for devising driving schemes and materials that result in non-trivial edge phenomena. However, this insight does not always follow from obtaining the invariants directly in terms of the time-evolution operator The topological singularities and the band-structure picture of the time-evolution operator give an intuitive way of understanding the topological phenomena in driven systems. This picture provides useful insight that can be used for devising driving schemes: one of the main conclusions of this thesis is that inducing non-trivial topological phenomena through periodic driving often amounts to introducing topological singularities into the phase bands of the bulk time-evolution operator.

In this paper, we have focused on 1- and 2-dimensional systems, but the band-flattening method is also applicable in higher dimensions, and topological singularities also appear there. In 3 dimensions, topological singularities appear as closed, oriented lines in $\mathbf{k}, t$-space. In 4 dimensions, a new type of topological singularity appears where the eigenvalues of 4 bands coincide. This type of singularity arises because the restriction of the time-evolution operator to the subspace of 4 bands can be expressed as a matrix exponential of a linear combination of the 5 Γ-matrices that generate SU(4). The momentum- and time coordinates in the 4+1-dimensional system can then tune all 5 gamma matrices to zero, and thereby prevent a lifting of the degeneracy between the 4 bands. The appearance of this new type of singularity seems to reflect the existence of a second Chern number in a 4+1D non-driven system, that can also only be nonzero if the system has 4 bands or more.

From the examples we have considered, it seems that for some symmetry classes, non-driven and driven systems can only have topologically non-trivial phases in dimensions where topological singularities are possible. Indeed, if a symmetry can be expressed as an instantaneous condition on the time-evolution operator, the symmetry only supports nontrivial topological phases if the time-evolution operator can have topological singularities in that dimension. This can be immediately seen by seeing the time-evolution operator as some interpolation of Floquet operators, with time being the interpolation parameter. Topological singularities then appear at the topological phase transitions of the system during the interpolation. For these types of symmetries, topological phase transitions are thus only possible if topological singularities are. For systems with the time-nonlocal condition however, the relationship is not so direct, but a similar argument can still be applied on a continuous interpolation of Floquet operators that satisfy the symmetry. In this way, considerations about topological singularities are enough to determine whether a symmetry can support non-trivial topological phases, both for non-driven and periodically driven systems.

In this thesis, we have primarily focused on obtaining bulk-edge correspondences for periodically driven systems. However, we have also encountered other topological invariants that the bulk system can have, for example, the zeroth winding number, or the $\mathbb{Z}$ invariant for a 2-band particle-hole symmetric system in 1D. This suggests that periodically driven systems can have other types of topological phenomena in addition to analogues of the edge-mode phenomena encountered in non-driven systems. This was also discussed in Ref. [40].

7.1 Outlook

In this thesis we demonstrated the usefulness of representing the time-evolution operator by its phase bands. This gave us a way of implementing continuous deformations of periodically driven systems, and made it clear that time-evolution operator in general could have protected degeneracies that played a role for its topological properties. Another nice result that followed from this band structure representation was the existence of a "physically meaningful" origin for labelling of quasi-energy bands - the natural quasi-energy zone described in chapter 6. This result was connected with the existence of an additional topological invariant, namely the zeroth winding number. The zeroth winding number is in the non-driven case often overlooked, but for Floquet systems it is more non-trivial. Although some physical consequences of these concepts were described, their implications still needs to be studied further.

In this thesis we found that inducing non-trivial topological phenomena through periodic driving often amounts to introducing topological singularities into the bulk time-evolution operator. For some cases, such as the particle-hole symmetric case, topological singularities can be intentionally created. Finding out whether/ how topological singularities can be intentionally created would be very useful for devising driving schemes that result in topologically non-trivial behaviour. This could also be an interesting subject of future study.

The diagonalization of the Floquet operator gives solutions to single-particle problems with periodically time-dependent Hamiltonians. The many-body problem - in particular the filling of quasi-energy levels when the system is connected to a particle reservoir - is currently not so well understood, and this field is a very active area of current research [11, 44–46]. In order to take advantage of the new possibilities for topological solid-state phenomena offered by periodic driving , this field still needs to be studied further.

Appendix A

List of known invariants

In this appendix we display the topological invariants so far obtained for periodically driven systems. We give expressions for them directly in terms of the time-evolution operator, as well as discrete expressions if they are known. If they are not known or relevant, or it is not clear whether such an expression exists, we indicate this with a question mark. We also give a reference to the source where the invariant was first derived. If a topological invariant can be defined for a system in dimension d, similar invariants can also be defined for systems any higher dimension. For example, a 3d system with no symmetries can be a weak topological insulator, classified by 3 invariants analogous to Chern numbers defined for 2d systems. In the tables, we therefore indicate the lowest dimension where an invariant first appears. Below the tables, a discussion and an explanation is given.

Symmetry Class A (No symmetry)			
Dimension	New topological invariant	Discrete expression	Obtained in
$d=0$	$\frac{1}{2\pi i}\int_0^T \mathrm{d}t \mathrm{Tr}\left[U_\xi^\dagger \partial_t U_\xi\right]$	$\sum_n w_n^\xi$	Chp. 6
$d=1$	0	0	–
$d=2$	$\frac{-1}{8\pi^2}\int \mathrm{d}^2\mathbf{k}\mathrm{d}t \mathrm{Tr}\left[\epsilon_{\mu_1\mu_2\mu_3}\prod_{i=1}^3 U_\xi^\dagger \partial_{\mu_i} U_\xi\right]$	$-\sum_n \mathcal{C}_n w_n^\xi + \sum_i q_i$	[10]
$d=3$	0	0	–
$d=4$	$\frac{i}{160\pi^3}\int \mathrm{d}^4\mathbf{k}\mathrm{d}t \mathrm{Tr}\left[\epsilon_{\mu_1\ldots\mu_5}\prod_{i=1}^5 U_\xi^\dagger \partial_{\mu_i} U_\xi\right]$	?	Chp. C

Symmetry Class AII (Time-reversal symmetry with $S^2 = -1$)			
Dimension	New topological invariant	Discrete expression	Obtained in
$d = 0$	0	0	–
$d = 1$	0	0	–
$d = 2$	$\nu_\xi[U] = \frac{-1}{8\pi^2} \int \mathrm{d}^2\mathbf{k}\mathrm{d}t\mathrm{Tr}\left[\epsilon_{\mu_1\mu_2\mu_3} \prod_{i=1}^{3} V_\xi^\dagger \partial_{\mu_i} V_\xi\right]$	?	[16]
$d = 3$	$\nu_\xi[U(\mathbf{k}, k_z, t)]_{k_z=0}^{k_z=\pi/a} \mod 2$	?	Chp. 5 / [16]

Symmetry Class AIII (Chiral symmetry)			
Dimension	New topological invariant	Discrete expression	Obtained in
$d = 0$	?	?	–
$d = 1$	$\nu_0 = \frac{1}{2\pi i} \int_0^{2\pi} \mathrm{d}k\mathrm{Tr}[B^{-1}(k)\partial_k B(k)]$ $\nu_\pi = \frac{1}{2\pi i} \int_0^{2\pi} dk\mathrm{Tr}[A^{-1}(k)\partial_k A(k)]$	? $Q[U_\pi]$	[13]

Symmetry Class D (Particle-hole symmetry with $S^2 = 1$)			
Dimension	New topological invariant	Discrete expression	Obtained in
$d = 0$	$\nu_0[U] = \mathrm{sgnPf}\left[\sqrt{U(T)} - \sqrt{U(T)}^{\mathrm{T}}\right]$ $\nu_\pi[U] = \mathrm{sgnPf}\left[U(T) - U(T)^{\mathrm{T}}\right]$	$\nu_{0d}[H(0)](-1)^{N_0}$ $(-1)^{N_\pi}$	[12]
$d = 1$	$\nu_0[U(0)]\nu_0[U(\pi/a)]$ $\nu_\pi[U(0)]\nu_\pi[U(\pi/a)]$	$\nu_{1d}[H(0)](-1)^{N_0}$ $(-1)^{N_\pi}$	[12]
$d = 2$	?	?	–

Explanations and comments

Symmetry class A

The operator $U_\xi(\mathbf{k}, t)$ is any time-evolution operator satisfying $U_\xi(\mathbf{k}, T) = 1$ that can be continuously deformed into the original time-evolution operator U such that the quasi-energy gap at ξ never closes. w_n^ξ is the phase winding number of band n and q_i is the charge of singularity i. $\mathcal{C}_n$ is the Chern number of band n. See Chp. 4 for more information. For symmetry class A, the topological invariants can be defined in every quasi-energy gap ξ. The invariant for $d = 2$ gives the number of chiral edge modes in the bulk quasi-energy gap. The relevance of the $d = 0$ invariant for the edge-mode spectrum is not currently clear.

Symmetry class AII

The operator V_ξ is found as follows: without breaking time-reversal symmetry of $U_\xi(\mathbf{k}, T) = 1$, continuously deform $U_\xi(\mathbf{k}, t)$ such that $U_\xi(\mathbf{k}, T/2) = 1$. V_ξ is then given by the deformed U_ξ in the first half of the driving. For 2d, ν_ξ give the parity of the number of Kramer's pairs of chiral edge mods in the quasi-energy gap ξ. The edge correspondence corresponding to the 3d invariant should also be analogous to the non-driven case, see for example Refs. [26, 32].

Symmetry class AIII

The operators $A(k)$ and $B(k)$ are found as follows. In a basis where the chiral symmetry operator S takes the form

$$S = \begin{bmatrix} 1 & 0 \\ 0 & -1 \end{bmatrix}, \tag{A.1}$$

the time-evolution operator at $T/2$ takes the form

$$U(k, T/2) = \begin{bmatrix} A(k) & B(k) \\ C(k) & D(k) \end{bmatrix}. \tag{A.2}$$

This defines A and B. For Chiral symmetry it is possible to define two invariants ν_0 and ν_π, corresponding to quasi-energy gaps 0 and π/T, respectively. For a 1d system, the parity of the invariants ν_0 and ν_π give the parity of 0- and π/T-quasi-energy edge modes, respectively. $Q[U_\pi]$ gives the number of singularities of $U_{\pi/T}(k, t)$ in some gap in the phase-band structure. The operator $U_{\pi/T}(k, t)$ is any time-evolution operator that can be continuously deformed into $U(k, t)$ without closing the quasi-energy gap at π/T or breaking chiral symmetry. The 1d invariants should have immediate generalizations to any odd dimension, analogous to the generalization of the static invariant [30].

Symmetry class D

The indices $\nu_{0,1d}[h] = \text{sgnPf}[h]$ are the $\mathbb{Z}_2$ indices found in Ref. [27] for static particle-hole symmetric Hamiltonians. $H(0)$ is the Hamiltonian of the driven system at the beginning of a driving period. For $d = 1$ ν_0 and ν_π give the parity of number of edge-modes with quasi-energy 0 and π/T, respectively. N_0 and N_π is the number of singularities at phase 0 and π, respectively.

Appendix B

Derivations

B.1 Derivation of Eq. (4.13)

In this appendix, we show that the time evolution operator $\tilde{U}_\xi$ given in Eqs. (4.9)-(4.11) has winding number $n|R|$, by explicit evaluation of the winding number formula (4.13). Inserting $\tilde{U}_\xi$ into this formula, we get

$$W = -\frac{1}{24\pi^2}\int_{|\mathbf{r}-\mathbf{r}_0|<\delta r} \mathrm{d}t\,\mathrm{d}^2k\ \mathrm{Tr}\left[M^\dagger\partial_i M\cdot M^\dagger\partial_j M\cdot M^\dagger\partial_k M\right]\epsilon_{ijk}, \tag{B.1}$$

where ε_{ijk} is the Levi-Civita symbol. Summation over repeated indices is used and will be used in the rest of this section. In order to exploit the symmetries of the time-evolution operator, we shift from Cartesian coordinates to polar coordinates centred at $\mathbf{r}_0$. Doing this we get

$$W = -\frac{1}{24\pi^2}\int_0^{\delta k}\mathrm{d}r\int_0^{\pi}\mathrm{d}\theta\int_0^{2\pi}\mathrm{d}\phi\ |J|J_{i\alpha}J_{j\beta}J_{k\gamma}\epsilon_{ijk}\cdot\mathrm{Tr}\left[M^\dagger\partial_\alpha M\cdot M^\dagger\partial_\beta M\cdot M^\dagger\partial_\gamma M\right], \tag{B.2}$$

where J is the Jacobian matrix of the coordinate transformation, and the Greek letters α,β,γ run over the polar coordinates r,θ,ϕ, where $r=|\mathbf{r}-\mathbf{r}_0|$. We now use the following useful identity for the Levi-Civita symbol that holds for any real invertible 3×3 matrix A [47]

$$A_{i\alpha}A_{j\beta}A_{k\gamma}\epsilon_{ijk} = \frac{\epsilon_{\alpha\beta\gamma}}{|A|}. \tag{B.3}$$

With this identity, we see that the winding number formula is independent on the choice of coordinates, as the Jacobian matrices always cancel out:

$$W = -\frac{1}{24\pi^2}\int_0^{\delta k}\mathrm{d}r\int_0^{\pi}\mathrm{d}\theta\int_0^{2\pi}\mathrm{d}\phi\ \mathrm{Tr}\left[M^\dagger\partial_\alpha M\cdot M^\dagger\partial_\beta M\cdot M^\dagger\partial_\gamma M\right]\epsilon_{\alpha\beta\gamma}.$$

We now use the cyclic property of the trace as well as the identity $\partial M M^\dagger = -M\partial M^\dagger$ to get

$$W = \frac{1}{8\pi^2}\int_0^{\delta k}\mathrm{d}r\int_0^{\pi}\mathrm{d}\theta\int_0^{2\pi}\mathrm{d}\phi\ \mathrm{Tr}\left[M^\dagger\partial_r M\partial_\theta M^\dagger\partial_\phi M\right] - \theta\leftrightarrow\phi. \tag{B.4}$$

Having rewritten the integral to polar coordinates, let us now see how M looks in terms of these coordinates. We have

$$M(r,\theta,\phi) = (-1)^{\nu} \exp\left(\frac{-i\pi n}{\delta k}\vec{p}\cdot\vec{\tau}\right), \tag{B.5}$$

where $\vec{p} = (\mathbf{r} - \mathbf{r}_0)$, and $\tau_i = R_{ij}\sigma_j$. Defining $\hat{r}(\theta,\phi) = \vec{p}/r$, we evaluate each of the factors in the integrand

$$\begin{aligned} M^{\dagger}\partial_r M &= \frac{i\pi\nu}{\delta k}\ \hat{r}\cdot\vec{\tau} \\ \partial_\theta M &= i\sin\left(\frac{i\pi\nu r}{\delta k}\right)\partial_\theta\hat{r}\cdot\vec{\tau} \\ \partial_\phi M &= i\sin\left(\frac{i\pi\nu r}{\delta k}\right)\partial_\phi\hat{r}\cdot\vec{\tau}. \end{aligned}$$

Hence

$$W = \frac{in}{16\pi}\int_0^{\pi} \mathrm{d}\theta \int_0^{2\pi} \mathrm{d}\phi \mathrm{Tr}\left[\hat{r}\cdot\vec{\tau}\ \partial_\theta\hat{r}\cdot\vec{\tau}\ \partial_\phi\hat{r}\cdot\vec{\tau}\right] - \theta \leftrightarrow \phi. \tag{B.6}$$

We now look for a simpler expression for the integrand:

$$\mathrm{Tr}\left[\hat{r}\cdot\vec{\tau}\ \partial_\theta\hat{r}\cdot\vec{\tau}\ \partial_\phi\hat{r}\cdot\vec{\tau}\right] = \hat{r}_i\partial_\theta\hat{r}_j\partial_\phi\hat{r}_k R_{ia}R_{jb}R_{kc}\mathrm{Tr}\left[\sigma_a\sigma_b\sigma_c\right].$$

Now, the Pauli matrices satisfy $\mathrm{Tr}[\sigma_i\sigma_j\sigma_k] = 2i\epsilon_{ijk}$. Hence

$$\begin{aligned} \mathrm{Tr}\left[\hat{r}\cdot\vec{\tau}\ \partial_\theta\hat{r}\cdot\vec{\tau}\ \partial_\phi\hat{r}\cdot\vec{\tau}\right] &= \hat{r}_i\partial_\theta\hat{r}_j\partial_\phi\hat{r}_k\cdot 2iR_{ia}R_{jb}R_{kc}\epsilon_{abc} \\ &= \hat{r}_i\partial_\theta\hat{r}_j\partial_\phi\hat{r}_k\cdot 2i|R|\epsilon_{ijk}, \end{aligned}$$

where we used the Levi-Civita symbol identity (B.3) and the fact that $|R|^{-1} = |R|$. Restoring antisymmetrization in θ and ϕ, and going back to vector notation, we then get

$$\mathrm{Tr}\left[\hat{r}\cdot\vec{\tau}\ \partial_\theta\hat{r}\cdot\vec{\tau}\ \partial_\phi\hat{r}\cdot\vec{\tau}\right] - \theta\leftrightarrow\phi = 4i|R|\ \hat{r}\cdot\partial_\theta\hat{r}\times\partial_\phi\hat{r} = 4i|R|\sin\theta. \tag{B.7}$$

Hence the integrand in Eq. (B.6) is simply $4i$ times the surface area element of the sphere. We thus have

$$\begin{aligned} W &= \frac{i\nu}{16\pi}\int_0^{\pi}\mathrm{d}\theta\int_0^{2\pi}\mathrm{d}\phi(-4i\sin\theta) \\ &= -\nu|R| \\ &= -q. \end{aligned} \tag{B.8}$$

This was what we wanted to prove.

B.2 $\mathbb{Z}_2$ indices for a particle-hole symmetric 1-d system

In this appendix we derive (5.10) from the the topological indices we obtained in Eqs. (5.7) and (5.8). To do this, we note that for $k \in \{0, \pi/a\}$ we can define the eigenstates $|\psi_k(t)\rangle$ and $|\psi_k^*(t)\rangle$

of $U(k,t)$ to be continuous in t. A main point in this paper is that it is not always possible to define the eigenstates of $U(\mathbf{k},t)$ globally in a continuous way. However, it is always possible to define the eigenstates and eigenvalues such that they are continuous along some arbitrary line in $\mathbf{k},t$-space. For $k \in \{0,\pi/a\}$ we can thus write

$$U(k,t) = \sum_n \left[\tilde{P}_{n,k}(t)e^{-i\tilde{\phi}_{n,k}(t)} + \tilde{P}^*_{n,k}(t)e^{i\tilde{\phi}_{n,k}(t)}\right], \tag{B.9}$$

where both $P_{n,k}(t)$ and $\phi_{n,k}(t)$ are continuous, but in contrast to earlier, the functions $\{\phi_{k,n}, -\phi_{k,n}\}$ are allowed to cross. It is convenient to choose $\{\phi_n(t)\}$ in Eq. (B.9) such that $\phi_n(t) \to 0^+$ in the limit $t \to 0$. A singularity occurs at phase 0 or π, whenever one of the $\phi'_{n,k}s$ reach $2\pi\mathbb{Z}$ or$(2\mathbb{Z}+1)\pi$. Then $N_0(k)$ counts how many times $\{\phi_n(k,t)\}$ cross $2\pi\mathbb{Z}$, and we have

$$(-1)^{N_0(k)} = \text{sgn} \prod_n \sin(\phi_n(k,t)/2). \tag{B.10}$$

We can find the rhs directly from the time-evolution operator: with $\sqrt{U(k,t)}$ defined by analytical continuation from $\sqrt{U(k,0)} = 1$, we introduce for $k \in \{0,\pi/a\}$ $Q_k(t) = \frac{1}{2i}[\sqrt{U(k,t)}^\dagger - \sqrt{U(k,t)}]$. We have

$$Q_k(t) = \sum_n \left[P_{n,k}(t)\sin\frac{\phi_{n,k}(t)}{2} - P^*_{n,k}(t)\sin\frac{\phi_{n,k}(t)}{2}\right]. \tag{B.11}$$

We see that $Q_k(t)$ is skew-symmetric and takes eigenvalues $\{\pm\sin\phi_{n,k}(t)/2\}$. General results for Pfaffians [28] then tell us that

$$\text{Pf}[Q_k(t)] = s_k \prod_n \sin(\phi_n(k,t)/2), \tag{B.12}$$

where $s_k \in \{\pm 1\}$ depends on the basis we choose. We can find s_k by taking the limit $t \to 0$ of the above equation. Since we choose $\phi_n(t) \to 0^+$ in this limit, we get

$$s_k = \text{sgn Pf}[h_0(k)]. \tag{B.13}$$

Hence, combining the above with Eqs. (B.12) and (B.10)

$$\text{sgn Pf}[Q_k(T)] = \text{sgn Pf}[h_0(k)](-1)^{N_0(k)}. \tag{B.14}$$

In Ref. [27] it was found that $\nu[h_0] = \text{sgn Pf}[h_0(0)]\text{Pf}[h_0(\pi/a)]$. Thus

$$\nu_0 = \nu[h_0](-1)^{N_0(0)+N_0(\pi/a)} = \text{sgn} \prod_{k\in\{0,\pi/a\}} \text{Pf}[Q_k(T)]. \tag{B.15}$$

In order to obtain a similar expression for ν_π, we note that the index ν_0 for the particle-hole symmetric system with time-evolution operator $\tilde{U}(k,t) = U^2(k,t)$ is given by

$$(-1)^{N_0+N_\pi}\nu[h_0] = \nu_0\nu_\pi. \tag{B.16}$$

This is because the static $\mathbb{Z}_2$ index of the initial Hamiltonian is the same for the systems with time-evolution operators $U(k,t)$ and $U^2(k,t)$, and $U^2(k,t)$ has a zero-phase singularity of for each π or 0-phase singularity of $U(k,t)$. This gives us

$$\nu_0\nu_\pi = \text{sgn} \prod_{k\in\{0,\pi/a\}} \text{Pf}\left[\frac{1}{2i}[U^\dagger(k,T) - U(k,T))\right]. \tag{B.17}$$

The expressions for ν_0 and ν_π obtained here are equivalent to the ones found in Ref. [12]. Here, the expressions for ν_0 and ν_π take the same form, but with $Q_k(T) = \log\sqrt{U(k,t)}$, where the logarithm is taken with branch cut at $-\pi$, and similarly for the $\nu_\pi\nu_0$-expression. The expression is seemingly different because $(-1)^{N_0(k)}$ can be obtained from the phases $\{\phi_{n,k}(T)\}$ in many ways. For example, we could in Eq. (B.10) also have taken

$$(-1)^{N_0(k)} = \text{sgn} \prod_n f\left[\phi_n(k,T)/2\right] \tag{B.18}$$

where $f(x)$ is the unique function that satisfies $f(x) \equiv x \mod 2\pi$ and takes values between $-\pi$ and π. When one repeats the subsequent steps, the expressions found in Ref. [12] are obtained.

B.3 Proof for the bulk-edge correspondence for a 2d system with time-reversal symmetry

In this appendix we show that the invariant in Eq. (5.18) gives the parity of the number of edge mode pairs, in a 2-dimensional driven system with time-reversal symmetry. To do this, we recall that it was possible to continuously deform $U(\mathbf{k},t)$ into the time-evolution operator

$$\tilde{U}_\xi(\mathbf{k},t) = \begin{cases} V_\xi(\mathbf{k},t), & t < T/2 \\ SV_\xi^*(-\mathbf{k},T-t)S, & t > T/2 \end{cases} \tag{B.19}$$

without breaking time-reversal symmetry or closing the quasi-energy gap at ξ. Now consider the following continuous deformation of $V_\xi(\mathbf{k},t)$:

$$V_\xi^s(\mathbf{k},t) = \begin{cases} V_\xi(k_x,k_y/s,,t), & k_y < 2\pi s \\ SV_\xi^*(k_x,0,t)S, & k_y > 2\pi s \end{cases} \tag{B.20}$$

for s from 1 to 2. Under this deformation $U_\xi(\mathbf{k},t)$ stays continuous and time-reversally symmetric, since $V_\xi(\mathbf{k},T/2) = 1$. Suppose now open boundary conditions are imposed on the system along the y-direction, such that the Floquet eigenstates, including any edge modes, still have well-defined y-momentum. The deformed system will then have a well-defined number of chiral edge modes in the $k_y \in [0,\pi]$ part of the 1-dimensional Brillouin zone. The net number of chiral edge modes here is given by $W[V_\xi]$. The system is still time-reversal symmetric however, so each of the edge modes in the $k_y \in [0,\pi]$ part of the Brillouin zone has a time-reversal (TR)-conjugate partner in the $k_y \in [\pi,2\pi]$ part. Hence the system has $W[V_\xi]$ TR-conjugate pairs of edge modes on each edge, and the number of pairs has parity ν_ξ. It is well-established that the parity of this number is a topological invariant [37]. Hence the number of edge-mode pairs in the quasi-energy gap ξ of the original system also parity ν_ξ.

B.4 Direct expressions for the chiral indices ν_0 and ν_π

In this appendix we show that the indices ν_0 and ν_π given in Eqs. (5.26) and (5.31) can be found from directly from time-evolution operator $U(k, T/2)$ in the expressions in Eq. (5.35). These expressions were also obtained in Ref. [13].

Expression for ν_0

We found in Eq. (5.26) that ν_0 can be found as the $\mathbb{Z}$ index $\nu[h_0]$ of the static chirally symmetric Hamiltonian h_0, given in Eq. (5.25). In the basis of eigenstates of S used in Eq. (A.2), h_0 takes the block off-diagonal form

$$h_0(k) = \begin{bmatrix} 0 & M(k) \\ M^\dagger(k) & 0 \end{bmatrix}. \tag{B.21}$$

ν_0 can then be found as [30]

$$\nu_0 = \frac{1}{2\pi i} \int_0^{2\pi} dk \mathrm{Tr}[M^{-1}(k)\partial_k M(k)]. \tag{B.22}$$

We note that the rhs is invariant under any continuous deformation of $M(k)$ that keeps $M(k)$ invertible for all k. In the basis of S-eigenstates used in Eq. (B.21), we remember $U(k, T/2)$ takes the form

$$U(k, T/2) = \begin{bmatrix} A(k) & B(k) \\ C(k) & D(k) \end{bmatrix}. \tag{B.23}$$

We recall from our analysis of 1-dimensional chirally symmetric systems Sec. 5.4, that $U(k, t)$ can be deformed into $e^{-ih_0(k)t}$ without breaking chiral symmetry or closing the quasi-energy gap at quasi-energy 0. From Eq. (5.25), we have that $e^{-ih_0(k)T/2} = -ih_0(k)T/\pi$. This means that under the deformation from $U(k, t)$ to $e^{-ih_0(k)t}$, $B(k)$ gets deformed into $-iM(k)T/\pi$. We claim that this deformation can be done without $B(k)$ ever becoming non-invertible.

To show this, suppose that somewhere during the deformation, $B(k_0)$ becomes non-invertible for some momentum k_0. At this point in the deformation, $B(k_0)v = 0$ for some nonzero vector v. However we always have

$$1 = U^\dagger(k, T/2)U(k, T/2)$$
$$U^\dagger(k, T) = U(k, T/2)SU^\dagger(k, T/2)S.$$

The first identity follows from unitarity of $U(k, T/2)$, while the second can be derived from the chiral symmetry condition eq. (5.22). By considering the matrix representation of $U(k, T/2)$ and S in this basis (B.23),(A.1), we deduce that at this point in the deformation,

$$U^\dagger(k_0, T) \begin{bmatrix} v \\ 0 \end{bmatrix} = \begin{bmatrix} v \\ 0 \end{bmatrix}. \tag{B.24}$$

Hence if $B(k_0)$ becomes non-invertible, during the deformation, the quasi-energy gap at 0 closes at k_0. However, we know that the quasi-energy gap at 0 stays open during the deformation. This

must mean that B stays invertible under the deformation, and hence it is possible to continuously deform $B(k)$ into $M(k)$ without $B(k)$ at any point becoming non-invertible. Thus

$$\nu_0 = \frac{1}{2\pi i}\int_0^{2\pi} dk \mathrm{Tr}[B^{-1}(k)\partial_k B(k)]. \tag{B.25}$$

Expression for ν_π

The proof follows an argument similar to the previous. We have that, in the same basis as the one used in Eq. (B.23), $U_\pi(k, T/2)$ takes the form

$$U_\pi(k, T/2) = \begin{bmatrix} N_\uparrow(k) & 0 \\ 0 & N_\downarrow(k) \end{bmatrix}, \tag{B.26}$$

where $N_\uparrow(k)$ and $N_\downarrow(k)$ are unitary matrices. As mentioned in our analysis of chirally symmetric systems, ν_π can be found directly from $U_\pi(k, T/2)$ as the winding number of the eigenvalues of $U_\pi(k, T/2)$ that correspond to eigenstates with S-eigenvalue 1, when k goes from 0 to 2π. In other words

$$\nu_\pi = \frac{1}{2\pi i}\int_0^{2\pi} dk \mathrm{Tr}[N_\uparrow^{-1}(k)\partial_k N_\uparrow(k)]. \tag{B.27}$$

As before, the rhs is invariant under any continuous deformation of $N_\uparrow(k)$ that keeps it invertible for all k. Consider the representation (B.23) of $U(k, T/2)$ in the same basis. Under the deformation from $U(k, t)$ to $U_\pi(k, t)$, $A(k)$ gets continuously deformed into $N_\uparrow(k)$. Suppose that at some point along the deformation, $A(k)$ becomes non-invertible. From a similar argument as for ν_0, it would then mean that $U^\dagger(k, T)$ would have eigenvalue -1, and the quasi-energy gap at π/T would close at k_0. We know that it is possible to continuously deform $U(k, t)$ into $U_\pi(k, t)$ without ever closing the quasi-energy gap at π/T. Hence it is possible to continuously deform $A(k)$ into $N_\uparrow(k)$ with $A(k)$ staying invertible under the entire deformation. This means that

$$\nu_\pi = \frac{1}{2\pi i}\int_0^{2\pi} dk \mathrm{Tr}[A^{-1}(k)\partial_k A(k)] \tag{B.28}$$

Appendix C

Frequency space approach

In this chapter, we present another complementary approach to the topological classification of periodically driven systems, namely the frequency space picture approach that was mentioned in Ref. [10]. This approach was followed in the first half of 2014. While the band-structure approach turned out to be more useful, the frequency space approach provides a complementary description of the problem that gives some further insight. Some of the contents of this chapter are furthermore helpful for the general understanding of periodically driven systems.

The basic idea is that there exists a well-defined mapping of any periodically driven systems in n dimensions a non-driven system in $n+1$ dimensions with an unbounded spectrum. The presently unknown topological invariants of the periodically driven system correspond to well-understood topological invariants of the non-driven system. The bulk-edge correspondence of a periodically driven system can thus be found form translating the time-dependent system to the non-driven system. This translation also requires imposing energy cutoff to deal with the unboundedness of the spectrum.

The challenge consists of finding a general way of doing this. I.e. using the approach to find the topological invariants directly from the time-evolution operator of the driven system.

The approach succeeded in deriving the bulk-edge correspondence for a $2d$ system without symmetries (the winding number obtained in Ref. [10]), and we found a generalization to $2n$ dimensions. In particular, we derived the Floquet analouge of the second Chern number, an invariant defined for a 4+1D system (see Ref. [48]). However, the approach turned out to be inconvenient when symmetries were introduced, and so it was eventually abandoned.

C.1 Setup of the system

The system we consider is a 2-dimensional lattice with M sites per unit cell, subject to a T-periodic time-dependent Hamiltonian with periodic boundary conditions.The Hamiltonian of the system is represented as an operator $H(\mathbf{k}, t)$ on the M-dimensional space $\mathcal{H}$ of periodic Bloch functions on the lattice. This space is spanned by the orbital eigenstates $\{|\alpha_i\rangle | i = 1...M\}$. Throughout this paper, Greek letters will indicate orbital eigenstates. The time evolution operator of the system is

$$U(k,t) = \mathcal{T} \exp\left(-i \int_0^t dt' H(\mathbf{k}, t')\right) \tag{C.1}$$

Where $\mathcal{T}$ the time-ordering operator. $U(\mathbf{k}, t)$ can be represented by an $M \times M$ matrix. Let us now take the $\mathbf{k}$-dependence to be implicit. Consider the operator $U(T)$, where T is the driving period. We can find and label the eigenstates of $U(T)$:

$$U(T)|n\rangle = e^{-iE_nT}|n\rangle, \quad n = 1...M \tag{C.2}$$

We will refer to these eigenstates as Floquet eigenstates, and the parameter E_n as the quasi-energy. This equation only defines E_n modulo $2\pi/T = \omega$ however, so there exists a Brillouin zone for quasi-energy, in the same way as there exists one for x and y-momentum.

The Floquet theorem and the frequency space picture

In general, it is impossible to obtain a nicer expression than (C.1) for the time evolution of the system, when the Hamiltonian is time-dependent. But when the time dependence is periodic, there is an exception. In the same way as a system with discrete translational symmetry can be solved with Bloch Functions, a system with discrete time-translation symmetry can be solved with a plane wave times a periodic pertubation. This is the central statement of the Floquet Theorem: for any eigenstate $|n\rangle$ of $U(T)$ with quasi-energy E_n, we can for some vector ${\phi^n}_\alpha(z)$ write

$$U(t)|n\rangle = e^{-iE_nt} \sum_{\alpha,z} {\phi^n}_\alpha(z)|\alpha\rangle e^{i\omega zt}. \tag{C.3}$$

In other words, we can write the time evolution $|n\rangle(t)$ of the Flouqet eigenstates as some periodic function $\sum {\phi^n}_\alpha(z) e^{i\omega zt}|\alpha\rangle$ times a "plane wave" e^{-iE_nt}. The vector components $\{{\phi^n}_\alpha(z)\}$ depend on the convention chosen for the quasi-energy: let E_n be a quasi-energy for the Floquet eigenstate $|n\rangle$ with ${\phi^n}_\alpha(z)$ solving the above equation. Then $E_n + \omega m$ is also a quasi-energy for the same eigenstate with ${\phi^n}_\alpha(z - m)$ solving the above equation. Here, m must be an integer. Hence picking a different "Brillouin zone" for the quasi-energy corresponds to a z-translation of ${\phi^n}_\alpha(z)$.

Extended Hilbert Space

Substituting (C.3) into the Schrodinger equation $H(t)U(t)|n\rangle = i\partial_t U(t)|n\rangle$ and projecting out the z'th Fourier component on both sides, we get

$$\sum_{z',\alpha} H^F_{\beta\alpha}(z, z'){\phi^n}_\alpha(z') = E_n {\phi^n}_\beta(z) \tag{C.4}$$

where

$$H^F_{\alpha\beta}(z,z') = \langle\beta|H(z-z') + \omega z\delta(z,z')|\alpha\rangle,\ H(t) = \sum_z e^{i\omega zt}H(z). \tag{C.5}$$

Here, $H(z)$ is the z'th fourier component of $H(t)$.

We can look at this as the Schrodinger equation of another system: Let $\mathcal{H}'$ be the Hilbert space spanned by the states $|\alpha, z\rangle\!\rangle$, where z is an integer, and α runs over the M orbital indices. On this new 3d lattice, we define the state $|n\rangle\!\rangle$ by

$$\langle\!\langle\alpha, z|n\rangle\!\rangle = \phi^n{}_\alpha(z) \tag{C.6}$$

and the operator H^F, which is called the Floquet Hamiltonian, by

$$\langle\!\langle z,\beta|H^F|z',\alpha\rangle\!\rangle = H^F_{\beta\alpha}(z,z') = \langle\beta|H(z-z') + \omega z\delta_{zz'}|\alpha\rangle. \tag{C.7}$$

In this picture, eq. (C.4) translates to an eigenvalue equation:

$$H^F|n\rangle\!\rangle = E_n|n\rangle\!\rangle. \tag{C.8}$$

$|n\rangle\!\rangle$ is related to the Flouqet eigenstate $|n\rangle$ through eq. (C.3), which in this picture becomes

$$U(t)|n\rangle = \sum_{\alpha,z}|\alpha\rangle\langle\!\langle\alpha, z|n\rangle\!\rangle e^{-i(E_n-\omega z)t} \tag{C.9}$$

Eqs. (C.8) and (C.9) determines the correspondence between the time evolution in the original Hilbert space $\mathcal{H}$ and the extended Hilbert space $\mathcal{H}'$. From now on, a single bracket $|\rangle$ indicates that the state lives in $\mathcal{H}$, while a double bracket $|\rangle\!\rangle$ indicates that the state lives in the extended Hilbert space $\mathcal{H}'$. Single-bracket states can be represented as M-dimensional vectors, while double-bracket states are represented by infinitely-dimensional vectors.

C.1.1 Labelling of Eigenstates

We now provide a labelling scheme for the eigenstates of H^F that will prove useful later on.

We found before that by translating an eigenstate of H^F in the z-direction, we can generate new eigenstates of H^F that all result in the same Floquet eigenstate. It therefore seems natural to split the set of eigenstates of H^F into families, where all eigenstates in one family corresponds to the same Floquet eigenstate. This means we will have to label the eigenstates of H^F with two indices: one index n denoting which Floquet eigenstate the state corresponds to and one index m distinguishing the different eigenstates in the same family. An obvious choice for the latter would be to sort the eigenstates according to their eigenvalues. Eigenstates with the same n but different m will then be copies of each other, just translated a number of steps in the z-direction, such that m by 1 means translating the state once in the z-direction. The space spanned by all eigenstates with the same m will be referred to as the *m'th quasi-energy zone*. This concept will be important later on for the derivation of anomalous bands.

In order to make the labelling complete, we have to pick out which states lie in the 0'th quasi-energy zone, since m runs from minus infinity to infinity. Later on, when we look at the number of edge modes in a gap, this free choice of the 0'th quasi-energy zone provides a compact way of dealing with the gap. I will now present the labelling scheme.

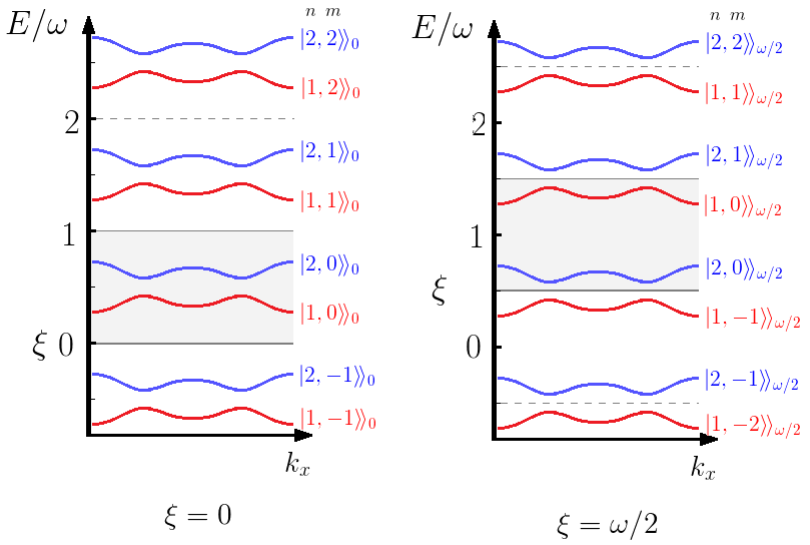

Figure C.1: Labelling of the bands of H^F for a 1-dimensional 2-level system with the scheme in C.1.1, given different values of ξ. The shaded area marks the first quasi-energy zone. The bands continue indefinitely in both directions

Labelling scheme Consider the Floquet eigenstate $|n\rangle$. For any $\xi \in \mathbb{R}$, we define the state $|n, m\rangle\!\rangle_\xi$ to be the unique eigenstate of H^F that results in the Floquet eigenstate $|n\rangle$ and has eigenvalue in the interval $[\xi + \omega m, \xi + \omega(m+1))$.
For the state $|n, m\rangle\!\rangle_\xi$, n indicates the Floquet eigenstate, and m denotes the number of the quasi-energy zone. The 0'th quasi-energy zone is defined to be spanned by all the eigenstates with eigenvalue between ξ and $\xi + \omega$. In this way, ξ marks the bottom of the 0'th quasi-energy zone. The index m corresponds to the variable z in the same way as the band number n corresponds to the orbital index α. A schematic example of the labelling scheme is provided in Fig. C.1.

For any choice of ξ, m, the physical solution to the time-dependent Schrodinger equation is simply

$$U(t)|n\rangle = \sum_{\alpha,z} |\alpha\rangle\langle\!\langle \alpha, z|n, m\rangle\!\rangle_\xi e^{-i(E(n)|_\xi + \omega(m-z))t} \tag{C.10}$$

where $|n\rangle$ is a Floquet eigenstate, and $E(n)|_\xi$ is the unique quasi-energy of $|n\rangle$ that lies in the interval $[\xi, \xi + \omega)$. In the subsequent sections, it turns out to be natural to define

$$U_\xi(t) = U(t)e^{iH^\xi_{\text{eff}}t}. \tag{C.11}$$

Here $H^\xi_{\text{eff}} = \frac{i}{T}\log(U(T))$ is the effective Hamiltonian, defined with the branch cut along $e^{-i\xi T}$. With this definition, H_{eff} returns the quasi-energy $E(n)|_\xi$ when acting on the Floquet eigenstate

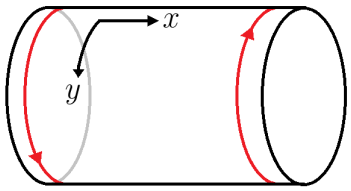

Figure C.2: Example of edge modes when edges are introduced in the x-direction. In this figure, the number of edge modes is -1

$|n\rangle$. As a result, eq. (C.10) becomes

$$U_\xi(t)|n\rangle = \sum_{\alpha,z} |\alpha\rangle\langle\!\langle \alpha, z|n, m\rangle\!\rangle_\xi e^{-i\omega(m-z))t}. \tag{C.12}$$

The operator $U_\xi(t)$ will be important for calculating the number of edge modes, as we will find in the next section.

C.2 Edge modes

In the same way as with energy, we can look at the quasi-energy spectrum as a band structure, the only difference being that the spectrum is not bounded above or below, but instead ω-periodic. We want to look at the number of edge modes arising when edges are introduced to the system. This number is defined as follows.

Consider a periodic system, whose bulk spectrum has a gap around some quasi-energy ξ. Now introduce edges in the x-direction, maintaining translational invariance in the y-direction. Thus k_y is still a good quantum number. As we wind k_y from 0 to 2π, consider the adiabatic evolution of the eigenstates and their quasi-energies. The number of edge modes in the gap, $n_{\text{edge}}(\xi)$, is defined as the net number of states on the upper edge of the sample which cross the gap during this evolution. See Fig C.2 for a picture of the system. By eq. (C.8), this is the same as the number of edge states of the Floquet Hamiltonian whose energies cross the gap at ξ.

There are two ways of calculating the number of edge modes, which we now review:

C.2.1 Method 1: Directly from the time evolution of the system

The following method is described in [10]. With this method, the number of edge modes is found directly from the time evolution operator $U(t)$ (the k-dependence of U is implicit). Referring to the proof in the article, let $U_\xi(t)$ be any operator that satisfies the following criteria

- $U_\xi(T) = 1$

- For some integer m, it is possible to smoothly deform $U_\xi(t)e^{i\omega mt}$ to $U(t)$[1].
- Throughout this deformation, the quasi-energy spectrum keeps its gap around ξ.

Then the number of edge modes crossing the gap at $E = \xi$ is

$$n_{\text{edge}}(\xi) = \frac{1}{8\pi^2}\int dtdk_xdk_y\ \text{Tr}[U_\xi^\dagger\partial_t U_\xi \cdot U_\xi^\dagger\partial_{k_x}U_\xi \cdot U_\xi^\dagger\partial_{k_y}U_\xi] - x \leftrightarrow y \tag{C.13}$$

An operator that has the above property property is

$$U_\xi(t) = U(t)e^{iH_{\text{eff}}^\xi t}. \tag{C.14}$$

Note that this operator is different from the one used in ref. [10].

Proof of property 1 The first property is trivially satisfied.

Proof of property 2 Let ξ be any real number. We note that there exists a ξ' and an integer m, such that $H_{\text{eff}}^\xi = H_{\text{eff}}^{\xi'} + \omega m$, where $\xi' \in [-\omega, 0)$. Consider the family

$$U^s(t) = U(t)e^{iH_{\text{eff}}^{\xi'}ts} \tag{C.15}$$

for $s \in [0, 1]$. This defines a smooth deformation as a function of s, and has $U^{s=0}(t) = U(t)$, $U^{s=1}(t) = U_\xi(t)e^{-i\omega mt}$. Thus property 2 is satisfied.

Proof of property 3 With the interpolation scheme above, consider the evolutions of quasi-energies $\{E(s)\}$. For requirement 1 to be satisfied the quasi-energy bands must be pushed to integer multiples of ω during the evolution, by property 3 the bands must never cross the gap during this evolution. Thus property 3 is equivalent to the requirement that if an evolution $E(s)$ satisfies $E(0) \in (\xi', \xi' + \omega)$, we must have $E(s) \in (\xi', \xi' + \omega)$ for all s between 0 and 1. Using $-\omega \leq \xi' \leq 0$, we have

$$\xi' \leq (1-s)\xi' < (1-s)E(0) < (1-s)(\omega + \xi') \leq (\omega + \xi') \tag{C.16}$$

Now consider $E(s)$. We have that $E(s) = E(0) - sE(0)|_{\xi'} = (1-s)E(0)$. Thus the requirement is fulfilled.

C.2.2 Method 2: From the bands of the Floquet Hamiltonian

Another method also described in [10] is to calculate the number of edge modes by considering the Floquet Hamiltonian defined in eq. (C.7). This can be seen as a Hamiltonian on a 3-d-lattice with translationally invariant local hopping terms. In addition to the hopping terms, a constant electric field of magnitude ω/e is applied in the z-direction, corresponding to the term ωz. The eigenstates of H^F on this lattice - including the edge states - will be localized in the z direction due

[1]That this is equivalent to the requirement in [10] can be seen by noting that the winding number in (C.13) is unchanged by the gauge transformation $U_\xi(t) \to e^{i\omega mt}U_\xi(t)$

to the boundedness of the kinetic energy. It is therefore meaningful to talk about the z-position of some energy.

If we place edges on the lattice in the z-direction, the eigenstates localized far away from the cutoff z's should therefore stay unchanged. In particular, the number of edge states in a gap should stay the same. Thus the number of edge states in the gap should be the same with or without the cutoff, if the "position" of the gap is far enough away from the cutoff.

With edges introduced, we can also look at the system as a 2-d system again, with the z index now denoting an additional orbital index rather than position. Due to the edges, the spectrum of H^F will be bounded. The number of edge states in a gap can then be found by summing the chern numbers of the bands below the gap. If we look at a gap far away from the cutoff, this gives a way of finding the number of edge modes in the untruncated system, c.f. the argument above.

C.3 Example: Edge modes of a 2-level system with single resonance and RWA

We consider a 2-level system subject to a time-dependent perturbation: $H(t) = H_0 + V\cos(\omega t)$ such that system has a single resonance. Here, V is a matrix. We have a time evolution operator associated with $H(t)$, defined by $U(t) = \mathcal{T}e^{-i\int_0^t dt' H(t')}$. We label the two Floquet bands associated with this Hamiltonian $|a\rangle$ and $|b\rangle$:

$$U(T)|a\rangle = e^{-iE_aT}|a\rangle, \quad U(T)|b\rangle = e^{-iE_bT}|b\rangle. \tag{C.17}$$

We will also make use of the bands $|\pm\rangle$ of the unperturbed Hamiltonian:

$$|\pm\rangle = \sum_\alpha u_{\pm,\alpha}|\alpha\rangle, \quad H_0|\pm\rangle = E_\pm|\pm\rangle. \tag{C.18}$$

We now look at the extended Hilbert space for the system. The Floquet Hamiltonian is

$$H^F = H_0 + \omega\hat{z} + \frac{1}{2}\sum_s V(s)(T + T^{-1}) \tag{C.19}$$

Where $V(s)$ is the s'th harmonic of the driving potential, and T is the z-translation operator: $T|\alpha, z\rangle\!\rangle = |\alpha, z+1\rangle\!\rangle$. $V(s)$ and H_0 only act on the 2-dimensional orbital space. The eigenstates of the unperturbed Floquet Hamiltonian are the states $\{|\pm, z\rangle\!\rangle\}$, where

$$|\pm, z\rangle\!\rangle = \sum_\alpha u_{\pm,\alpha}|\alpha, z\rangle\!\rangle, \quad (H_0 + \omega\hat{z})|\pm, z\rangle\!\rangle = (E_\pm + \omega z)|\pm, z\rangle\!\rangle \tag{C.20}$$

In order to find the eigenstates of H^F, we do the rotating wave approximation. This means that we only consider the driving potential to be relevant when there is a resonance. In the extended Hilbert space picture, this translates to only considering the perturbation when it couples bands that become degenerate somewhere in k-space. We assumed the existence of a single resonance, which means that the bands $|+, z\rangle\!\rangle$ and $|-, z+1\rangle\!\rangle$ become degenerate for some values of k. Degeneracy between any other pair of bands will imply higher resonances, which we

assumed didn't exist. Hence the perturbation can only mix the unperturbed bands two by two, and we can write the perturbed bands of the form

$$\begin{aligned} |a\rangle\!\rangle_z &= A_{+a}|+,z\rangle\!\rangle + A_{-a}|-,z+1\rangle\!\rangle \\ |b\rangle\!\rangle_z &= A_{+b}|+,z\rangle\!\rangle + A_{-b}|-,z+1\rangle\!\rangle \end{aligned} \tag{C.21}$$

See fig C.3. Here the a-states correspond to the Floquet eigenstate $|a\rangle$ through (C.9); the same holds for b. A is some matrix that can be found using perturbation theory in V.

Knowing the form of the eigenstates of H^F, we can now try to find the number edge modes that appear when edges are introduced. We will try to calculate this number using both methods described in the previous section.

Method 2

If we truncate the system at $z = 0$, we will get the 2d anomalous edge state $|-,0\rangle\!\rangle$ (see Fig. C.3), corresponding to the unperturbed eigenstate $|-\rangle$. It is easy to show that the Chern number of the a-bands equals minus the Chern number of the b-bands. Thus, summing the Chern numbers below the gap, we get (again referring to the figure)

$$n_{\text{edge}}(\omega) = C_- \quad n_{\text{edge}}(\omega/2) = C_- + C_a \tag{C.22}$$

where C_- is the Chern number of the band $|-,0\rangle\!\rangle$ which is the same as the chern number of the real-space band $|-\rangle$. In the same way, $C(a)$ is the Chern number of the real-space band $|a\rangle$.

Method 1

We now show that this is the same result gotten when using method 1. The energies of the states $|a\rangle_z$ and $|b\rangle_z$ are, respectively

$$E_a(z) = \omega(z + 1/2) - \epsilon \tag{C.23}$$

$$E_b(z) = \omega(z + 1/2) + \epsilon, \tag{C.24}$$

Where $0 < \epsilon < \omega/2$. We now try to express the eigenstates in terms of the labelling scheme we developed in sec. C.1.1. If we take $\xi = 0$, we must have the eigenvalue corresponding to $|a,0\rangle\!\rangle_\omega$ lying between 0 and ω. Looking at the expression for $E_a(z)$, we see that z must be zero for this to hold. Thus $|a,0\rangle\!\rangle_{\xi=0} = |a\rangle\!\rangle_0$. In this way, we get

$$\begin{aligned} |a,0\rangle\!\rangle_{\xi=0} &= |a\rangle\!\rangle_0 \\ |b,0\rangle\!\rangle_{\xi=0} &= |b\rangle\!\rangle_0 \\ |a,0\rangle\!\rangle_{\xi=\omega/2} &= |a\rangle\!\rangle_0 \\ |b,0\rangle\!\rangle_{\xi=\omega/2} &= |b\rangle\!\rangle_{-1} \end{aligned}$$

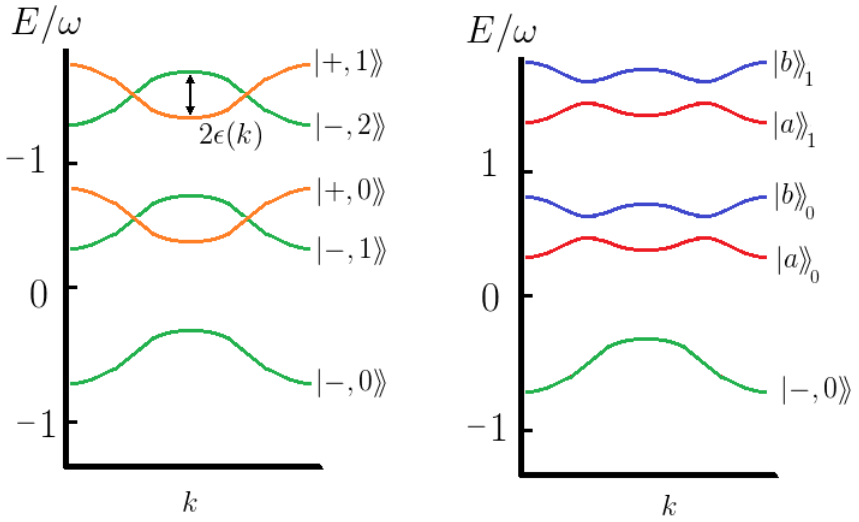

Figure C.3: Labelling of the bands of a truncated 2-level system (see eq. (C.21)). On the left is the unperturbed system, and on the right the system with the driving field pertubation. With the truncation, the lowest level state $|-,0\rangle\!\rangle$ is unaffected by the perturbation

Thus, setting $m = 0$ and $\xi = 0$ in eq. (C.12), and using the above

$$U_0(t)|a\rangle = \sum_{\alpha,z} |\alpha\rangle\langle\!\langle \alpha, z|a, 0\rangle\!\rangle_0 e^{i\omega z t} = A_{+a}|+\rangle + e^{i\omega t}A_{-a}|-\rangle$$

Doing the same for the other states, we get

$$\begin{aligned} U_0(t)|a\rangle &= A_{+a}|+\rangle + e^{i\omega t}A_{-a}|-\rangle \\ U_0(t)|b\rangle &= A_{+b}|+\rangle + e^{i\omega t}A_{-b}|-\rangle \\ U_{\omega/2}(t)|a\rangle &= A_{+a}|+\rangle + e^{i\omega t}A_{-a}|-\rangle \\ U_{\omega/2}(t)|b\rangle &= e^{-i\omega t}A_{+b}|+\rangle + A_{-b}|-\rangle \end{aligned} \tag{C.25}$$

Putting $t = 0$ we see that $A_{+a} = \langle +|a\rangle$, and so on. Thus

$$\begin{aligned} U_0(t) &= |+\rangle\langle +|a\rangle\langle a| + |+\rangle\langle +|b\rangle\langle b| + |-\rangle\langle -|a\rangle\langle a|e^{i\omega t} + |-\rangle\langle -|b\rangle\langle b|e^{i\omega t} \\ &= P_+ + P_- e^{i\omega t} \end{aligned} \tag{C.26}$$

Where $P_\pm = |\pm\rangle\langle\pm|$. We can do the same for $U_{\omega/2}$.

$$U_{\omega/2}(t) = (P_+ + e^{i\omega t}P_-)(P_a + e^{-i\omega t}P_b) \tag{C.27}$$

Where $P_a = |a\rangle\langle a|$ and same with b. We now look at the number of edge modes in the quasi-energy gap around $E = \omega$. We make use of

$$U_0^\dagger \partial_t U_0 = i\omega P_-, \quad \partial_k U_0 = (1 - e^{i\omega t})\partial_k P_+$$

Thus, using the formula given in [10]

$$\begin{aligned} n_{\text{edge}}(0) &= -\frac{1}{8\pi^2}\int dtd^2k\text{Tr}\left(U_0^\dagger\partial_t U_0\ \partial_{k_x}U_0^\dagger\ \partial_{k_y}U_0\right) - x \leftrightarrow y \\ &= -\frac{i\omega}{8\pi^2}\int dtd^2k\text{Tr}\left(P_-\partial_{k_x}P_-\partial_{k_y}P_-\right)(1-e^{i\omega t})(1-e^{-i\omega t}) - x \leftrightarrow y \\ &= -\frac{i\omega}{8\pi^2}\cdot 2\cdot\frac{2\pi}{\omega}\int dk_xdk_y\text{Tr}(P_-\partial_{k_x}P_-\partial_{k_y}P_-) - x \leftrightarrow y \\ &= \frac{1}{2\pi i}\int dk_xdk_y\text{Tr}(P_-\partial_{k_x}P_-\partial_{k_y}P_-) - x \leftrightarrow y \\ &= C_- \end{aligned} \tag{C.28}$$

Where C_- is the Chern number of the $-$-band. In the same way, we can look at the number of edge modes in the gap around $E = \omega/2$. There, we should use $U_{\omega/2}$ from (C.27) instead of U_0. Plugging in this operator in the above equation, one gets,

$$n_{\text{edge}}(\omega/2) = C_a + C_-$$

Although this requires some more algebra to show. Hence the two methods give the same result for this system.

C.4 Equivalence of the two methods in the general case

The above result is not a coincidence. We will now prove that method 1 and 2 are equivalent. We will do this under the assumption that the Floquet eigenstates only contain a finite range of harmonics. In other words, we assume that some $N \in \mathbb{Z}$ exists, such that the z'th fourier coefficient of $U_\xi(t)$ is zero if $|z| > N$. In the extended Hilbert space picture this translates to the physically sound approximation that the eigenstates of H^F are only nonzero within some z-range of width $2N$ (recall that they must be localized due to the boundedness of the kinetic energy).

Having proven the equivalence of the two methods under this assumption, we then note that even if no such N exist, we can still approximate any $U_\xi(t)$ arbitrarily well by an operator that satisfies the assumption for some sufficiently large N. We also expect the number of edge modes to be locally continuous as a function of $U_\xi(t)$: a small enough change of $U_\xi(t)$ shouldn't affect the presence of absence of edge modes. Thus, if the result holds for all finite N, the result will also hold in the limit $N \to \infty$.

C.4.1 Relating $U_\xi(t)$ to the extended Hilbert space picture

In order to relate the two methods, we begin by finding an expression for $U_\xi(t)$ in the extended Hilbert space picture. We found this operator in the end of sec. C.1.1. Beginning with eq. (C.12), we can write $U_\xi(t)$ in the spectral representation

$$U_\xi(t) = \sum_{\alpha,n,z} |\alpha\rangle\!\langle\!\langle \alpha, z|n, m\rangle\!\rangle_\xi \langle n|e^{-i\omega(m-z))t}. \tag{C.29}$$

This holds for any choice of quasi-energy zone ξ, m. The relation between the frequency space picture and the time evolution of the system can thus be summed up as follows: Let $U(T)|n\rangle = e^{-iE_nT}|n\rangle$. Then

$$H^F|n,m\rangle_\xi = (E(n)|_\xi + \omega m)|n,m\rangle\!\rangle_\xi \quad \text{and} \quad U_\xi(t) = \sum_{\alpha,n,z} |\alpha\rangle\langle\!\langle \alpha, z|n,m\rangle\!\rangle_\xi \langle n|e^{-i\omega(m-z))t} \tag{C.30}$$

Now, we make some general considerations about the state $|n,m\rangle\!\rangle_\xi$. We know that $|n,m\rangle\!\rangle_\xi$ lives in the extended Hilbert space $\mathcal{H}'$. It can therefore can be written in terms of the basis states $\{|\alpha,z\rangle\!\rangle\}$. We also know that changing m by one means translating $|n,m\rangle\!\rangle_\xi$ once in the z-direction. Hence, for any choice of unit cell n,ξ, we can write $|n,m\rangle\!\rangle_\xi$ on the form

$$|n,m\rangle\!\rangle_\xi = \sum_{\alpha,z} F^\xi_{n\alpha}(z)|\alpha, z+m\rangle\!\rangle$$

Also, the Floquet eigenstates can be expressed on the form

$$|n\rangle = \sum_\alpha A_{n\alpha}|\alpha\rangle \tag{C.31}$$

The matrices $F^\xi(z)$ and A are unitary, with $F^\xi(z)$ satisfying $\sum_z F^\xi(z)F^{\xi\dagger}(z) = I$. Due to the boundedness of the kinetic energy, $|n,m\rangle\!\rangle_\xi$ will be localized at some z, meaning $F^\xi(z)$ will go to zero for large $|z|$. Define now $B^\xi(z)$ by

$$B^\xi_{\alpha\beta}(z) = A^\dagger F^\xi_{\beta\alpha}(z). \tag{C.32}$$

Fixing $m = 0$ this allows us to write

$$U_\xi(t) = \sum_{\alpha,z,n} |\alpha\rangle\langle\!\langle \alpha, z|n,0\rangle\!\rangle_\xi \langle n|e^{i\omega zt} = \sum_{\alpha\beta z} |\alpha\rangle\langle\beta|B^\xi_{\alpha\beta}(z)e^{i\omega zt} \tag{C.33}$$

Thus $B_\xi(z) = \sum_{\alpha\beta}|\alpha\rangle\langle\beta|B^\xi_{\alpha\beta}(z)$ is simply the z'th fourier coefficient of U_ξ. Our assumption about $U_\xi(t)$ then means that $B_\xi(z) = 0$ for $|z| > N$. .

In the following, we will make extensive use of the projector into the m'th quasi-energy zone. (see sec. C.1.1 for definition). We can write it in terms of the B matrices

$$P_m = \sum_n |n,m\rangle\!\rangle_\xi \langle\!\langle n,m|_\xi = \sum_{n,\beta,\alpha,z} A_{n\alpha_1}A^*_{n\alpha_2}B^\xi_{\alpha_1\beta_1}(z_1-m)B^{\xi*}_{\alpha_1\beta_2}(z_2-m)|\beta_1,z_1\rangle\!\rangle\langle\!\langle\beta_2,z_2|. \tag{C.34}$$

Using the unitarity of A, we get

$$P_m = \sum_{z_1,z_2}\sum_{\alpha,\beta_1,\beta_2} B^\xi_{\alpha\beta_1}(z_1-m)B^{\xi*}_{\alpha\beta_2}(z_2-m)|\beta_1,z_1\rangle\!\rangle\langle\!\langle\beta_2,z_2|. \tag{C.35}$$

C.4.2 The Anomalous Projector

In the rest of this section we will take the ξ dependence of B to be implicit. Also, implicit summation over repeated orbital indices is used (i.e. summation over repeated greek letters).

Furthermore, we will make extensive use of the following identity that is equivalent to $U_\xi^\dagger(t)U_\xi(t) = 1$:

$$\delta_{\alpha\beta}\delta(m,n) = \sum_{z=-\infty}^{\infty} B^{\xi *}_{\alpha\gamma}(z+m)B^{\xi}_{\beta\gamma}(z+n). \tag{C.36}$$

Now we continue with the proof. Let $P_<$ be the projector into the subspace of all bands with quasi-energy below ξ, i.e. below our chosen 0'th quasi-energy zone. With the labelling scheme introduced in sec. C.1.1, we have

$$P_< = \sum_{m=-\infty}^{-1} P_m \tag{C.37}$$

We look closer at the semi-infinite sum of projectors on the rhs using eq. (C.35). We start by splitting the sum into two parts: the sum over terms where z_1 and z_2 are both greater than $-N$, and the sum over terms where this is not the case:

$$\begin{aligned}\sum_{m=-\infty}^{-1} P_m = &\sum_{z_1,z_2=-N+1}^{\infty}\sum_{m=1}^{\infty} B_{\alpha,\beta_1}(m+z_1)B^*_{\alpha,\beta_2}(m+z_2)|\beta_1,z_1\rangle\!\rangle\langle\!\langle\beta_2,z_2| \\ &+ \sum_{\min z_1,z_2\le -N}\sum_{m=1}^{\infty} B_{\alpha,\beta_1}(m+z_1)B^*_{\alpha,\beta_2}(m+z_2)|\beta_1,z_1\rangle\!\rangle\langle\!\langle\beta_2,z_2|.\end{aligned} \tag{C.38}$$

Here we also changed the sign of m. For the second term, we notice that if $m \le 0$, the terms vanish anyway since then either $z_1 + m \le -N$ or $z_2 + m \le -N$, $B(z) = 0$ for $z < -N$. Thus we might as well drop the boundary of summation for m. Then for this term we get, using eq. (C.36)

$$\sum_{\min(z_1,z_2)\le -N}\sum_{m=-\infty}^{\infty} B_{\alpha,\beta_1}(m+z_1)B^*_{\alpha,\beta_2}(m+z_2)|\beta_1,z_1\rangle\!\rangle\langle\!\langle\beta_2,z_2| = \sum_{z=-\infty}^{-N}|\alpha,z\rangle\!\rangle\langle\!\langle\alpha,z| \tag{C.39}$$

Thus the second term in eq. (C.38) is just the projector into the part of the lattice below $z = -N+1$. The first term which we call the anomalous projector, P^a, gives rise to the winding number, as will be proven in the following. It is given by

$$P^a = \sum_{z_i=-N}^{\infty}\sum_{m=0}^{\infty} B_{\alpha,\beta_1}(m+z_1)B^*_{\alpha,\beta_2}(m+z_2)|\beta_1,z_1\rangle\!\rangle\langle\!\langle\beta_2,z_2| \tag{C.40}$$

To sum up, we have found

$$P_< = \sum_{z=-\infty}^{-N} P_z + P^a \tag{C.41}$$

A graphical representation of this identity is shown in Fig. C.4

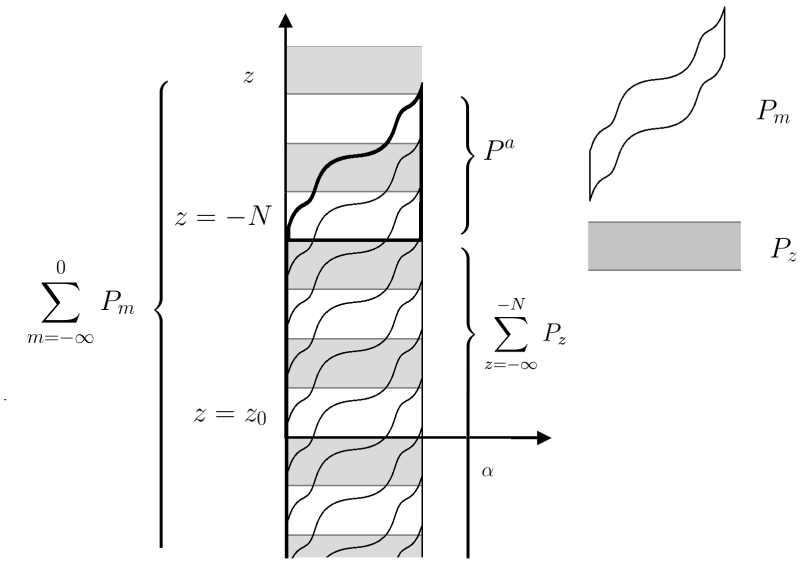

Figure C.4: A schematic representation of the Hilbert space and its subspaces. The horizontal direction indicates some abstract orbital index of the states, and the vertical axis indicates the harmonic index z. The interpretation is that the m'th subspace (projected into by P_m) consists of z-eigenstates with eigenvalues within some range. When stacking enough m-subspaces on top of each other, it should therefore be possible to "build" a complete z-subspace. Stacking infinitely many m-subspaces on top of each other should then result in an infitite sum of z-projectors, plus some residue, which we name the anomalous projector .

Relation between the anomalous projector and the edge modes

We now show that the number of edge modes can be found from the anomalous projector.

A truncation at z_0 can be implemented as follows: Let P_c project out all states with $z < z_0$. Then the Hamiltonian of the truncated system is $\bar{H} = P_c H P_c$. Let $P_<$ and $P_>$ be the the projectors into the states with energy below and above the gap centered at ξ, respectively, for the untruncated system, and let $\bar{P}_>$ and $\bar{P}_>$ denote the same for the truncated system (excluding the states that are projected out). We expect that when the system is truncated for some sufficiently large, negative z_0, the eigenstates of the Hamiltonian above the gap should be unaffected[2]. Thus the projector into the states with energy above the gap $P_>$ is the same for the truncated and untruncated system:

$$\bar{P}_> = P_>.$$

But then, since $\bar{P}_> + \bar{P}_< = P_c$

$$\bar{P}_< = P_c - \bar{P}_> = P_c - P_> = P_c(1 - P_>) = P_c P_<.$$

Here we used that $P_c P_> = P_>$, which follows from our hypothesis that $P_> = \bar{P}_>$. Now plugging in $P_<$ from eq. (C.41), we thus have

$$\bar{P}_< = \sum_{z=z_0}^{-N} P_z + P^a. \tag{C.42}$$

In order to find the sum of chern numbers below the gap in the truncated system we use the formula

$$\begin{aligned} n_{\text{edge}}(\xi) &= \frac{1}{2\pi i} \int dk_x dk_y \text{Tr}\left(\bar{P}_< \partial_{k_x} \bar{P}_< \partial_{k_y} \bar{P}_<\right) - x \leftrightarrow y \\ &= \frac{1}{2\pi i} \int dk_x dk_y \text{Tr}\left(P^a \partial_{k_x} P^a \partial_{k_y} P^a + \sum_{z=z_0}^{N} P_z \; \partial_{k_x} \sum_{z=z_0}^{N} P_z \; \partial_{k_y} \sum_{z=z_0}^{N} P_z\right) - x \leftrightarrow y \\ &= \frac{1}{2\pi i} \int dk_x dk_y \text{Tr}\left(P^a \partial_{k_x} P^a \partial_{k_y} P^a\right) - x \leftrightarrow y. \end{aligned} \tag{C.43}$$

Between the second and third line we usd the fact that $\partial_{k_i} \sum_{z=z_0}^{-N} P_z = 0$ to eliminate the second term. Now all that is left is to prove that the number of edge modes obtained with this formula is the same as the formula given in [10].

Example: 2-level system

To gain a better understanding for the steps above, we can again consider the single resonance 2-level system. By changing basis from $B_{\alpha\beta}$ to B_{+a} and so on, and examining eqs. (C.27) and (C.33), we find that

$$\begin{aligned} B(1) &= P_- P_a \\ B(0) &= P_+ P_a + P_- P_b \\ B(-1) &= P_+ P_b \end{aligned} \tag{C.44}$$

[2]This can be proven from our assumption about B

In this case, owing to the rotating wave approximation, we exactly have that $B(z) = 0$ if $|z| > 1$. So the anomalous projector can be taken to be

$$\begin{aligned} P^a &= \sum_{m=0}^{\infty} \sum_{z_1,z_2=0}^{\infty} B^\dagger(m+z_1)B(m+z_2) \\ &= B^\dagger(0)B(0) + B^\dagger(0)B(1) + B^\dagger(1)B(0) + 2B^\dagger(1)B(1) \\ &= P_a + P_- \end{aligned} \tag{C.45}$$

Plugging this into (C.43), we obtain the expected Chern number. For the case $\xi = \omega$, it is even easier to show that $P^a = P_-$.

C.4.3 Proof of equivalence of the winding number formula and the sum anomalous chern numbers

Having defined the sum of chern numbers within the anomalous projector, we have to prove that this is the same as the winding number in eq. (C.13).

Part 1 - Eliminating redundant variables and summation bounds

Plugging the anomalous projector from eq. (C.38) into eq. (C.43) we have:

$$n_{\text{edge}}(\xi) = \frac{1}{2\pi i} \int dk_x dk_y \text{Tr}[I(\xi)] - x \leftrightarrow y \tag{C.46}$$

where the integrand $I(\xi)$ is defined by

$$I(\xi) = \sum_{m_i=0}^{\infty} \sum_{z_i=-N}^{\infty} B(m_1+z_1)B^\dagger(m_1+z_2)\partial_x \left[B(m_2+z_2)B^\dagger(m_2+z_3)\right] \partial_y \left[B(m_3+z_3)B^\dagger(m_3+z_1)\right]. \tag{C.47}$$

In the subsequent, we will make use of the fact that we are only using the trace of $I(\xi)$, and that the result has to be antisymmetrized in x and y. Changing variables to

$$a = m_1 + z_2 \quad b = m_2 + z_2 \quad c = m_3 + z_2 \quad r = z_1 - z_2 \quad s = z_3 - z_2$$

we get for $I(\xi)$

$$I(\xi) = \sum_{abc=-N}^{\infty} \sum_{z_2=-N}^{\min(a,b,c)} \sum_{r=-N-z_2}^{\infty} \sum_{s=-N-z_2}^{\infty} B(a+r)B^\dagger(a)\partial_x \left[B(b)B^\dagger(b+s)\right] \partial_y \left[B(c+s)B^\dagger(c+r)\right] \tag{C.48}$$

Now, we can perform the sum on z_2. In order to save space, we introduce

$$f(a,b,c,r,s) = B(a+r)B^\dagger(a)\partial_x \left[B(b)B^\dagger(b+s)\right] \partial_y \left[B(c+s)B^\dagger(c+r)\right]$$

For each (a, b, c, r, s), this term appears several times in the sum, namely once for each z_2 in the interval $[-N, \min(a, b, c)]$ for which $r \geq -N - z_2$ and $s \geq -N - z_2$. This is just the number of integers between $\max(-N, -N - r, -N - s)$ and $\min(a, b, c)$. Thus

$$I(\xi) = \sum_{abc=-N}^{\infty} \sum_{r,s=-N-\min(a,b,c)}^{\infty} N_{abcrs} f(a, b, c, r, s), \tag{C.49}$$

where N_{abcrs} is

$$N_{abcrs} = \min(a, b, c) + \min(r, s, 0) + N. \tag{C.50}$$

The fact that number must never be negative is taken care of by the summation bounds: for all terms, $\min(r, s, 0) \geq -N - \min(a, b, c)$. Now, we notice that we can relax the summation bounds. Firstly, we see that we can take the lower bound on the abc sum to minus infinity without changing the sum. Secondly, we note, that if $r < -N - \min(a, b, c)$, we have that $\min(a + r, b + r, c + r) < -N$. The only case where this doesn't result in vanishing terms is when $\min(a, b, c) = b$. Hence $r < -N - \min(a, b, c)$ implies $r < -N - b$ for the nonvanishing terms. However, if $r < -N - b$, then $-N \leq r + c < -N - b + c$. This implies $c > b$. In the same way, we find $a > b$. Thus $r < -N - b$ implies $\min(a, b, c) = b$. All together, these arguments provide a bi-implication for nonvanishing terms:

$$r < -N - \min(a, b, c) \Leftrightarrow r < -N - b$$

As well as

$$r < -N - b \Rightarrow \min(a, b, c) = b$$

With this in mind, we rewrite $I(\xi)$:

$$\begin{aligned} I(\xi) = &\sum_{abc=-N}^{\infty} \sum_{r=-\infty}^{\infty} \sum_{s=-N-\min(a,b,c)}^{\infty} N_{abcrs} f(a, b, c, r, s) \\ &- \sum_{abc=-N}^{\infty} \sum_{r=-\infty}^{-N-\min(a,b,c)-1} \sum_{s=-N-\min(a,b,c)}^{\infty} N_{abcrs} f(a, b, c, r, s) \end{aligned}$$

For the second term, we use the above results to redefine the summation domain:

$$\begin{aligned} &\sum_{abc=-N}^{\infty} \sum_{r=-\infty}^{-N-\min(a,b,c)-1} \sum_{s=-N-\min(a,b,c)}^{\infty} N_{abcrs} f(a, b, c, r, s) \\ &= \sum_{abc=-\infty}^{\infty} \sum_{r=-\infty}^{-N-b-1} \sum_{s=-N-b}^{\infty} (N + \min(r, s, 0) + b) f(a, b, c, r, s) \end{aligned}$$

Then, using the identity (C.36), we can perform the sum over c to obtain zero

$$\begin{aligned} \sum_{c=-\infty}^{\infty} f(a, b, c, r, s) &= B(a + r) B^{\dagger}(a) \partial_x \left[B(b) B^{\dagger}(b + s) \right] \partial_y \left[\sum_{c=-\infty}^{\infty} B(c + s) B(c + r) \right] \\ &= B(a + r) B^{\dagger}(a) \partial_x \left[B(b) B^{\dagger}(b + s) \right] \partial_y \delta_{rs} = 0. \end{aligned} \tag{C.51}$$

Thus we don't have to impose $r < -N - \min(a,b,c)$, since the terms below $r < -N - \min(a,b,c)$ cancel each other out anyway. In the same way we can relax the summation bound for s. We are now left with

$$C = \sum_{abcrs=-\infty}^{\infty} (\min(a,b,c) + N + \min(r,s,0)) f(a,b,c,r,s) \tag{C.52}$$

Now, the two last terms don't depend on b or c, so for these, we can sum out b or c and obtain a zero, in the same way as we did in eq. (C.51). Thus we are finally down to

$$I(\xi) = \sum_{abcrs=-\infty}^{\infty} \min(a,b,c) B(a+r)B^\dagger(a)\partial_x \left[B(b)B^\dagger(b+s)\right] \partial_y \left[B(c+s)B^\dagger(c+r)\right] \tag{C.53}$$

Part 2 - Simplifying the sum

Expanding the derivatives in the above expression, and changing the sign of s, we have

$$\begin{aligned}
I(\xi) &= \sum_{abcrs=-\infty}^{\infty} \min(a,b,c) B(a+r)B^\dagger(a)\partial_x \left[B(b)B^\dagger(b-s)\right] \partial_y \left[B(c-s)B^\dagger(c+r)\right] \\
&= \sum_{-\infty}^{\infty} \min(a,b,c) \left[B(a+r)B^\dagger(a) \cdot \partial_x B(b)B^\dagger(b-s) \cdot \partial_y B(c-s)B^\dagger(c+r)\right] && T_1 \\
&+ \sum_{-\infty}^{\infty} \min(a,b,c) \left[B(a+r)B^\dagger(a) \cdot B(b)\partial_x B^\dagger(b-s) \cdot \partial_y B(c-s)B^\dagger(c+r)\right] && T_2 \\
&+ \sum_{-\infty}^{\infty} \min(a,b,c) \left[B(a+r)B^\dagger(a) \cdot \partial_x B(b)B^\dagger(b-s) \cdot B(c-s)\partial_y B^\dagger(c+r)\right] && T_3 \\
&+ \sum_{-\infty}^{\infty} \min(a,b,c) \left[B(a+r)B^\dagger(a) \cdot B(b)\partial_x B^\dagger(b-s) \cdot B(c-s)\partial_y B^\dagger(c+r)\right] && T_4.
\end{aligned} \tag{C.54}$$

Here we have labeled the four terms T_1, T_2, T_3, T_4. We will evaluate these terms separately. In order to do his, we will make use of an identity derived from eq. (C.36):

$$\sum_z \partial_x B^\dagger(z+y)B(z) = -\sum_z B^\dagger(z+y)\partial_x B(z) \tag{C.55}$$

Evaluating T_1: For T_1, we start by eliminating two B's using the identity (C.36) for the sum over r.

$$T_1 = \sum \min(a,b) B^\dagger(a)\partial_x B(b)B^\dagger(b-s)\partial_y B(a-s)$$

By doing the variable shift $a, b \to b+s, a+s$, we get

$$T_1 = \sum (\min(a,b)+s) B^\dagger(a+s)\partial_x B(b+s)B^\dagger(b)\partial_y B(a).$$

Now we switch a and b and let $s \to -s$

$$T_1 = \sum (\min(a,b)-s) B^\dagger(b-s)\partial_x B(a-s)B^\dagger(a)\partial_y B(b).$$

Exploiting the cyclic property of the trace and xy antisymmetrization:

$$T_1 = -\sum(\min(a,b)-s)B^\dagger(a)\partial_x B(b)B^\dagger(b-s)\partial_y B(a-s)$$

We recognize the first term as $-T_1$, so we finally have

$$T_1 = \frac{1}{2}\sum s\ B^\dagger(a)\partial_x B(b)B^\dagger(b-s)\partial_y B(a-s) \tag{C.56}$$

Evaluating T_2: To evaluate the second term we make a similar approach. Eliminating two $B's$ with the identity (C.36) and changing variables $a, b \to a+s, b+s$:

$$T_2 = (\sum \min(a,b)+s)B^\dagger(a+s)B(b+s)\cdot\partial_x B^\dagger(b)\partial_y B(a)$$

For the first term we can again sum out 2 B's to obtain

$$T_2 = \sum a\partial_x B^\dagger(a)\partial_y B(a) + sB^\dagger(a+s)B(b+s)\cdot\partial_x B^\dagger(b)\partial_y B(a) \tag{C.57}$$

Using the antisymmetrization and restoring x-integration, we can rewrite the first term:

$$\begin{aligned}\sum a\partial_x B^\dagger(a)\partial_y B(a) - x\leftrightarrow y &= \sum\int dk_x\partial_x(aB^\dagger(k_x,a)\partial_y B(k_x,a)) - x\leftrightarrow y \\ &= \sum a(B^\dagger(2\pi,a)\partial_y B(2\pi,a)) - B^\dagger(0,a)\partial_y B(0,a)) - x\leftrightarrow y \end{aligned}\tag{C.58}$$

However, we must have $B(k_x,z) = B(k_x+2\pi,z)$[3]. Thus we can throw this term away. For the second term in eq. (C.57), we shift the x-derivative once, using the identity (C.55) to get

$$T_2 = -\sum sB^\dagger(a+s)\partial_x B(b+s)\cdot B^\dagger(b)\partial_y B(a)$$

With a proper variable shift and comparing with the expression for T_1 (C.56), we recognize this as

$$T_2 = -2T_1 \tag{C.59}$$

Evaluating T_3: Now we look at T_3. Here we can also sum out two B's at first:

$$T_3 = \sum \min(a,b)B(a+s)B^\dagger(a)\cdot\partial_x B(b)\partial_y B^\dagger(b+s)$$

Making use of the trace cyclicity and shifting the y-derivative

$$T_3 = -\sum \min(a,b)B^\dagger(a)\partial_x B(b)\cdot B^\dagger(b+s)\partial_y B(a+s)$$

Changing $s\to -s$ we recognize this as

$$T_3 = -T_1 \tag{C.60}$$

[3]Since the Hamiltonian satisfies $H(k_x) = H(k_x+2\pi)$, and $U_\xi(k,t)$ is fully determined by the Hamiltonian at momentum k, its fourier coefficients $B(k,z)$ must also satisfy $B(k_x,z) = B(k_x+2\pi,z)$.

Evaluating T_4: Finally, we have T_4. We cannot sum any pair of B's out immediately, but doing the variable shift $r \to r-s$, $a, b, c \to a, b, c+s$

$$T_4 = \sum (\min(a,b,c)+s) B(a+r) B^\dagger(a+s) \cdot B(b+s)\partial_x B^\dagger(b) \cdot B(c)\partial_y B^\dagger(c+r)$$

Now we can sum out the s's for the first term and the a's for the second term:

$$\begin{aligned} T_4 = &\sum \min(a,c) B(a+r)\partial_x B^\dagger(a) \cdot B(c)\partial_y B^\dagger(c+r) && T_{41} \\ &+ \sum s B(a+r) B^\dagger(a+s) \cdot B(b+s)\partial_x B^\dagger(b) \cdot B(c)\partial_y B^\dagger(c+r) && T_{42} \end{aligned}$$

Where we named the first term T_{41} and the second T_{42}. For T_{41} we start by shifting the y derivative and changing variables $a, c \to a-r, c-r$:

$$T_{41} = \sum (\min(a,c)-r) \cdot \partial_y B(a)\partial_x B^\dagger(a-r) \cdot B(c-r) B^\dagger(c)$$

For the second term, we can sum out the c's to obtain something xy symmetric, so this can be thrown away. For the first term we shift the x derivative and use the cyclic property of the trace:

$$T_{41} = \sum \min(a,c) \cdot B^\dagger(c)\partial_y B(a) \cdot B^\dagger(a-r)\partial_x B(c-r)$$

Using the antisymmetrization, we recognize this as

$$T_{41} = -T_1 \tag{C.61}$$

For T_{42} we can sum out the a's to get

$$T_{42} = \sum s \cdot B(b+s)\partial_x B^\dagger(b) \cdot B(c)\partial_y B^\dagger(c+s)$$

Shifting both ∂_x and ∂_y we get

$$T_{42} = \sum s B^\dagger(c+s)\partial_x B(b+s) \cdot B^\dagger(b)\partial_y B(c)$$

By changing variables, we finally see

$$T_{42} = \sum s B^\dagger(c)\partial_x B(b) \cdot B^\dagger(b-s)\partial_y B(c-s) = 2T_1 \tag{C.62}$$

So $T_4 = T_1$. Remembering $T_2 = -2T_1$, $T_3 = -T_1$, we finally find

$$n_{\text{edge}}(\xi) = (1-2-1+1)T_1 = -T_1 = -\frac{1}{2}\sum s\ B^\dagger(a)\partial_x B(b) \cdot B^\dagger(b-s)\partial_y B(a-s) \tag{C.63}$$

Part 3 - Relating the sum to the winding number formula

Restoring the prefactor, trace, and integrals

$$n_{\text{edge}}(\xi) = -\frac{1}{4\pi i}\int dk_x dk_y \text{Tr}\left[s \sum_{abs=-\infty}^{\infty} B^\dagger(a)\partial_{k_x} B(b) \cdot B^\dagger(b-s)\partial_{k_y} B(a-s) \right] \tag{C.64}$$

Rearranging the factors and summation variables, and adding a vanishing term gives

$$\begin{aligned} n_{\text{edge}}(\xi) &= \frac{1}{4\pi i}\int dk_x dk_y \text{Tr}\left[(s+b)\sum_{abs=-\infty}^{\infty} B^\dagger(a+s)B(b+s)\cdot\partial_{k_x}B^\dagger(b)\partial_{k_y}B(a)\right] \\ &= \frac{1}{4\pi i}\int dk_x dk_y \text{Tr}\left[\sum_{z_i=-\infty}^{\infty} z_2\ B^\dagger(z_1)B(z_2)\cdot\partial_{k_x}B^\dagger(z_3)\partial_{k_y}B(z_4)\delta(z_2+z_4-z_1-z_3)\right] \end{aligned} \tag{C.65}$$

Re-expressing the delta function by its Fourier transform:

$$\begin{aligned} n_{\text{edge}}(\xi) &= \frac{1}{4\pi iT}\int dk_x dk_y \int_0^T dt \text{Tr}\left[\sum_{z_i=-\infty}^{\infty} z_2\ B^\dagger(z_1)B(z_2)\cdot\partial_{k_x}B^\dagger(z_3)\partial_{k_y}B(z_4)e^{i\omega t(z_2+z_4-z_1-z_3)}\right] \\ &= -\frac{1}{8\pi^2}\int dk_x dk_y \int_0^T dt \text{Tr}\left[\sum_{z_i=-\infty}^{\infty} i\omega z_2\ B^\dagger(z_1)B(z_2)\cdot\partial_{k_x}B^\dagger(z_3)\partial_{k_y}B(z_4)e^{i\omega t(z_2+z_4-z_1-z_3)}\right] \end{aligned} \tag{C.66}$$

Going back to eq. (C.33) we see that this is just a product of U_ξ's expressed in terms of their fourier coefficients:

$$\begin{aligned} n_{\text{edge}}(\xi) &= -\frac{1}{8\pi^2}\int dt dk_x dk_y \text{Tr}\left[U_\xi^\dagger(t)\partial_t U_\xi(t)\cdot\partial_{k_x}U_\xi^\dagger(t)\partial_{k_y}U_\xi(t)\right] \\ &= \frac{1}{8\pi^2}\int dt dk_x dk_y \text{Tr}\left[U_\xi^\dagger(t)\partial_t U_\xi(t)\cdot U_\xi^\dagger(t)\partial_{k_x}U_\xi(t)\cdot U_\xi^\dagger(t)\partial_{k_y}U_\xi(t)\right] - x\leftrightarrow y \end{aligned} \tag{C.67}$$

So the sum of Chern numbers in the anomalous projector gives the winding number, eq. (C.13), derived in ref. [10]. We have thus shown that method 1 and 2 are equivalent.

C.5 The topological invariant corresponding to the n'th Chern number

Here, we generalize the result of the previous section to obtain the invariant analogous to the n'th Chern number. The invariant is defined for a periodically driven system in $2n$ spatial dimensions. For $2n$ dimensional system, the n'th Chern number is [48]

$$C_n = \frac{(-1)^n}{(2\pi i)^n n!}\int d^{2n}k \text{Tr}\left[P_<\prod_{i=1}^{2n}\partial_{k_{n_i}}P_<\right]\cdot\epsilon_{n_1 n_2 \ldots n_{2n}} \tag{C.68}$$

Where $P_<$ is already defined. Since $P_< = P_a + P_{z<-N}$, we can replace $P_<$ with P_a, since the derivatives of the other term vanish. Hence

$$C_n = \frac{(-1)^n}{(2\pi i)^n n!}\int d^{2n}k\ I(\xi), \quad I(\xi) = \text{Tr}\left[P_a\prod_{i=1}^{2n}\partial_{n_i}P_a\right]\cdot\epsilon_{n_1 n_2 \ldots n_{2n}} \tag{C.69}$$

Plugging in the expression for P_a,

$$I(\xi) = \sum_{M\geq 0}\sum_{z_i\geq -N}\sum_{m_i\geq 0}\left[U(z_{2n+1}+M)U^\dagger(z_1+M)\prod_{i=1}^{2n}\partial_{n_i}\left[U^\dagger(z_i+m_i)U(z_{i+1}+m_i)\right]\right]\cdot\epsilon_{n_1n_2\ldots n_{2n}} \tag{C.70}$$

Changing variables, $z_i \to z_i - M$, $m_i \to m_i + M$,

$$I(\xi) = \sum_{M\geq 0}\sum_{z_i\geq -N+M}\sum_{m_i\geq -M}\left[U(z_{2n+1})U^\dagger(z_1)\prod_{i=1}^{2n}\partial_{n_i}\left[U^\dagger(z_i+m_i)U(z_{i+1}+m_i)\right]\right]\cdot\epsilon_{n_1n_2\ldots n_{2n}} \tag{C.71}$$

Now, for every configuration of $(z_1...z_{2n+1}, m_1...m_{2n})$, the same term appears a number of times, namely the number of M's that satisfy the following

$$M \geq 0, \quad z_i \geq -N + M, \quad m_i \geq -M \tag{C.72}$$

Call this number $N(z_1...z_{2n+1}, m_1...m_{2n})$. We have

$$\begin{aligned} N(z_1...z_{2n+1}, m_1...m_{2n}) &= \min(z_1...z_{2n+1}) + N - \max(-m_1... - m_{2n}, 0) \\ &= \min(z_1...z_{2n+1}) + \min(0, m_1...m_{2n}) + N \end{aligned} \tag{C.73}$$

Hence

$$\begin{aligned} I(\xi) = \sum_{(z_1...z_{2n+1}, m_1...m_{2n})\in C} &(\min(z_1...z_{2n+1}) + \min(0, m_1...m_{2n}) + N) \\ &\left(U(z_{2n+1})U^\dagger(z_1)\prod_{i=1}^{2n}\partial_{n_i}\left[U^\dagger(z_i+m_i)U(z_{i+1}+m_i)\right]\right)\cdot\epsilon_{n_1n_2\ldots n_{2n}} \end{aligned}$$

Where C is the set of configurations $(z_1...z_{2n+1}, m_1...m_{2n})$ where an integer M exists such that

$$\max(0, -m_1... - m_{2n}) \leq M \leq \min(z_1...z_{2n+1}) + N \tag{C.74}$$

Hence it is equal to the set of configurations where

$$\max(0, -m_1... - m_{2n}) \leq \min(z_1...z_{2n+1}) + N \tag{C.75}$$

This is the set of all configurations $(z_1...z_{2n+1}, m_1...m_{2n})$ where $z_i \geq -N + \max(0, -m_1... - m_{2n}) = -N - \min(0, m_1...m_{2n})$. Thus

$$\begin{aligned} I(\xi) = \sum_{m_i=-\infty}^{\infty}\sum_{z_i\geq -N-\min(0,m_1...m_{2n})} &(\min(z_1...z_{2n+1}) + \min(0, m_1...m_{2n}) + N) \\ &\left(U(z_{2n+1})U^\dagger(z_1)\prod_{i=1}^{2n}\partial_{n_i}\left[U^\dagger(z_i+m_i)U(z_{i+1}+m_i)\right]\right)\cdot\epsilon_{n_1n_2\ldots n_{2n}} \end{aligned}$$

Now, we note that if $z_j < -N - \min(0, m_1...m_{2n})$, we have for nonvanishing terms

$$\min(0, m_1...m_{2n}) \notin \{m_j, m_{j-1}\} \tag{C.76}$$

Otherwise either $z_j + m_j < -N$ or $z_j + m_{j-1} < -N$, and one of the factors in the product would be zero[4]. But this means that $\min(0, m_1...m_{2n}) = \min(0, m_1...m_{j-2}, m_{j+1}..., m_{2n})$. But then the only part of the summand that depends on m_j is the factor

$$\partial_{n_j}\left[U^\dagger(z_j + m_j)U(z_{j+1} + m_j)\right].$$

Thus the terms with $z_j < -N - \min(0, m_1...m_{2n})$ will contain the following factor

$$\sum_{m_j=-\infty}^{\infty} \partial_{n_j}\left[U^\dagger(z_j + m_j)U(z_{j+1} + m_j)\right] = \partial_{n_j}\left[\delta_{z_j z_{j+1}}\right] = 0$$

Hence terms with $z_j < -N - \min(0, m_1...m_{2n})$ vanish. The result can easily be generalized to cases where multiple z's are smaller than $-N - \min(0, m_1...m_{2n})$ or if $j = 1$ or $j = 2n + 1$. Thus

$$\begin{aligned} I(\xi) = &\sum_{m_i=-\infty}^{\infty} \sum_{z_i \geq -N - \min(0, m_1...m_{2n})} (\min(z_1...z_{2n+1}) + \min(0, m_1...m_{2n}) + N) \\ &\left(U(z_{2n+1})U^\dagger(z_1)\prod_{i=1}^{2n}\partial_{n_i}\left[U^\dagger(z_i + m_i)U(z_{i+1} + m_i)\right]\right)\cdot\epsilon_{n_1 n_2 ... n_{2n}} \\ = &\sum_{m_i=-\infty}^{\infty}\sum_{z_i=-\infty}^{\infty} (\min(z_1...z_{2n+1}) + \min(0, m_1...m_{2n}) + N) \\ &\left(U(z_{2n+1})U^\dagger(z_1)\prod_{i=1}^{2n}\partial_{n_i}\left[U^\dagger(z_i + m_i)U(z_{i+1} + m_i)\right]\right)\cdot\epsilon_{n_1 n_2 ... n_{2n}} \end{aligned}$$

Now for terms with the prefactor $\min(z_1...z_{2n+1}) + N$, we can sum out the m's as before to get the vanishing derivative of a delta function, so

$$I(\xi) = \sum_{m_i, z_i=-\infty}^{\infty} \min(0, m_1...m_{2n})\left(U(z_{2n+1})U^\dagger(z_1)\prod_{i=1}^{2n}\partial_{n_i}\left[U^\dagger(z_i + m_i)U(z_{i+1} + m_i)\right]\right)\cdot\epsilon_{n_1 n_2 ... n_{2n}} \tag{C.77}$$

We recognize this as

$$I(\xi) = \sum_{m_i}\min(0, m_1...m_{2n})\cdot\left(P_0\prod_{i=1}^{2n}\partial_{n_i}P_{m_i}\right)\cdot\epsilon_{n_1...n_{2n}} \tag{C.78}$$

Where P_m is the m'th quasi-energy zone projector. This is a nice expression, since it gives the winding number in terms of bulk operators on $\mathcal{H}^a$. No truncation has to be made to calculate the winding number.

[4]Strictly speaking, thiss is only a proof for the case $1 < j < 2n + 1$, but the argument is easily generalized to $j = 1$ and $j = 2n + 1$

C.5.1 Calculating the second Chern number

For $n = 2$, we expand the derivatives and obtain sixteen terms. Using the projector property, we reduce this to four terms:

$$\begin{aligned} I(\xi) = \sum_{m_i} \epsilon_{\mu\nu\lambda\sigma} \mathrm{Tr} & \\ & 4\min(m_1, m_2, 0) \cdot \partial_\mu |m_1\rangle\!\rangle \partial_\nu \langle\!\langle m_1| \cdot \partial_\lambda |\nu, 0\rangle\!\rangle \partial_\sigma \langle\!\langle 0| P_{m_2} && 4T_1 \\ & + 3\min(m_1, m_2, 0) \cdot \partial_\mu |0\rangle\!\rangle \partial_\nu \langle\!\langle 0| \cdot \partial_\lambda |m_1\rangle\!\rangle \partial_\sigma \langle\!\langle m_1| P_{m_2} && 3T_2 \\ & - 1\min(m_1, m_2, 0) \cdot \partial_\mu |m_1\rangle\!\rangle \partial_\nu \langle\!\langle m_1| \cdot \partial_\lambda |m_2\rangle\!\rangle \partial_\sigma \langle\!\langle m_2| P_0 && -T_3 \\ & - \min(m_1, m_2, m_3, 0) \cdot P_{m_1} \partial_\mu |m_2\rangle\!\rangle \partial_\nu \langle\!\langle m_2| \cdot P_{m_3} \partial_\lambda |0\rangle\!\rangle \partial_\sigma \langle\!\langle 0| && T_4 \end{aligned}$$

Where we named the terms T_1, T_2, T_3, T_4. Doing some long and tedious gymnastics that are explained in sec. C.6, we obtain

$$C_2 = \frac{i}{160\pi^3} \int d^4k dt \mathrm{Tr}[U^\dagger \partial_\mu U \cdot U^\dagger \partial_\nu U \cdot U^\dagger \partial_\lambda U \cdot U^\dagger \partial_\sigma U \cdot U^\dagger \partial_\tau U] \epsilon_{\mu\nu\lambda\sigma\tau} \tag{C.79}$$

C.5.2 A time domain expression for the n'th Chern number

The above suggests the general formula for the invariant corresponding to the n'th Chern number.

$$C_n = K_n \int d^{2n+1}k \mathrm{Tr} \left[\prod_{i=1}^{2n+1} U^\dagger \partial_{\mu_i} U \right] \epsilon^{\mu_1 \mu_2 \ldots \mu_{2n+1}} \tag{C.80}$$

It is easy to show that the above is a topological invariant. Here K_n is some normalization constant, that can be calculated in the same way as for $n = 1$, $n = 2$. The constants are, for $n = 0, 1, 2$:

$$K_0 = \frac{1}{2\pi i}, \quad K_1 = -\frac{1}{24\pi^2}, \quad K_2 = \frac{i}{160\pi^3}$$

The case $n = 0$ is explained below:

C.5.3 Zeroth Chern number

Eq. (C.80) can in fact be generalized to $n = 0$. In the non-driven case the 0'th Chern number just tells you the number of occupied bands, as can be easily seen from eq. (C.69). However, in the driven case, the invariant corresponding to C_0 is slightly less trivial. The "zeroth" chern number is

$$C_0 = \frac{1}{2\pi i} \int dt U^\dagger \partial_t U \tag{C.81}$$

The constant in front is chosen such C_0 is an integer and can be any integer. This is simply the winding number of the determinant of $U_\xi(t)$. If ξ lies in a gap, C_0 is well defined in any dimension, since it is the same for all $\mathbf{k}$ in the BZ.C_0 can easily be found directly from the Hamiltonian:

$$C_0 = -\frac{1}{\omega} \left[\mathrm{Tr} H_0 - \mathrm{Tr} H_{\mathrm{eff}}(\xi) \right] \tag{C.82}$$

Where H_0 is the zeroth fourier component of $H(t)$. (there might be sign errors in the two above equations).

In non-driven systems, the zeroth Chern number is the number of occupied bands, and in the Floquet Hilbert space, it determines the dimension d_{anom} of the anomalous subspace. The formula is

$$d_{\text{anom}}(\xi) = \text{Tr}P_a = M(N+1) + C_0 \tag{C.83}$$

Here N is the cutoff, and M the number of orbitals. Note that the invariant corresponding to the zeroth chern number is not the result gotten when extending eq. (C.69), to $n = 0$, as this is ill defined. There seems to appear some kind of "regularization" term $M(N+1)$. It could be interesting to examine what this says about winding numbers in general.

C.6 Deriving eq. (C.79)

Evaluating T_4

We have

$$\begin{aligned}
T_4 &= -\sum_{m_i} \mathrm{Tr}\min(m_1,m_2,m_3,0)\cdot P_{m_1}\partial_\mu|m_2\rangle\!\rangle\partial_\nu\langle\!\langle m_2|\cdot P_{m_3}\partial_\lambda|0\rangle\!\rangle\partial_\sigma\langle\!\langle 0| \\
&= -\sum_{m_i} \mathrm{Tr}\min(m_1,m_2,m_3,0)\cdot P_0\partial_\mu|m_2-m_1\rangle\!\rangle\partial_\nu\langle\!\langle m_2-m_1|\cdot P_{m_3-m_1}\partial_\lambda|-m_1\rangle\!\rangle\partial_\sigma\langle\!\langle -m_1| \\
&= -\sum_{m_i} \mathrm{Tr}\min(m_1,m_2+m_1,m_3+m_1,0)\cdot P_0\partial_\mu|m_2\rangle\!\rangle\partial_\nu\langle\!\langle m_2|\cdot P_{m_3}\partial_\lambda|-m_1\rangle\!\rangle\partial_\sigma\langle\!\langle -m_1| \\
&= -\sum_{m_i} \mathrm{Tr}\min(-m_1,m_2-m_1,m_3-m_1,0)\cdot P_0\partial_\mu|m_2\rangle\!\rangle\partial_\nu\langle\!\langle m_2|\cdot P_{m_3}\partial_\lambda|m_1\rangle\!\rangle\partial_\sigma\langle\!\langle m_1| \\
&= -\sum_{m_i} \mathrm{Tr}[\min(0,m_2,m_3,m_1)-m_1]\cdot P_0\partial_\mu|m_2\rangle\!\rangle\partial_\nu\langle\!\langle m_2|\cdot P_{m_3}\partial_\lambda|m_1\rangle\!\rangle\partial_\sigma\langle\!\langle m_1|
\end{aligned}$$

The first term is

$$\begin{aligned}
T_{41} &= -\sum_{m_i} \mathrm{Tr}\min(0,m_2,m_3,m_1)\cdot P_0\partial_\mu|m_2\rangle\!\rangle\partial_\nu\langle\!\langle m_2|\cdot P_{m_3}\partial_\lambda|m_1\rangle\!\rangle\partial_\sigma\langle\!\langle m_1| \\
&= -\sum_{m_i} \mathrm{Tr}\min(0,m_2,m_3,m_1)\cdot \partial_\sigma|0\rangle\!\rangle\partial_\mu\langle\!\langle 0|P_{m_2}\partial_\nu|m_3\rangle\!\rangle\partial_\lambda\langle\!\langle m_3|\cdot P_{m_1}
\end{aligned}$$

Renaming m_i and remembering antisymmetrization

$$\begin{aligned}
T_{41} &= -\sum_{m_i} \mathrm{Tr}\min(0,m_2,m_3,m_1)\cdot P_{m_1}\partial_\nu|m_2\rangle\!\rangle\partial_\lambda\langle\!\langle m_2|\cdot P_{m_3}\partial_\sigma|0\rangle\!\rangle\partial_\mu\langle\!\langle 0| \\
&= +\sum_{m_i} \mathrm{Tr}\min(0,m_2,m_3,m_1)\cdot P_{m_1}\partial_\mu|m_2\rangle\!\rangle\partial_\nu\langle\!\langle m_2|\cdot P_{m_3}\partial_\lambda|0\rangle\!\rangle\partial_\sigma\langle\!\langle 0| \\
&= -T_4
\end{aligned}$$

Hence

$$\begin{aligned}
T_4 &= \frac{1}{2}\sum_{m_i} m_1 P_0\partial_\mu|m_2\rangle\!\rangle\partial_\nu\langle\!\langle m_2|\cdot P_{m_3}\partial_\lambda|m_1\rangle\!\rangle\partial_\sigma\langle\!\langle m_1| \\
&= \frac{1}{2}\sum_{m_i} m_1 P_0\partial_\mu|m_2\rangle\!\rangle\partial_\nu\langle\!\langle m_2|\cdot \partial_\lambda|m_1\rangle\!\rangle\partial_\sigma\langle\!\langle m_1|
\end{aligned}$$

Evaluating T_2

We have

$$\begin{aligned}
T_2 &= \sum_{m_i} \mathrm{Tr}\min(m_1, m_2, 0)\partial_\mu|0\rangle\!\rangle\partial_\nu\langle\!\langle 0|\cdot\partial_\lambda|m_1\rangle\!\rangle\partial_\sigma\langle\!\langle m_1|P_{m_2} \\
&= \sum_{m_i} \mathrm{Tr}\min(m_1, m_2, 0)\partial_\mu|-m_2\rangle\!\rangle\partial_\nu\langle\!\langle -m_2|\cdot\partial_\lambda|m_1-m_2\rangle\!\rangle\partial_\sigma\langle\!\langle m_1-m_2|P_0 \\
&= \sum_{m_i} \mathrm{Tr}\min(m_1+m_2, m_2, 0)\partial_\mu|-m_2\rangle\!\rangle\partial_\nu\langle\!\langle -m_2|\cdot\partial_\lambda|m_1\rangle\!\rangle\partial_\sigma\langle\!\langle m_1|P_0 \\
&= \sum_{m_i} \mathrm{Tr}\min(m_1-m_2, -m_2, 0)\partial_\mu|m_2\rangle\!\rangle\partial_\nu\langle\!\langle m_2|\cdot\partial_\lambda|m_1\rangle\!\rangle\partial_\sigma\langle\!\langle m_1|P_0 \\
&= \sum_{m_i} \mathrm{Tr}(\min(m_1, 0, m_2)-m_2)\partial_\mu|m_2\rangle\!\rangle\partial_\nu\langle\!\langle m_2|\cdot\partial_\lambda|m_1\rangle\!\rangle\partial_\sigma\langle\!\langle m_1|P_0 \\
&= T_3 - \sum_{m_i} m_2\partial_\mu|m_2\rangle\!\rangle\partial_\nu\langle\!\langle m_2|\cdot\partial_\lambda|m_1\rangle\!\rangle\partial_\sigma\langle\!\langle m_1|P_0 \\
&= T_3 + T_{2R}
\end{aligned}$$

Where T_{2R} was defined.

Evaluating T_1

We have

$$\begin{aligned}
T_1 &= \sum_{m_i} \mathrm{Tr}\min(m_1, m_2, 0)\partial_\mu|m_1\rangle\!\rangle\partial_\nu\langle\!\langle m_1|\cdot\partial_\lambda|0\rangle\!\rangle\partial_\sigma\langle\!\langle 0|P_{m_2} \\
&= \sum_{m_i} \mathrm{Tr}\min(m_1, m_2, 0)\partial_\mu|m_1-m_2\rangle\!\rangle\partial_\nu\langle\!\langle m_1-m_2|\cdot\partial_\lambda|-m_2\rangle\!\rangle\partial_\sigma\langle\!\langle -m_2|P_0 \\
&= \sum_{m_i} \mathrm{Tr}\min(m_1+m_2, m_2, 0)\partial_\mu|m_1\rangle\!\rangle\partial_\nu\langle\!\langle m_1|\cdot\partial_\lambda|-m_2\rangle\!\rangle\partial_\sigma\langle\!\langle -m_2|P_0 \\
&= \sum_{m_i} \mathrm{Tr}\min(m_1-m_2, -m_2, 0)\partial_\mu|m_1\rangle\!\rangle\partial_\nu\langle\!\langle m_1|\cdot\partial_\lambda|m_2\rangle\!\rangle\partial_\sigma\langle\!\langle m_2|P_0 \\
&= \sum_{m_i} \mathrm{Tr}[\min(m_1, m_2, 0)-m_2]\partial_\mu|m_1\rangle\!\rangle\partial_\nu\langle\!\langle m_1|\cdot\partial_\lambda|m_2\rangle\!\rangle\partial_\sigma\langle\!\langle m_2|P_0 \\
&= T_3 - \sum_{m_i} \mathrm{Tr}\ m_2\partial_\mu|m_1\rangle\!\rangle\partial_\nu\langle\!\langle m_1|\cdot\partial_\lambda|m_2\rangle\!\rangle\partial_\sigma\langle\!\langle m_2|P_0 \\
&= T_3 - \sum_{m_i} \mathrm{Tr}\ m_1\partial_\mu|m_2\rangle\!\rangle\partial_\nu\langle\!\langle m_2|\cdot\partial_\lambda|m_1\rangle\!\rangle\partial_\sigma\langle\!\langle m_1|P_0 \\
&= T_3 + T_{1R}
\end{aligned}$$

Hence $L_1 = 4T_1 + 3T_2 - T_3 = -6T_3 + 4T_{1R} + 3T_{2R}$. Also, by partial integration, it can be easily shown that $T_1 + T_2 + T_3 = 0$. But then

$$T_1 + T_2 + T_3 = 3T_3 + T_{1R} + T_{2R} = 0 \tag{C.84}$$

Thus $T_3 = \frac{1}{3}(T_{1R} + T_{2R})$ And

$$L_1 = -2T_{1R} - 2T_{2R} + 4T_{1R} + 3T_{2R} = 2T_{1R} + T_{2R} \tag{C.85}$$

Now

$$\begin{aligned}
T_{2R} &= -\sum_{m_i} m_2 \partial_\mu |m_2\rangle\!\rangle \partial_\nu \langle\!\langle m_2| \cdot \partial_\lambda |m_1\rangle\!\rangle \partial_\sigma \langle\!\langle m_1|P_0 \\
&= -\sum_{m_i} m_2 \partial_\mu |0\rangle\!\rangle \partial_\nu \langle\!\langle 0| \cdot \partial_\lambda |m_1 - m_2\rangle\!\rangle \partial_\sigma \langle\!\langle m_1 - m_2|P_{-m_2} \\
&= -\sum_{m_i} m_2 \partial_\mu |0\rangle\!\rangle \partial_\nu \langle\!\langle 0| \cdot \partial_\lambda |m_1\rangle\!\rangle \partial_\sigma \langle\!\langle m_1|P_{-m_2} \\
&= \sum_{m_i} m_2 \partial_\mu |0\rangle\!\rangle \partial_\nu \langle\!\langle 0| \cdot \partial_\lambda |m_1\rangle\!\rangle \partial_\sigma \langle\!\langle m_1|P_{m_2}
\end{aligned}$$

Since $T_{41} = -T_{1R}/2$, we get,

$$\begin{aligned}
I(\xi) &= \frac{3}{2} T_{1R} + T_{2R} \\
&= -\sum_{m_i} (3m_1/2 + m_2) \mathrm{Tr}\left[\partial_\mu |m_2\rangle\!\rangle \partial_\nu \langle\!\langle m_2| \cdot \partial_\lambda |m_1\rangle\!\rangle \partial_\sigma \langle\!\langle m_1|P_0\right]
\end{aligned}$$

Plugging in the expressions for $|m, n\rangle\!\rangle$,

$$\begin{aligned}
I(\xi) = &- \sum_{m_i \beta_i z_i} (3m_1/2 + m_2) \mathrm{Tr}[\\
&\partial_\mu U_{\beta_1 \alpha_1}(z_1) |z_1 \beta_1\rangle\!\rangle \partial_\nu U^*_{\beta_2 \alpha_1}(z_2) \langle\!\langle z_2 \beta_2| \cdot \partial_\lambda U_{\beta_3 \alpha_2}(z_3 - m_1) |z_3 \beta_3\rangle\!\rangle \partial_\sigma U^*_{\beta_4 \alpha_2}(z_4 - m_1) \langle\!\langle z_4 \beta_4| \\
&|z_5 \beta_5\rangle\!\rangle U_{\beta_5 \alpha_3}(z_5 - m_1) U^*_{\beta_6 \alpha_3}(z_6 - m_1) \langle\!\langle z_6 \beta_6|] \\
&= - \sum_{m_i \beta_i z_i} (3m_1/2 + m_2) \\
&\mathrm{Tr}[\partial_\mu U(z_1 - m_2) \partial_\nu U^\dagger(z_2 - m_2) \partial_\lambda U(z_2 - m_1) \partial_\sigma U^\dagger(z_3 - m_1) U(z_3) U^\dagger(z_1)]
\end{aligned}$$

Letting $z_i \to z_i - m_1$, $m_2 \to m_2 - m_1$,

$$\begin{aligned}
I(\xi) = &- \sum_{m_i \beta_i z_i} (m_1/2 + m_2) \\
&\mathrm{Tr}[\partial_\mu U(z_1 - m_2) \partial_\nu U^\dagger(z_2 - m_2) \partial_\lambda U(z_2) \partial_\sigma U^\dagger(z_3) U(z_3 - m_1) U^\dagger(z_1 - m_1)]
\end{aligned}$$

The second term vanishes because it can be written as the integral of a derivative, and adding another vanishing term,

$$\begin{aligned}
I(\xi) = &\sum_{m_i \beta_i z_i} (z_3 - m_1)/2 \\
&\mathrm{Tr}[\partial_\mu U(z_1 - m_2) \partial_\nu U^\dagger(z_2 - m_2) \partial_\lambda U(z_2) \partial_\sigma U^\dagger(z_3) U(z_3 - m_1) U^\dagger(z_1 - m_1)] \\
&= \frac{1}{2i\omega T} \int dt \mathrm{Tr}[\partial_\mu U \partial_\nu U^\dagger \partial_\lambda U \partial_\sigma U^\dagger \partial_t U \cdot U^\dagger]
\end{aligned}$$

Expanding $\partial_\mu U^\dagger$, and restoring the Levi-Civita tensor,

$$\begin{aligned} I(\xi) &= \frac{1}{4\pi i}\int dt \mathrm{Tr}[\partial_\mu U\cdot U^\dagger \partial_\nu U\cdot U^\dagger \partial_\lambda U\cdot U^\dagger \partial_\sigma U\cdot U^\dagger \partial_t U\cdot U^\dagger]\epsilon_{\mu\nu\lambda\sigma} \\ &= \frac{1}{20\pi i}\int dt \mathrm{Tr}[U^\dagger \partial_\mu U\cdot U^\dagger \partial_\nu U\cdot U^\dagger \partial_\lambda U\cdot U^\dagger \partial_\sigma U\cdot U^\dagger \partial_\tau U]\epsilon_{\mu\nu\lambda\sigma\tau} \end{aligned}$$

Plugging this expression into eq. (C.69),

$$\begin{aligned} C_2 &= \frac{(-1)^2}{(2\pi i)^2 2!}\int d^{2\cdot 2}k\ I(\xi) \\ &= \frac{-1}{8\pi^2}\frac{1}{20\pi i}\int d^4k dt \mathrm{Tr}[U^\dagger \partial_\mu U\cdot U^\dagger \partial_\nu U\cdot U^\dagger \partial_\lambda U\cdot U^\dagger \partial_\sigma U\cdot U^\dagger \partial_\tau U]\epsilon_{\mu\nu\lambda\sigma\tau} \\ &= \frac{i}{160\pi^3}\int d^4k dt \mathrm{Tr}[U^\dagger \partial_\mu U\cdot U^\dagger \partial_\nu U\cdot U^\dagger \partial_\lambda U\cdot U^\dagger \partial_\sigma U\cdot U^\dagger \partial_\tau U]\epsilon_{\mu\nu\lambda\sigma\tau} \end{aligned}$$

Bibliography

[1] K. v. Klitzing, G. Dorda, and M. Pepper. New method for high-accuracy determination of the fine-structure constant based on quantized hall resistance. *Phys. Rev. Lett.*, 45:494–497, Aug 1980.

[2] Takuya Kitagawa, Takashi Oka, Arne Brataas, Liang Fu, and Eugene Demler. Transport properties of nonequilibrium systems under the application of light: Photoinduced quantum hall insulators without landau levels. *Phys. Rev. B*, 84:235108, Dec 2011.

[3] T. Oka and H. Aoki. Photovoltaic hall effect in graphene. *Phys. Rev. B*, 79:081406, Feb 2009.

[4] Zhenghao Gu, H. A. Fertig, Daniel P. Arovas, and Assa Auerbach. Floquet spectrum and transport through an irradiated graphene ribbon. *Phys. Rev. Lett.*, 107:216601, Nov 2011.

[5] Balázs Dóra, Jérôme Cayssol, Ferenc Simon, and Roderich Moessner. Optically engineering the topological properties of a spin hall insulator. *Phys. Rev. Lett.*, 108:056602, Jan 2012.

[6] N. H. Lindner, G. Refael, and V. Galitski. Floquet topological insulator in semiconductor quantum wells. *Nat. Phys.*, 7:490–495, Jun 2011.

[7] T. Vu, Q. H. Haug, D. Mücke, O. T. Tritschler, M. Wegener, G. Khitrova, and M. Gibbs, H. ˙ Light-induced gaps in semiconductor band-to-band transitions. *Phys. Rev. Lett.*, 92:217403, May 2004.

[8] J. W. McIver, D. Hsieh, H. Steinberg, P. Jarillo-Herrero, and N. Gedik. Control over topological insulator photocurrents with light polarization. *Nat. Nano.*, 7:96–100, Feb 2012.

[9] Marin Bukov and Anatoli Polkovnikov. Stroboscopic versus nonstroboscopic dynamics in the floquet realization of the harper-hofstadter hamiltonian. *Phys. Rev. A*, 90:043613, Oct 2014.

[10] M. S. Rudner, N. H. Lindner, E. Berg, and M. Levin. Anomalous edge states and the bulk-edge correspondence for periodically driven two-dimensional systems. *Phys. Rev. X*, 3:031005, Jul 2013.

[11] L. D'Alessio and M. Rigol. Long-time behavior of periodically driven isolated interacting lattice systems. *ArXiv e-prints*, February 2014.

[12] Liang Jiang, Takuya Kitagawa, Jason Alicea, A. R. Akhmerov, David Pekker, Gil Refael, J. Ignacio Cirac, Eugene Demler, Mikhail D. Lukin, and Peter Zoller. Majorana fermions in equilibrium and in driven cold-atom quantum wires. *Phys. Rev. Lett.*, 106:220402, Jun 2011.

[13] J. K. Asbóth, B. Tarasinski, and P. Delplace. Chiral symmetry and bulk-boundary correspondence in periodically driven one-dimensional systems. *Phys. Rev. B*, 90:125143, Sep 2014.

[14] Liang Fu and C. L. Kane. Topological insulators with inversion symmetry. *Phys. Rev. B*, 76:045302, Jul 2007.

[15] B. Andrei Bernevig, Taylor L. Hughes, and Shou-Cheng Zhang. Quantum spin hall effect and topological phase transition in hgte quantum wells. *Science*, 314(5806):1757–1761, 2006.

[16] D. Carpentier, P. Delplace, M. Fruchart, and K. Gawędzki. A topological index for periodically driven time-reversal invariant 2D systems. *arXiv*, July 2014.

[17] Conyers Herring. Accidental degeneracy in the energy bands of crystals. *Phys. Rev.*, 52:365–373, Aug 1937.

[18] www.issp.ac.ru/lpcbc.

[19] www.physicsworld.com (from Laurens W. Molenkamp).

[20] www.nobelprize.org.

[21] www.jqi.umd.edu (from Alejandro Lobos).

[22] Jason Alicea. Exotic matter: Majorana modes materialize. *Nat. Nano.*, 8:623–624, 09 2013. From Leo Kouwenhoven's group.

[23] Yasuhiro Hatsugai. Chern number and edge states in the integer quantum hall effect. *Phys. Rev. Lett.*, 71:3697–3700, Nov 1993.

[24] J. E. Avron, L. Sadun, J. Segert, and B. Simon. Topological invariants in fermi systems with time-reversal invariance. *Phys. Rev. Lett.*, 61:1329–1332, Sep 1988.

[25] D. J. Thouless, M. Kohmoto, M. P. Nightingale, and M. den Nijs. Quantized hall conductance in a two-dimensional periodic potential. *Phys. Rev. Lett.*, 49:405–408, Aug 1982.

[26] B. A. Bernevig and T. L. Hughes. *Topological Insulators and Supercondutors*. Princeton University Press, 2013.

[27] A Yu Kitaev. Unpaired majorana fermions in quantum wires. *Physics-Uspekhi*, 44(10S):131, 2001.

[28] T. Voronov. *Concise Encyclopedia of Supersymmery*. Springer Netherlands, 2003.

[29] Alexander Altland and Martin R. Zirnbauer. Nonstandard symmetry classes in mesoscopic normal-superconducting hybrid structures. *Phys. Rev. B*, 55:1142–1161, Jan 1997.

[30] Shinsei Ryu, Andreas P Schnyder, Akira Furusaki, and Andreas W W Ludwig. Topological insulators and superconductors: tenfold way and dimensional hierarchy. *New Journal of Physics*, 12(6):065010, 2010.

[31] Alexei Kitaev. Periodic table for topological insulators and superconductors. *AIP Conference Proceedings*, 1134(1), 2009.

[32] M. Z. Hasan and C. L. Kane. *Colloquium* : Topological insulators. *Rev. Mod. Phys.*, 82:3045–3067, Nov 2010.

[33] B. I. Halperin. Quantized hall conductance, current-carrying edge states, and the existence of extended states in a two-dimensional disordered potential. *Phys. Rev. B*, 25:2185–2190, Feb 1982.

[34] Alexander Tzalenchuk, Samuel Lara-Avila, Alexei Kalaboukhov, Sara Paolillo, Mikael Syvajarvi, Rositza Yakimova, Olga Kazakova, JanssenT. J. B. M., Vladimir Fal'ko, and Sergey Kubatkin. Towards a quantum resistance standard based on epitaxial graphene. *Nat. Nano.*, 5:186–189, Mar 2010.

[35] S. Das Sarma, M. Freedman, and C. Nayak. Majorana Zero Modes and Topological Quantum Computation. *ArXiv e-prints*, January 2015.

[36] C. L. Kane and E. J. Mele. Quantum spin hall effect in graphene. *Phys. Rev. Lett.*, 95:226801, Nov 2005.

[37] C. L. Kane and E. J. Mele. Z_2 topological order and the quantum spin hall effect. *Phys. Rev. Lett.*, 95:146802, Sep 2005.

[38] G. Floquet. Sur les equations differentielles lineaires a coefficients periodiues. *Annales scientifiques*, 2:47–48, 1883.

[39] M. Bukov, L. D'Alessio, and A. Polkovnikov. Universal High-Frequency Behavior of Periodically Driven Systems: from Dynamical Stabilization to Floquet Engineering. *ArXiv e-prints*, July 2014.

[40] Takuya Kitagawa, Erez Berg, Mark Rudner, and Eugene Demler. Topological characterization of periodically driven quantum systems. *Phys. Rev. B*, 82:235114, Dec 2010.

[41] Takuya Kitagawa, Matthew A. Broome, Alessandro Fedrizzi, Mark S. Rudner, Erez Berg, Ivan Kassal, Alan Aspuru-Guzik, Eugene Demler, and Andrew G. White. Observation of topologically protected bound states in photonic quantum walks. *Nat. Comm.*, 3:882, Jun 2012.

[42] K. J. Riley, M. P. Hobson, and S. J. Bence. *Mathematical Methods for Physics and Engineering.* Cambridge University Press, 3 edition, 2006.

[43] Xiao-Liang Qi, Taylor L. Hughes, and Shou-Cheng Zhang. Topological field theory of time-reversal invariant insulators. *Phys. Rev. B*, 78:195424, Nov 2008.

[44] Achilleas Lazarides, Arnab Das, and Roderich Moessner. Equilibrium states of generic quantum systems subject to periodic driving. *Phys. Rev. E*, 90:012110, Jul 2014.

[45] Achilleas Lazarides, Arnab Das, and Roderich Moessner. Periodic thermodynamics of isolated quantum systems. *Phys. Rev. Lett.*, 112:150401, Apr 2014.

[46] Angelo Russomanno, Alessandro Silva, and Giuseppe E. Santoro. Periodic steady regime and interference in a periodically driven quantum system. *Phys. Rev. Lett.*, 109:257201, Dec 2012.

[47] K. J. Riley, M. P. Hobson, and S. J. Bence. *Mathematical Methods for Physics and Engineering*. Cambridge University Press, 3 edition, 2006.

[48] Emil Prodan, Bryan Leung, and Jean Bellissard. The non-commutative n th-chern number. *Journal of Physics A: Mathematical and Theoretical*, 46(48):485202, 2013.